DISTINGUISHING CARBOHYDRATE ISOMERS WITH ION-MOLECULE REACTIONS AND INSIGHTS INTO METAL CATIONIZATION

Matthew T. Campbell

A dissertation submitted to the faculty at the University of North Carolina at Chapel Hill in partial fulfillment of the requirements for the degree of Doctor of Philosophy in the Department of Chemistry.

Chapel Hill
2018

Approved by:

Gary L. Glish

Leslie Hicks

James Jorgenson

Russell Grant

Cynthia Schauer

ABSTRACT

Matthew T. Campbell: Distinguishing Carbohydrate Isomers with Ion-Molecule Reactions and Insights into Metal Cationization
(Under the direction of Gary L. Glish)

Mass spectrometry has become a powerful analytical technique because it provides high sensitivity, short analysis times, and provides quantitative measurements of chemical and biological systems. Mass spectrometry also provides a high degree of selectivity, separating ions based on their mass-to-charge ratio. Isobaric or isomeric ions which have the same mass-to-charge ratio are more difficult to distinguish with mass spectrometry. Methods have been developed for distinguishing isobaric/isomeric compounds, the most common of which is collision induced dissociation (CID). Isomeric ions can also be distinguished by unique reaction with other ions (ion-ion reactions) or molecules (ion-molecule reactions). One example of an ion-molecule reaction is the adduction of water to lithium cationized molecules, $[M+Li]^+$, in a quadrupole ion trap, producing $[M+Li+H_2O]^+$ observed 18 mass-to-charge units higher than $[M+Li]^+$. This water adduction reaction was used to distinguish several different monosaccharide isomers including an exhaustive list of D-pentoses and several biologically relevant hexoses, hexosamines, and N-acetyl hexosamaines. These isomers could be distinguished by at least one of two metrics of the water adduction reaction. The first metric is the water adduction reaction rate. The second metric is the fraction of $[M+Li]^+$ that will not adduct water, even when allowed very long reaction times. This fraction is very reproducible and unique for different isomers. The chemistry behind the unreactive fraction is studied with a combination of density functional theory calculations and experimental results. Together the

reaction rate and the unreactive fraction of ions were then used to determine the relative concentration of two different hexoses in a binary mixture and determine the anomeric ratio of glucose in different solvents. Water adduction was used to distinguish several different glucose-glucose disaccharides, determining both the linkage position and anomericity of the glycosydic linkage.

"In the temple of science are many mansions, and various indeed are they that dwell therein and the motives that have led them thither. Many take to science out of a joyful sense of superior intellectual power; science is their own special sport to which they look for vivid experience and the satisfaction of ambition; many others are to be found in the temple who have offered the products of their brains on this altar for purely utilitarian purposes. Were an angel of the Lord to come and drive all the people belonging to these two categories out of the temple, the assemblage would be seriously depleted, but there would still be some men, of both present and past times, left inside. I am quite aware that we have just now light-heartedly expelled in imagination many excellent men who are largely, perhaps chiefly, responsible for the buildings of the temple of science; and in many cases our angel would find it a pretty ticklish job to decide. But of one thing I feel sure: if the types we have just expelled were the only types there were, the temple would never have come to be, any more than a forest can grow which consists of nothing but creepers. For these people any sphere of human activity will do, if it comes to a point; whether they become engineers, officers, tradesmen, or scientists depends on circumstances. Now let us have another look at those who have found favor with the angel. Most of them are somewhat odd, uncommunicative, solitary fellows, really less like each other, in spite of these common characteristics, than the hosts of the rejected. What has brought them to the temple? That is a difficult question and no single answer will cover it."

TABLE OF CONTENTS

LIST OF TABLES

LIST OF FIGURES

LIST OF ABBREVIATIONS AND SYMBOLS

A	arbitrary reactant
A_t	concentration of reactant at a time, t
A_0	concentration of reactant at time = 0
B3LYP	Becke, 3-parameter, Lee-Yang-Parr
BOMD	Born-Oppenheimer molecular dynamics
CID	collision-induced dissociation
°C	degrees Celsius
CO_2	carbon dioxide
CRM	charged residue model
DFT	density functional theory
ΔΔG	the difference in the change in Gibbs free energy
$\Delta G_{WaterAddcution}$	change in Gibbs free energy after water adduction
ESI	electrospray ionization
EESI	extractive electrospray ionization
Fru	fructose
$G_{Hydrated}$	Gibbs free energy of the hydrated complex
$G_{Lithiated\ Hexose}$	Gibbs free energy of the lithium cationized hexose
G_{Water}	Gibbs free energy of water
Glc	glucose
I_{187}	Signal intensity for mass-to-charge ratio 187, [M+Li]+
I_{205}	Signal intensity for mass-to-charge ratio 205, [+Li+H2O]+
IEM	ion evaporation model

K	Kelvin
k	Boltzmann constant
K_{eq}	equilibrium constant
Kcal/mol	kilocalories per mole
L	liter
M06-2X	Minnesota ’06 family of functionals
µM	micromolar
$[M+H]^+$	protonated molecule
$[M+K]^+$	potassium cationized molecule
$[M+Li]^+$	lithium cationized molecule
$[M+Na]^+$	sodium cationized molecule
mg	milligram
µL	microliter
µm	micrometer
MP2	Møller-Plesset perturbation theory
MS	mass spectrometry
ms	millisecond
MS/MS	mass-spectrometry/mass-spectrometry
MS^2	two stages of tandem mass spectrometry
MS^3	three stages of tandem mass spectrometry
m/z	mass-to-charge ratio
nM	nanomolar
QIT	quadrupole ion trap

RSD	relative standard deviation
R_R	reactive fraction of ions
R_U	unreactive fraction of ions
T	temperature
t	time
V	volt
Zn	Zinc

CHAPTER 1: INTRODUCTION TO ION-MOLECULE REACTIONS AND WATER ADDUCTION TO LITHIUM CATIONIZED MOLECULES

1.1. Introduction to Analysis of Carbohydrate Molecules

Carbohydrates are important biological molecules because of their role in cell-cell interactions, cell growth, inflammation, and other physiological processes[1–5]. In biological systems carbohydrates are found as free monomers, chains of polysaccharides, and modifications to lipids and proteins[6]. Structural elucidation of complex carbohydrates requires knowing sequence, linkage positions, branching points, and any modifications such as N-acetylation, phosphorylation, or methylation[7–9]. Complete structural elucidation begins with identification of the monosaccharide and disaccharide building blocks[10].

Distinguishing carbohydrates is analytically challenging because the high degree of structural similarity. The monosaccharide subunits differ by as little as one stereocenter. Aldohexoses such as D-glucose have three chiral centers (excluding the anomeric carbon) creating eight possible diastereomers. Conventional methods such as NMR and x-ray crystallography have had some success in elucidating monosaccharide structures[11]. However, these techniques usually require relatively large amounts of sample (hundreds of nanomoles for analyses with the best limits of detection) of highly purified sample, which can be very labor intensive. Though some carbohydrates such as glucose and fructose are typically found in mM concentrations at physiological conditions, more sensitive methods are required for minimizing the amount of sample needed and/or diluting a complex matrix such as blood, serum, or an extraction from tissue. Mass spectrometry can be used to analyze samples from complex

matrices, and analysis is completed in seconds. Most importantly, with the selectivity of MS, background molecules that do not ionize or ionize with a different mass-to-charge ratio as the analyte are unlikely to affect the analysis.

1.2. Distinguishing Isomers with Pre- and Post-Ionization Separations Coupled to Mass Spectrometry

The drawback to using mass spectrometry to study carbohydrates is the inherent difficulty distinguishing conformational isomers and stereoisomers[12,13]. Liquid chromatography (LC) is often used prior to mass analysis, providing an orthogonal separation step before mass analysis. However, chromatographic methods used to separate carbohydrates require lengthy separation and column regeneration times, and some methods require a specialized chiral column [5,14–16]. Separation of carbohydrates has also been successfully performed by gas chromatography-mass spectrometry (GC-MS); however, gas chromatography also suffers from the same drawbacks as LC-MS with an additional need for prior derivatization to increase volatility of the carbohydrates. Additionally, some chromatographic methods can also result in different peaks for α and β anomers and/or pyranose and furanose forms of a single compound, which can lead to overlapping peaks for different isomers, further complicating data analysis [17,18].

Another method that has been used to separate carbohydrate isomers prior to mass analysis is ion mobility spectrometry-mass spectrometry (IMS-MS). IMS separates ions based upon their mobility in an electric field and is capable of separating ions on millisecond timescales, significantly reducing analysis time compared to LC or GC separations [19–21]. IMS separations have had the most success with carbohydrates that are typically tetrasaccharides or larger chains. The larger number of monosaccharide units increases the likelihood for differences in size, and therefore mobility, compared to smaller molecules such as disaccharides and monosaccharides. Recently, a method was reported for distinguishing unmodified hexoses with

drift tube ion mobility spectrometry [22]. This required forming a tetrameric complex of the hexose, divalent transition metal cation, and two chiral molecules (typically amino acids). The subsequent complex resulted in different drift times for several different hexoses; however, a concentration of 30 mM hexose as well as millimolar concentrations of divalent metal cation and amino acids were required to form these multiunit noncovalent complexes. These high sample concentrations ultimately translate to large amounts of sample, providing no major benefits over identification using NMR.

1.3. Distinguishing Carbohydrates without a Prior Separation Step

Mass spectrometry without prior chromatographic or ion mobility separations is often considered unable to distinguish diastereomers, but methods have been reported for carbohydrate isomer identification using only mass spectrometry. Dissociative methods are the most common techniques used for distinguishing isomeric compounds with mass spectrometry. The most prevalent form of dissociation is collision induced dissociation (CID), where the ions are accelerated into neutral atoms or molecules (typically argon or helium atoms). Several consecutive collisions may cause the internal energy of the ion to increase enough that bonds begin to dissociate. The product ions resulting from dissociation can be mass analyzed, and if the product ions are unique to a given isomer, then the isomers can be distinguished.

When considering distinguishing carbohydrate isomers, dissociative techniques have had the most success with disaccharides and longer chain carbohydrates. The viability of a particular dissociative technique is often proven by analyzing an array of glucosyl-glucose disaccharides varying in linkage position and anomericity. CID was reported to distinguish the linkage position for several disaccharides but not anomericity.[23,24] CID was then used to determine the anomericity of several disaccharides first derivatized with Zn(II)-diethylenetriamine chloride

prior to mass spectral analysis.[25] Since then other methods have been developed to determine linkage position and the anomericity of some linkages which do not require a prior derivatization step[26–33]. Most of these methods report relatively high concentrations (typically ≥ 100 μM) to provide sufficient signal intensity to confidently distinguish isomers. High concentrations are necessary for determining the anomericity of the linkage because there are only very small differences in product ions ratios. However, these methods did not demonstrate the ability to distinguish linkage position and anomericity for both reducing and non-reducing disaccharides. Infrared multi-photon dissociation has also been used to determine some linkage position and anomericity of some disaccharides but requires separate tandem mass spectrometry (MS/MS) experiments and the additional cost and complexity of a tunable CO_2 laser.[12,34] Recently, a method was reported that was capable of distinguishing linkage position and anomeric configuration for both reducing and non-reducing disaccharides by measuring collisional cross-section of the MS^2 product using ion mobility.[35] However, this method requires the extra cost/complexity of the Ion Mobility Cell.

Monosaccharides are particularly difficult to distinguish with dissociative methods, because their small and similar structures do not produce unique product ions. Some methods involve first derivatizing the carbohydrate of interest by covalently binding a transition metal complex (usually zinc-diethylenetriamine) and subsequently performing CID on the resulting metal N-glycosides. The method results in unique product ions for different isomers and has been used for identification of hexoses, but the derivatization reaction requires heating the sample for 20 minutes, increasing analysis time. Dissociative methods have had little success with underivatized monosaccharides, though identification has been reported by using ammonium cationized hexoses [1,36,37]. Unmodified monosaccharides have very similar structures

making it difficult for dissociative methods to obtain unique product ions capable of distinguishing the large number of stereoisomers. Methods that can successfully distinguish monosaccharides typically require concentrations of analyte greater than 100 μM to achieve reproducible data.

One successful dissociative method for identifying monosaccharides without a separation step uses the kinetic method [38]. The kinetic method requires addition of a divalent metal cation (M^{II}), and a chiral reference molecule (crm), to the analyte solution prior to electrospray ionization (ESI). These species form a complex $[M^{II}(A)(crm)_2 – H)]^+$ where (A) is the monosaccharide of interest. Once the complex is formed, CID results in both $[M^{II}(crm)_2 – H]^+$ and $[M^{II}(A)(crm) – H]+$. The resulting product ion ratio of $[M^{II}(A)(crm) – H]^+$/ $[M^{II}(crm)_2 – H]^+$ is unique for each isomer, allowing the isomers to be identified. Because the desired tetrameric complex is not easily formed and several other undesired complexes form, depleting the population of available hexose, the kinetic method requires relatively high concentrations (100s of μM to 10s of mM) of each the chiral reference, and monosaccharide. A previous application of this method to determine the relative concentration of each hexose in mixtures of D-fructose, D-glucose, and D-galactose required concentrations of 200 μM for both the sugar and reference compound and 100 μM transition metal[39].

A slightly more complicated method, the fixed ligand kinetic method, has also been used to discriminate pentose isomers and hexose isomers [17,18,40]. The chiral fixed ligand (FL) replaces the adduction of one of the chiral reference molecules used in the previously described kinetic method to form $[M^{II}(A)(crm)(FL – H)]^+$. CID results in product ions of $[M^{II}(A)(FL – H)]+$ and $[M^{II}(crm)(FL – H)]^+$ [40,41]. The fixed ligand is a molecule where deprotonation occurs solely at one site, decreasing the number of ways the $[M^{II}(A)(crm)(FL– H)]^+$ complex can form, thereby

increasing the selectivity of the analysis. The fixed ligand kinetic method requires the same high concentrations needed as the kinetic method. The fixed ligand kinetic method was applied to both identify and determine absolute configuration (D-configuration versus L-configuration) of all hexoses[17]. Two sets of fixed ligand experiments were necessary to distinguish all isomers: one using Cu^{II}/L-Serine/5'GMP and the other using Mn^{II}/L-Aspartate/L-phenylalanine-glycine (divalent cation/chiral reference/fixed ligand). Concentrations of 100 µM or higher for all reagents were necessary to form the tetrameric complexes. Because identification of monosaccharides from biological media are often sample limited, a more sensitive method is ultimately desired[42,43].

1.4. Distinguishing Carbohydrates via Water Adduction to Lithium Cationized Molecules

This dissertation focuses on developing a method to distinguish carbohydrate isomers using water adduction to the lithium cationized molecules in a quadrupole ion trap mass spectrometer [44–46]. This method does not require a derivatization step, pre- or post-ionization separations. Only the addition of a lithium salt to the analyte solution is required. It is well known that carbohydrates have a high affinity for metal cations [47–54]. For this reason the protonated sugar, $[M+H]^+$, is usually not observed in an ESI mass spectrum, and instead $[M+Na]^+$ is observed because of ambient sodium. Adding a lithium salt to the analyte solution allows lithium to adduct to monosaccharides, producing $[M+Li]^+$. In a quadrupole ion trap trace water present adducts to the lithium cationized molecules [55]. Water adducting to a lithium cationized molecule causes the mass-to-charge ratio to increase by 18 units. Two metrics of the water adduction reaction can be used to distinguish isomers. First, the rate of water adduction can be used to distinguish the different hexoses by varying the reaction time. Second, each isomer has at least one unreactive (non-water adducting) and at least one reactive (water

adducting) sites where the lithium cation will bind. This results in a mass spectrum with peaks for both $[M+Li]^+$ and $[M+Li+H_2O]^+$. The unreactive fraction of ions, measured as the ratio of $[M+Li]^+/([M+Li]^+ + [M+Li+H_2O]^+)$ after all the reactive ions have adducted water, can be used to distinguish isomers.

Different lithiation sites in a single compound are expected have potentially different reaction rates or possibly not be reactive at all. Experimental evidence along with quantum mechanical calculations using density functional theory was used to determine likely sites for the lithium cation to bind for several molecules. The relative free energies of several different lithiation sites were compared to determine which lithiation sites are the most thermodynamically favorable.

All of the molecules studied were ionized by electrospray ionization (ESI). ESI is used to easily transfer analytes dissolved in solution to the gas phase. There is a significant amount of work being done to determine if molecules retain their solution phase conformation after being transferred into the gas phase via ESI [56–58]. Therefore, it is important to determine which lithiation sites are favorable in the solution phase and which are favorable in the gas phase. Experiments and DFT calculations presented in this dissertation provide insight that solution phase structures are remain kinetically trapped after ESI, but increasing the internal energy of the kinetically trapped ions allows them to isomerize into gas phase structures.

1.5 Summary

The purpose of this chapter has been to give an introduction to distinguishing isomeric compounds with mass spectrometry and water adduction, allowing the reader to understand the experiments and results described throughout the remainder of the work. Much of the work presented in this dissertation depends on an understanding that water adduction occurs in a

quadrupole ion trap mass spectrometer. A trapping time can be added between accumulation of ions in the ion trap and before the ions are ejected from the ion trap for mass analysis (Figure 1.1). This allows for a reaction time where ions can adduct, and this reaction time can be easily changed directly in the instrument control software. After the reaction time, ions are ejected from the ion trap for mass analysis. Ions that have not adducted water are observed at the mass-to-charge ratio where the reaction time can be easily controlled, and the amounts of reactant and product from the reaction can be easily measured. Thus, information detailing this reaction have been the focus of a majority of **Chapter 1**.

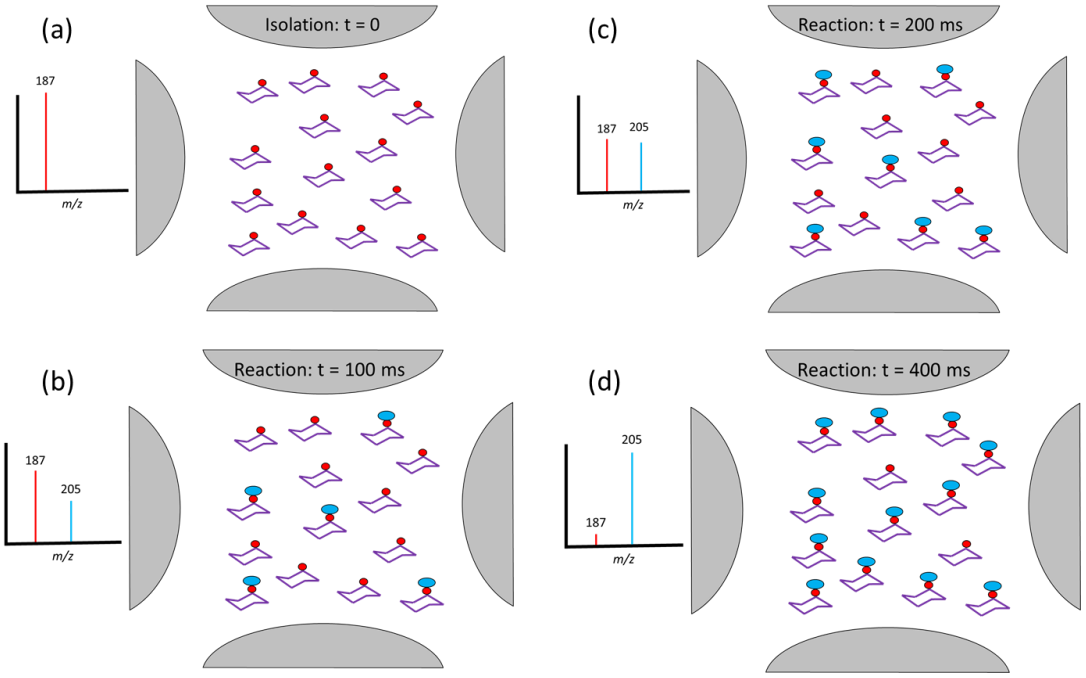

Figure 1.1. A schematic of the water adduction reaction in a quadrupole ion trap for a lithium cationized hexose, where the lithium cation is shown as a red circle and the hexose as purple chair. (a) shows an expected mass spectrum immediately after isolation, and (b – d) shows how the mass spectrum would change as the reaction time (delay time) increases. Water (blue oval) adducts to the lithium cationized hexoses, and the mass-to-charge shifts 18 units.

The experimental methods used in the subsequent chapters are provided in **Chapter 2**. Details about the reagents used are included. The instrumentation used is also covered, including information about the electrospray ionization source, the ion optics used to transfer ions from atmosphere to the high vacuum of the mass spectrometer, and the quadrupole ion trap. Methods for measuring the rate of water adduction and the unreactive fraction are given in detail.

The work presented in **Chapter 3** describes the application of the water adduction reaction to distinguish an exhaustive list of D-pentoses and biologically relevant hexoses,

hexosamines, and N-acetyl hexoses individually. The average reaction rate and unreactive fraction are reported for each monosaccharide, along with the standard deviation of the measurement.

Chapter 4 goes into details explaining the chemistry responsible for the unreactive fraction. Developing an understanding of the water adduction reaction is achieved through a combination of experiments and density functional theory calculations. The calculations are used to optimize the $[M+Li]^+$ and $[M+Li+H_2O]^+$ structures. Because the monosaccharide isomers have several different hydroxyl oxygens to which the lithium cation can coordinate, several different unique structures for $[M+Li]^+$ were optimized. The relative free energy of these ions can then be compared, determining which sites for lithiation are most thermodynamically favorable. The energetics of the water adduction can then be compared, and the number of oxygen atoms coordinated to the lithium cation can be used to predict the unreactive fraction of a molecule (Figure 1.2).

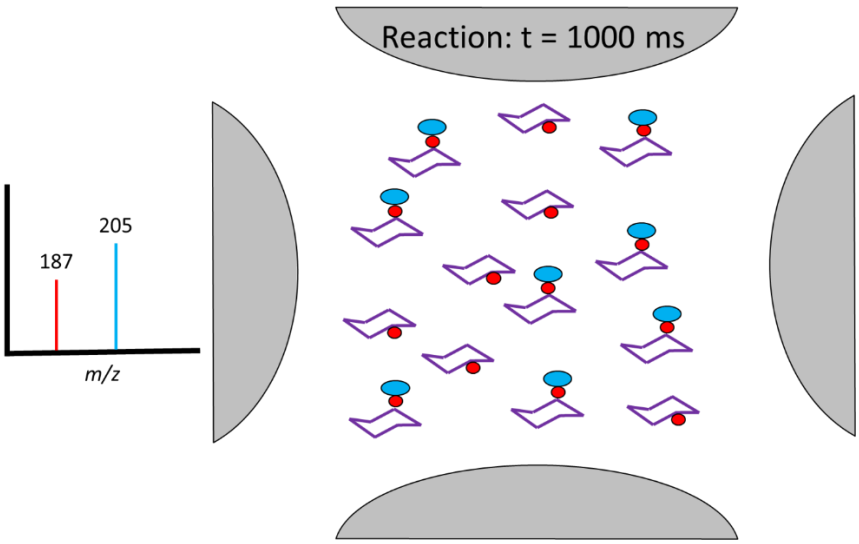

Figure 1.2. The unreactive fraction is measured after 1000 ms. After this time, all the reactive species (with the lithium cation coordinated to the top of the hexose) have adducted water, and all the unreactive species (with the lithium cation coordinated to the bottom of the hexose) still have not adducted water.

The water adduction method is used to distinguish ten different glucose-glucose disaccharides in **Chapter 5**. The ten disaccharides differ in both position and anomericity of the glycosidic linkage. The reaction rate and unreactive fraction can be used together to distinguish all ten different linkages, including those from both reducing and non-reducing disaccharides. This method is further extended to disaccharides containing monosaccharide subunits other than glucose. Sucrose (glucose-fructose), lactose (galactose-glucose), and lactulose (galactose-fructose) were distinguished from each other and the other 10 disaccharides previously mentioned using water adduction. This method is applied to various applications such as analysis of disaccharides in food, biological samples, and the vaping liquid used in an electronic cigarette.

Chapter 6 uses the information learned from experiments discussed in the previous chapters and applies it to distinguishing binary mixtures of monosaccharides and mixtures of disaccharides. The relative concentration of fructose is measured in samples of high-fructose

corn syrup based on a calibration curve of the reaction rate versus percent fructose or unreactive fraction versus percent fructose. This same method is then used to determine the anomeric ratio of glucose in water. Mixtures of disaccharides are also analyzed. Collision induced dissociation of disaccharides results in product ions that are unique for each linkage position but not the anomericity of the linkage. Water adduction to the fragment ions formed during CID allows for mixtures of disaccharides that have unique product ions to be distinguished in a mixture.

Chapter 7, the final chapter, provides a summary of the results of each chapter presented and considers potential future directions related to this work.

REFERENCES

1 G. Li, Z. Huang, C. Fu, P. Xu, Y. Liuaand and Y. Zhao, L-valine assisted distinction between the stereo-isomers of D-hexoses by positive ion ESI tandem mass spectrometry, *J. Mass Spectrom.*, 2010, **45**, 643–650.

2 S. J. Park, J. C. Gildersleeve, O. Blixt and I. Shin, Carbohydrate microarrays, *Chem. Soc. Rev.*, 2013, **42**, 4310.

3 T. M. Gloster and D. J. Vocadlo, Developing inhibitors of glycan processing enzymes as tools for enabling glycobiology, *Nat. Chem. Biol.*, 2012, **8**, 683.

4 V. K. Tiwari, R. C. Mishra, A. Sharma and R. P. Tripathi, Carbohydrate based Potential Chemotherapeutic Agents: Recent Developments and their Scope in Future Drug Discovery, *Mini-Rev. Med. Chem.*, 2012, **12**, 1497.

5 J. Pazourek, Monitoring of mutarotation of monosaccharides by hydrophilic interaction chromatography, *J. Sep. Sci.*, 2010, **33**, 974–981.

6 D. L. Nelson and M. M. Cox, in *Principles of Biochemistry*, W. H. Freeman and Company, New York, 2013, vol. 6, pp. 235–260.

7 S. P. Gaucher and J. A. Leary, Stereochemical Differentiation of Mannose, Glucose, Galactose, and Talose Using Zinc(II) Diethylenetriamine and ESI-Ion Trap Mass Spectrometry, *Anal. Chem.*, 1998, **70**, 3009–3014.

8 M. Remko, P. T. Van Duijnen and R. Broer, Effect of metal ions (Li+, Na+, K+,Mg+ and Ca2+) and water on the conformational changes of glycosidic bonds in heparin oligosaccharides, *RSC Adv.*, 2013, **3**, 9843–9853.

9 V. N. Reinhold, B. B. Reinhold and C. E. Costello, Carbohydrate Molecular Weight Profiling, Sequence, Linkage, and Branching Data: ES-MS and CID, *Anal. Chem.*, 1995, **67**, 1772–1784.

10 K. E. Mutenda and R. Matthiesen, in *Mass Spectrometry Data Analysis in Proteomics*, ed. R. Matthiesen, Humana Press, Totowa, 2007, vol. 1, p. 289.

11 J. Ø. Duus, C. H. Gotfredsen and K. Bock, Carbohydrate Structural Determination by NMR Spectroscopy: Modern Methods and Limitations †, *Chem. Rev.*, 2000, **100**, 4589–4614.

12 S. E. Stefan and J. R. Eyler, Differentiation of glucose-containing disaccharides by infrared multiple photon dissociation with a tunable CO2 laser and Fourier transform ion cyclotron resonance mass spectrometry, *Int. J. Mass Spectrom.*, 2010, **297**, 96–101.

13 T. T. Fang and B. Bendiak, The Stereochemical Dependence of Unimolecular

Dissociation of Monosaccharide-Glycolaldehyde Anions in the Gas Phase: A Basis for Assignment of the Stereochemistry and Anomeric Configuration of Monosaccharides in Oligosaccharides by Mass Spectrometry via a, *J. Am. Chem. Soc.*, 2007, **129**, 9721–9736.

14 Y.-H. Wang, B. Avula, X. Fu, M. Wang and I. A. Khan, Simultaneous Determination of the Absolute Configuration of Twelve Monosaccharide Enantiomers from Natural Products in a Single Ijection by a UPLC-UV/MS Method, *Planta Med*, 2012, **78**, 834–837.

15 J. F. Lopes and E. M. S. M. Gaspar, Simultaneous chromatographic separation of enantiomers, anomers, and structural isomers of some biologically relelvant monosaccharides, *J. Chromatogr. A*, 2008, **1188**, 34–42.

16 M. Akabane, A. Yamamoto, S. Aizawa, A. Taga and S. Kodama, Simultaneous Enantioseparation of Monosaccharides Derivatized with L-Tryptophan by Reversed Phase HPLC, *J Soc Anal Chem*, 2014, **30**, 739–743.

17 G. Nagy and N. L. B. Pohl, Complete Hexose Isomer Identifcation with Mass Spectrometry, *J Am Soc Mass Spectrom*, 2015, **26**, 677–685.

18 G. Nagy and N. L. B. Pohl, Monosaccharide Identifcation as a First Step toward de Novo Carbohydrate sequencing: Mass Spectrometry Strategy for the Identifcation and Differentiation of Diastereomic and Enantiomeric Pentose Isomers, *Anal Chem*, 2015, **87**, 4566–4571.

19 A. A. Shvartsburg and R. D. Smith, Fundamentals of Traveling Wave Ion Mobility Spectrometry, *Anal. Chem.*, 2008, **80**, 9689–9699.

20 B. G. Santiago, R. A. Harris, S. L. Isenberg, M. E. Ridgeway, A. L. Pilo, D. A. Kaplan and G. L. Glish, Improved Differential Ion Mobility Separations Using Linked Scans of Carrier Gas Composition and Compensation Field, *J. Am. Soc. Mass Spectrom.*, 2015, **26**, 1746–1753.

21 R. A. Sowell, S. L. Koeniger, S. J. Valentine, M. H. Moon and D. E. Clemmer, Nanoflow LC/IMS-MS and LC/IMS-CID/MS of Protein Mixtures, *J. Amer. Soc. Mass Spectrom.*, 2004, **15**, 1341–1353.

22 M. M. Gaye, G. Nagy, D. E. Clemmer and N. L. B. Pohl, Multidimensional Analysis of 16 Glucose Isomers by Ion Mobility Spectrometry, *Anal. Chem.*, 2016, **88**, 2335–2344.

23 G. E. Hofmeister, Z. Zhou and L. J.A., Linkage position determination in lithium-cationized disaccharides: Tandem mass spectrometry and semiempirical calculations, *J. Am. Chem. Soc.*, 1991, **113**, 5964–5970.

24 M. R. Asam and G. L. Glish, Tandem mass spectrometry of alkali cationized polysaccharides in a quadrupole ion trap, *J. Am. Soc. Mass Spectrom.*, 1997, **8**, 987–995.

25 M. D. Leavell, S. P. Gaucher and J. A. Leary, Conformational Studies of Zn-Ligand-Hexose Diastereomers Using Ion Mobility Measurements and Density Functional Theory Calculations, *J. Am. Soc. Mass Spec.*, 2002, **13**, 284–293.

26 Á. Kuki, L. Nagy, K. E. Szabó, B. Antal, M. Zsuga and S. Kéki, Activation Energies of Fragmentations of Disaccharides by Tandem Mass Spectrometry, *J. Am. Soc. Mass Spectrom.*, 2014, **25**, 439–443.

27 T. T. Fang, J. Zirrolli and B. Bendiak, Differentiation of the anomeric configuration and ring form of glucosyl-glycolaldehyde anions in the gas phase by mass spectrometry: isomeric discrimination between m/z 221 anions derived from disaccharides and chemical synthesis of m/z 221 standards, *Carbohydr. Res.*, 2007, **342**, 217–235.

28 H. Yang, L. Shi, W. Yao, Y. Wang, L. Huang, D. Wan and S. Liu, Differentiation of Disaccharide Isomers by Temperature-Dependent In-Source Decay (TDISD) and DART-Q-TOF MS/MS, *J. Am. Soc. Mass Spectrom.*, 2015, **26**, 1599–1605.

29 H. Yuan, L. Liu, J. Gu, Y. Liu, M. Fang and Y. Zhao, Distinguishing isomeric aldohexose-ketohexose disaccharides by electrospray ionization mass spectrometry in positive mode, *Rapid Commun. Mass Spectrom.*, 2015, **29**, 2167–2174.

30 D. Wan, H. Yang, C. Yan, F. Song, Z. Liu and S. Liu, Differentiation of glucose-containing disaccharides isomers by fragmentation of the deprotonated non-covalent dimers using negative electrospray ionization tandem mass spectrometry, *Talanta*, 2013, **115**, 870–875.

31 A. El Firdoussi, M. Lafitte, J. Tortajada, O. Kone and J.-Y. Salpin, Characterization of the glycosidic linkage of underivatized disaccharides by interaction with Pb2 ions, *J. mass Spectrom.*, 2007, **42**, 999; 999-1011; 1011.

32 J. Simoes, P. Domingues, A. Reis, F. M. Nunes, M. A. Coimbra and M. R. M. Domingues, Indentification of Anomeric Configuration of Underivatized Reducing Glucopyranosyl-glucose Disaccharides by Tandem Mass Spectrometry and Multivariate Analysis, *Anal. Chem.*, 2007, **79**, 5896–5905.

33 H. Zhang, S. M. Brokman, N. Fang, N. L. Pohl and E. S. Yeung, Linkage position and residue identification of disaccharides by tandem mass spectrometry and linear discriminant analysis, *Rapid Commun. Mass Spectrom.*, 2008, **22**, 1579–1586.

34 Y. Tan and N. C. Polfer, Linkage and Anomeric Differentiation in Trisaccharides by Sequential Fragmentation and Variable-Wavelength Infrared Photodissociation, *J. Am. Soc. Mass Spectrom.*, 2015, **26**, 359–368.

35 C. J. Gray, B. Schindler, L. G. Migas, M. Pičmanová, A. R. Allouche, A. P. Green, S. Mandal, M. S. Motawia, R. Sánchez-Pérez, N. Bjarnholt, B. L. Møller, A. M. Rijs, P. E.

Barran, I. Compagnon, C. E. Eyers and S. L. Flitsch, Bottom-Up Elucidation of Glycosidic Bond Stereochemistry, *Anal. Chem.*, 2017, **89**, 4540–4549.

36 K. P. Madhusudanan, Tandem mass spectra of ammonium adducts of monosaccharides: Differentiation of diastereomers, *J. Mass Spectrom.*, 2006, **41**, 1096–1104.

37 X. Zhu and T. Sato, The distinction of underivatized monosaccharides using electrospray ionization ion trap mass spectrometry, *Rapid Comm. Mass Spectrom.*, 2007, **21**, 191–198.

38 L. Wu, W. A. Tao and R. G. Cooks, Kinetic method for the simultaneous chiral analysis of different amino acids in mixtures, *J. Mass Spectrom.*, 2003, **38**, 386–393.

39 T. Fouquet and L. Charles, Distinction and Quantitation of Sugar Isomers in Ternary Mixtures Using the Kinetic Method, *J. Am. Soc. Mass Spectrom.*, 2010, **21**, 60–67.

40 L. Wu and R. G. Cooks, Chiral Analysis Using the Kinetic Method with Optimized Fixed Ligands: Applications to Some Antibiotics, *Anal. Chem.*, 2003, **75**, 678–684.

41 L. Wu and R. G. Cooks, Chiral and isomeric analysis by electrospray ionization and sonic spray ionization using the fixed-ligand kinetic method., *Anal. Chem.*, 2005, **11**, 678–684.

42 M. Wuhrer, Glycomics using mass spectrometry, *Glycoconj J*, 2013, **30**, 11–22.

43 A. Dell and H. R. Morris, Glycoprotein Structure Determination by Mass Spectrometry, *Science (80-.).*, 2001, **291**, 2351–2356.

44 M. T. Campbell, D. Chen and G. L. Glish, Distinguishing Linkage Position and Anomeric Configuration of Glucose–Glucose Disaccharides by Water Adduction to Lithiated Molecules, *Anal. Chem.*, 2018, acs.analchem.7b04162.

45 M. T. Campbell, D. Chen and G. L. Glish, Identifying the D-Pentoses Using Water Adduction to Lithium Cationized Molecule, *J. Am. Soc. Mass Spectrom.*, 2017, **28**, 1420–1424.

46 M. T. Campbell and G. L. Glish, Fragmentation in the ion transfer optics after differential ion mobility spectrometry produces multiple artifact monomer peaks, *Int. J. Mass Spectrom.*, 2018, **425**, 47–54.

47 D. Toczek, K. Kubas, M. Turek, S. Roszak and R. Gancarz, Theorectical studies of structure, energetics and properties of Ca2+ complexes with alizarin glucoside, *J Mol Model*, 2013, **19**, 4209–4214.

48 J.-Y. Salpin and J. Tortajada, Gas-Phase Reactivity of Lead(II) Ions with D-Glucose. Combined Eelctrospray Ionization Mass Spectrometry and Theoretical Study, *J. Phys. Chem. A*, 2003, **107**, 2943–2953.

49 B. a. Cerda and C. Wesdemiotis, Thermochemistry and structures of Na+ coordinated

mono- and disaccharide stereoisomers, *Int. J. Mass Spectrom.*, 1999, **189**, 189–204.

50 C. H. S. Wong, F. M. Siu, N. L. Ma and C. W. Tsang, Interaction of Ca2+ with mannose: a density functional study, *Theochem*, 2001, **536**, 227–234.

51 S. Karamat and W. F. Fabian, Interaction of Methyl ß-D-Xylopyranoside with Metal Ions: Density Functional Theory Study of Cationic and Neutral Bridging and Pendant Complexes, *J. Phys. Chem. A*, 2008, **112**, 1823–1831.

52 L. Yang, Y. Su, Y. Xu, Z. Wang, Z. Gua, S. Weng, C. Yan, S. Zhang and J. Wu, Interactions between Metal Ions and Carbohydrates. Coordination Behavior of Neutral Erythritol to Ca(II) and Lanthanide Ions, *Inorg. Chem.*, 2003, **42**, 5844–5856.

53 B. Gyurcsik and L. Nagy, Carbohydrates as Ligands: Coordination Equilibria and Structure of Metal Complexes, *Coord. Chem.Rev.*, 2000, **203**, 81–149.

54 M. T. Cancilla, S. P. Gaucher, H. Desaire and J. A. Leary, Combined Partial Acid Hydrolysis and Electrospray Ionization-Mass Spectrometry for the Structural Determination of Oligosaccharides, *Anal. Chem.*, 2000, **72**, 2901–2907.

55 O. Hernandez, S. Isenberg, V. Steinmetz, G. L. Glish and P. Maitre, Probing Mobility-Selected Saccharide Isomers: Selective Ion–Molecule Reactions and Wavelength-Specific IR Activation, *J. Phys. Chem. A*, 2015, **119**, 6057–6064.

56 R. G. McAllister, H. Metwally, Y. Sun and L. Konermann, Release of Native-like Gaseous Proteins from Electrospray Droplets via the Charged Residue Mechanism: Insights from Molecular Dynamics Simulations, *J. Am. Chem. Soc.*, 2015, **137**, 12667–12676.

57 L. Konermann, E. Ahadi, A. D. Rodriguez and S. Vahidi, Unraveling the mechanism of electrospray ionization, *Anal. Chem.*, 2013, **85**, 2–9.

58 E. Ahadi and L. Konermann, Surface charge of electrosprayed water nanodroplets: A molecular dynamics study, *J. Am. Chem. Soc.*, 2010, **132**, 11270–11277.

CHAPTER 2: EXPERIMENTAL

2.1 Materials

Methanol (optima grade), water (optima grade), and lactulose were purchased from Fisher Scientific (Fairlawn, NJ, USA). D-Glucose, α-D-glucose, D-galactose, D-fructose, D-mannose, D-ribose, D-glucose-$^{13}C_6$, maltose, lactose, cellobiose, maltotriose, isomaltotriose, palitunose, deuterium oxide, sorbitol, mannitol, 1,2-propandiol, 1,3-propandiol, 1,2,3-propantriol, and lithium acetate were purchased from Sigma Aldrich (St. Louis, MO, USA). D-talose, L-glucose, L-galactose, L-mannose, D-arabinose, D-xylose, D-ribulose, D-ribulose, isomaltose, nigerose, laminarbiose, sophorose, kojibiose, gentibiose, trehalose, isotrehalose, levoglucosan, 2-deoxyglucose, 1,5-anhydrosorbitol, α-methyl glucoside, and ß-methyl glucoside were purchased from Carbosynth (Berkshire, UK). Samples of high fructose corn syrup were gifted from Sweeteners Plus (Lakeville, NY, USA).

All samples were prepared to a total analyte concentration of 10 µM unless otherwise stated. Solutions were either prepared in 50/50 methanol/water (v/v) or were completely aqueous. Beer (Yuengling, from Pottsville, PA, USA) was analyzed after diluting by a factor of 1,000 in 50:50 methanol:water and used without further purification. Dried shiitake mushrooms (Red Bunny Farms) were ground up using mortar and pestle. Approximately 1 g of ground mushroom was added to a 2-mL Eppendorf tube along with 1 mL of water. The sample was centrifuged for 5 minutes using an Eppendorf 5414 Microcentrifuge at 15,600G. The resulting supernatant was diluted by a factor of 2,000 in 50:50 methanol:water and analyzed without further purification. A vaping liquid, menthol tobacco, was acquired from Vapor Girl (Chapel

Hill, NC) and diluted by a factor of ~2,000 in 50:50 methanol:water and analyzed without further purification[1].

All samples were analyzed on either an HCTUltra quadrupole ion trap mass spectrometer or an Esquire quadrupole ion trap mass spectrometer. The schematic of the HCTUltra is illustrated in Figure 2.1. Ions are generated from the ESI emitter, and nebulization of the spray is aided by a coaxial nitrogen gas at 10 psi. Desolvation of the nebulized droplets is aided by a heated nitrogen desolvation gas (typically heated to 300°C) that is passed coaxially over the glass inlet capillary. The entrance and exit of the glass capillary has a metal coat so that a potential can be applied. The electrospray emitter is held at ground potential, while the entrance to the inlet capillary is held at -5,000 V (for positive mode ESI) unless otherwise mentioned. Ions pass through the glass capillary into the first differentially pumped region of the mass spectrometer. A voltage is applied to the end of the glass capillary, and a more negative voltage is applied to the skimmer, which is used to block neutrals from the high vacuum region of the mass spectrometer. The voltage difference between the exit of the glass inlet capillary and the skimmer is referred to as the capillary/exit offset voltage. Increasing this voltage can be used to increase the internal energy of the ions once they are in the gas phase. The most significant difference between the Esquire and the HCTUltra is the ion optics used to transfer ions from atmosphere to the high vacuum. The HCTUltra has two lenses used to guide ions into the quadrupole ion trap, while the Esquire only has one. Both instruments have two octopoles, which are also used to focus ions to the center of the instrument. The quadrupole ion trap acts as the mass analyzer, and an electron multiplier serves as the detector. Signal intensities were measured by summing the peak area (± 0.5 m/z) from the centroid of the peak measured as the average of

approximately 50 MS scans. All data presented are the calculated averages and standard deviations of these intensities based on three replicate samples[1–3].

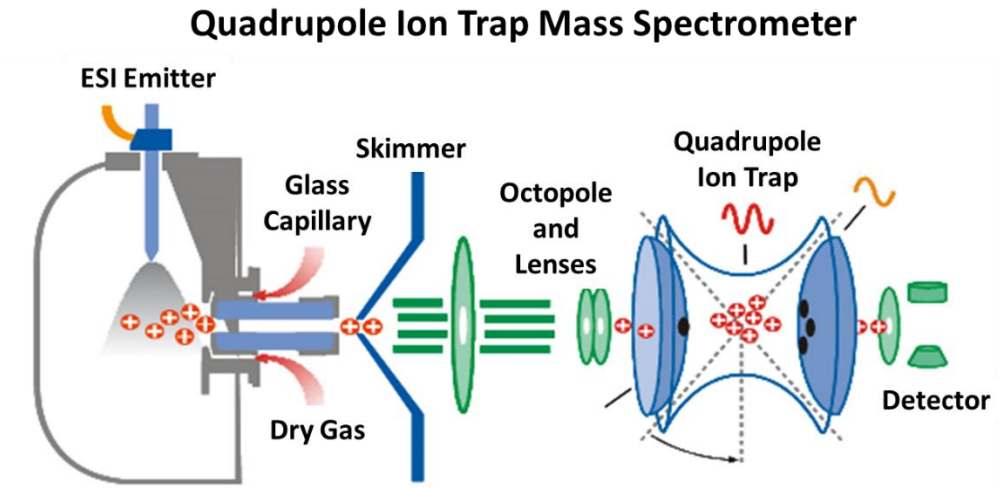

Figure 2.1. A schematic of the HCTUltra.

Mixtures of glucose and fructose as well as samples of high-fructose corn syrup were analyzed by GC-MS. BSTFA:TMCS (99:1) and pyridine were purchased from Sigma Aldrich and used without further purification. Solutions of glucose, fructose, and high fructose corn syrup were trimethylsilanated by dissolving them in pyridine and adding BSTFA:TMCS (99:1) in 100-fold excess. The solutions were allowed to react at room temperature for at least 15 minutes before injection into a Bruker EVOQ 456 GC-TQ. A DB5-MS capillary column (30 m x 0.25 mm I.D. and film thickness of 0.25µm, Agilent, Palo Alto, CA, USA) was used with helium (Airgas, 99.999% purity) as the carrier gas at a constant linear velocity of 30 cm/s. The injector and MS source temperatures were maintained at 270°C and 200°C, respectively. The column temperature program consisted of injection at 90°C and hold for 1 minute, temperature increase of 20°C/min to 250°C, followed by an isothermal hold at 250°C for 5 minutes. The MS was operated in electron ionization mode with an ionization energy of 70 eV. The scan range was set

from 60 to 500 Da at 2.0 scan/s. The samples were analyzed in splitless mode. Multiple peaks were observed for both glucose and fructose, and relative quantitation was performed by summing the total peak area measured under each of the multiple peaks of the TIC[1].

2.2. Controlling Water Adduction

The water adduction reaction occurs in the quadrupole ion trap mass spectrometer (QIT-MS). Ions generated from ESI are allowed to accumulate in the trap for 1 – 200 ms depending on the number of ions generated from the sample during electrospray. After accumulation $[M+Li]^+$ is isolated in the QIT, serving as t = 0 for the water adduction reaction. A delay time can be added in the instrument software after ion accumulation but before detection. The delay time allows the reaction time to be easily controlled with the instrument software. The total reaction time is the sum of the delay time and the time required to scan the ions from the QIT, typically 3 to 15 ms, depending on scan speed of the mass spectrometer (13,000 *m/z* per second for the Esquire and 26,000 *m/z* per second for the HCTUltra) and the mass range scanned.

The proportion of unreactive species, R_U, was determined by measuring the ratio of the signal intensities $[M+Li]^+/([M+Li]^+ + [M+Li+H_2O]^+)$ after a reaction time of 1000 ms. The rate of water adduction was determined for each hexose by measuring the intensity of the lithiated hexose and the intensity of the water adducted species after delay times of 0, 10, 20, 30, 40, and 50 ms. Because the concentration of water in the QIT-MS is significantly greater than the concentration of ions, pseudo-first order kinetics can be assumed. The signal intensity for $[M+Li]^+ + [M+Li+H_2O]^+$ approximates the amount of $[M+Li]^+$ initially present immediately after isolation (assuming negligible ion losses during the trapping time). The exact concentration of the water in the quadrupole ion trap is unknown. Therefore, the calculated rate will be a function of the rate constant times the unknown concentration of water in the quadrupole ion

trap, herein referred to as k´. The concentration is not expected to vary greatly with time, and this is confirmed by the measured reaction rates remaining constant over periods of several months[2].

Only the reactive portion of $[M+Li]^+$ should be used in determining the rate constant, and therefore, the unreactive fraction must be subtracted from the total when determining k´. Equation 1 was used to find the proportion of reactive species remaining at given delay time, R_R, for the determination of the corrected reaction rate.

$$R_R = \frac{(1-R_U)(I_{187}+I_{205})-I_{205}}{(1-R_U)(I_{187}+I_{205})} \qquad \textbf{Eq. 2.1}$$

Plotting $\ln(R_R)$ vs. time yields a linear trend as expected, and provides the true reaction rate (i.e. the rate constant times the concentration of water in the QIT-MS). Using R_R is preferred to simply using the signal intensity of $[M+Li]^+$ because the ratio is unaffected by fluctuations in absolute signal intensity from multiple MS scans.

2.3. Methods Used for Computations

Density functional theory calculations performed with the Gaussian 09 program[4] were used to determine likely lithium cation binding sites and the relative energy for each unique structure. Additionally, the change in Gibb's Free Energy of water adduction ($\Delta G_{\text{Water Adduction}}$) was measured for each unique structure.

The lowest energy structures for gas phase structures of the alpha and beta anomers for D-glucose, D-galactose, D-mannose, and D-talose were previously determined by molecular dynamics or simulated annealing. The structure with the lowest energy (global minimum) was reproduced for each anomer studied, and the energies matched (within 0.01%) at the B3LYP/6-311++G(d,p) level of theory. Each optimized anomer was lithiated systemically by adding a single lithium cation to each of four locations around all oxygen atoms. These four locations were the vertices of an imaginary tetrahedron such that the lithium was always 1.4 Å from the

targeted oxygen, the typical bond distance after optimization. Adding a single lithium cation in four locations around each of six oxygens results in 24 unique structures. The structures were optimized using B3LYP at the 3-21G level of theory using the conductor-like polarizable continuum (cpcm) implicit solvation model[5,6] with water as a solvent. The resulting optimized structures are again optimized and vibrational calculations are performed with B3LYP functional at the 6-311++G(d,p) level of theory while the lithiated molecule is still solvated, still using the implicit solvation model.

The structures previously optimized at the 6-311++G(d,p) level of theory were again optimized at the 6-311++G(d,p) level of theory in vacuum to make the computational modelling process as similar as possible to the electrospray process, where ions are transferred from solution phase to gas phase. This allows the energies for lithiation to be compared in both the aqueous phase as well as the gas phase. After optimization of $[M+Li]^+$ in the gas phases, a single water molecule is then added to each optimized gas phase structure, and each structure is then optimized at the 3-21G level of theory before a subsequent optimization and subsequent vibrational calculations were performed at the 6-311++G(d,p) level of theory. Additionally, all structures previously described (solvated and in vacuum) also had vibrational calculations performed at the M06-2X/cc-pTZV level of theory. The M06-2X functional[7] was previously shown to provide more accurate vibrational calculations compared to the B3LYP functional[8,9], and values calculated with each functional are compared below. Vibrational calculations were also performed at the MP2/6-311++G(d,p) level of theory for several structures to ensure maximum accuracy.

REFERENCES

1 M. T. Campbell, D. Chen, N. J. Wallbillich and G. L. Glish, Distinguishing Biologically Relevant Hexoses by Water Adduction to the Lithium Cationized Molecule, Anal. Chem., 2017, acs.analchem.7b02647.

2 M. T. Campbell, D. Chen and G. L. Glish, Identifying the D-Pentoses Using Water Adduction to Lithium Cationized Molecule, J. Am. Soc. Mass Spectrom., 2017, 28, 1420–1424.

3 M. T. Campbell, D. Chen and G. L. Glish, Distinguishing Linkage Position and Anomeric Configuration of Glucose–Glucose Disaccharides by Water Adduction to Lithiated Molecules, Anal. Chem., 2018, acs.analchem.7b04162.

4 M. J. Frisch, G. W. Trucks, H. B. Schlegel, G. E. Scuseria, M. A. Robb, J. R. Cheeseman, G. Scalmani, V. Barone, B. Mennucci and G. A. Petersson, Gaussian 09, Revision D. 01; Gaussian: Wallingford, CT, USA, 2009, There is no Corresp. Rec. this Ref.

5 Y. Takano and K. N. Houk, Benchmarking the Conductor-like Polarizable Continuum Model (CPCM) for Aqueous Solvation Free Energies of Neutral and Ionic Organic Molecules, J. Chem. Theory Comput., 2005, 1, 70–77.

6 B. Mennucci, J. Tomasi, R. Cammi, J. R. Cheeseman, M. J. Frisch, F. J. Devlin, S. Gabriel and P. J. Stephens, Polarizable continuum model (PCM) calculations of solvent effects on optical rotations of chiral molecules, J. Phys. Chem. A, 2002, 106, 6102–6113.

7 Y. Zhao and D. G. Truhlar, The M06 suite of density functionals for main group thermochemistry, thermochemical kinetics, noncovalent interactions, excited states, and transition elements: Two new functionals and systematic testing of four M06-class functionals and 12 other function, Theor. Chem. Acc., 2008, 120, 215–241.

8 G. I. Csonka, A. D. French, G. P. Johnson and C. a Stortz, Evaluation of Density Functionals and Basis Sets for Carbohydrates, J. Chem. Theory Comput., 2009, 5, 679–692.

9 W. M. C. Sameera and D. A. Pantazis, A Hierarchy of Methods for the Energetically Accurate Modeling of Isomerism in Monosaccharides, J. Chem. Theory Comput., 2012, 8, 2630–2645.

CHAPTER 3: DISTINGUISHING MONOSACCHRIDES WITH WATER ADDUCTION: HEXOSES, PENTOSES, HEXOSAMINES, AND N-ACEYTL HEXOSAMINES

3.1 Electrospray Ionization of Carbohydrates and Analysis of Hexose Isomers

Electrospray ionization of a solution containing monosaccharides results in metal cationized molecules such as $[M+Na]^+$. Adding other metal salts to solution prior to electrospray will produce different metal adducts. Metals besides sodium are commonly used to explore different fragmentation chemistries for disaccharides and larger carbohydrates[1,2].

ESI of a solution containing a hexose and a lithium salt produces $[M+Li]^+$ at *m/z* 187. The signal intensity of the sodium cationized hexose (*m/z* 203) is less than 5% the relative intensity of the *m/z* 187 peak when using concentrations of 100 µM lithium acetate. Four biologically relevant hexoses including glucose, galactose, mannose, and fructose were studied. No differences in MS/MS spectra after collision induced dissociation (CID) of the lithium cationized molecules of each hexose isomer shown Figure 3.1. While there are no significant differences in the CID spectra, the formation of an unusual ion (*m/z* 205) in the MS/MS spectrum is observed: the addition of water to the parent ion (Figure 3.2). This is not a product ion resulting from dissociation, but instead it is the result of an ion-molecule reaction in the 11.3 ms after CID but before ejection of *m/z* 187.

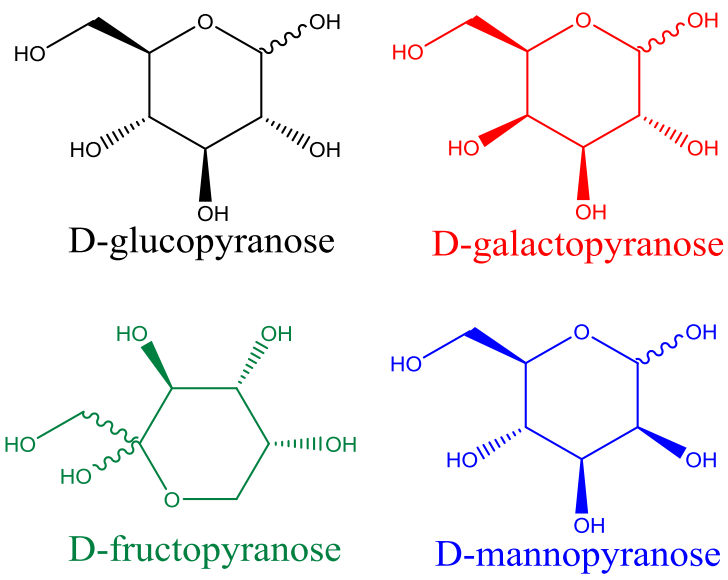

Figure 3.1: The hexoses studied in this chapter showed in their pyranose conformation

The water adduction reaction was studied for each of the hexose isomers individually. Plotting the ratio signal intensity of hexose that has not yet reacted (I_{187}) to the total hexose that has and has not adducted water (I_{205} + I_{187}) versus the delay time results in an exponential decay (Figure 3.3). The decay curves all asymptote before all the lithium cationized hexose has reacted. This is caused by some fraction of the lithium cationized molecules being unreactive for each hexose. The ratio of unreacted lithium cationized hexose to total hexose $\frac{I_{187}}{I_{187}+I_{205}}$ (i.e. the unreactive fraction of the lithiated adduct) was measured after a reaction time of 1011.3 ms. The unreactive fraction was found to be unique for each of the isomers studied and can be used to distinguish the biologically relevant hexoses (Table 3.1).

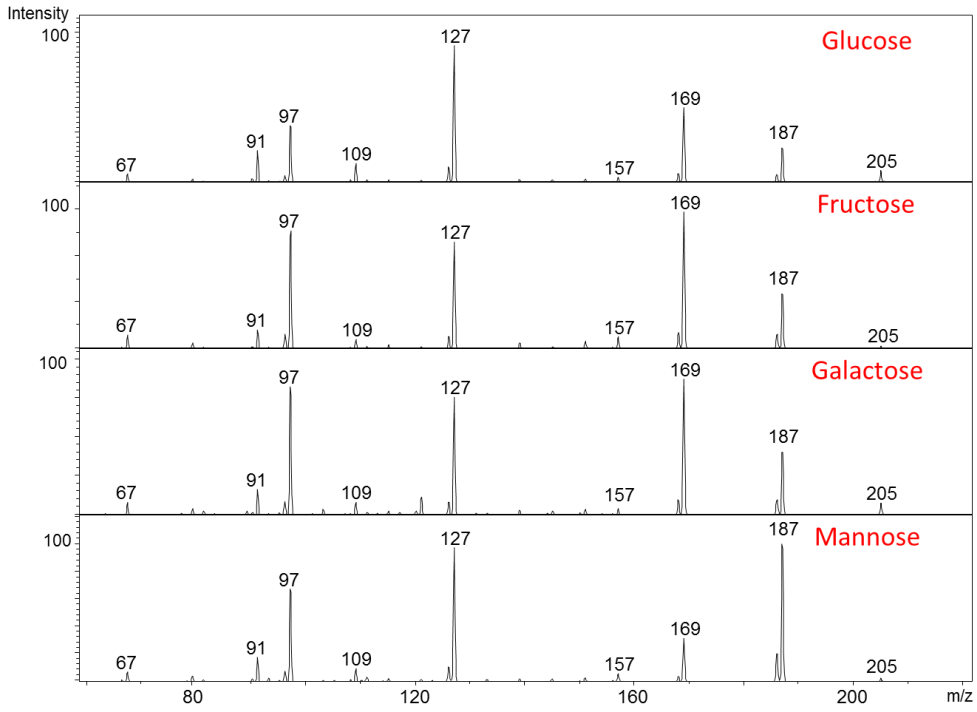

Figure 3.2. MS/MS spectra for the four hexoses studied. The ion observed at *m/z* 205 is caused by water adduction to the $[M+Li]^+$ parent ion at *m/z* 187. Possible differences in the product ion ratios are a result of water adduction to the product ions themselves.

It is well known that metal cations typically form multi-dentate interactions with hexoses [35, 37, 41]. The reactivity for a given lithium cationized hexose conformation is expected to depend on the number of oxygen atoms to which the lithium cation is coordinated. Experimental measurements made by CID with guided ion beam mass spectrometry of $Li+(H_2O)_n$ (where n = 1 – 6) suggest that four waters bind to lithium in the first hydration shell[3]. As each water molecule is dissociated from the complex, the subsequent bond dissociation enthalpy increases. Therefore, the bond energy for each subsequent water binding to the lithium cation will be smaller than the previous hydration. A greater number of coordinations to the lithium from oxygen atoms in the hexose (such as a tridentate or tetradentate structure compared to a bidentate structure) will cause

a hydration to the lithium cation in the ion trap to become less energetically favorable. Therefore, the fraction of ions that are reactive will depend on the number of the oxygen atoms coordinated to the lithium cation. More information about this topic can be found in Chapter 5.

Using the reaction rate for the water adduction reaction provides a second metric for distinguishing hexoses. The rate of water adduction was determined for each hexose by first measuring the signal intensity of the lithium cationized hexose and the signal intensity of the water adducted species at reaction times of 11.3, 21.3, 31.3, 41.3, 51.3, and 61.3 ms. Because the number density of water in the quadrupole ion trap is significantly greater than the number density of ions, pseudo-first order kinetics can be assumed (Equation 2.1). $I_{187} + I_{205}$ is used to approximate the amount of $[M+Li]^+$ initially present immediately after isolation (assuming negligible ion losses during the trapping time). The concentration of the water in the quadrupole ion trap is unknown. Therefore, the calculated rate will be a function of the rate constant times the unknown concentration of water in the quadrupole ion trap, herein referred to as k'. The concentration is not expected to vary greatly with time, and this is confirmed by the measured reaction rates remaining constant over periods of several months.

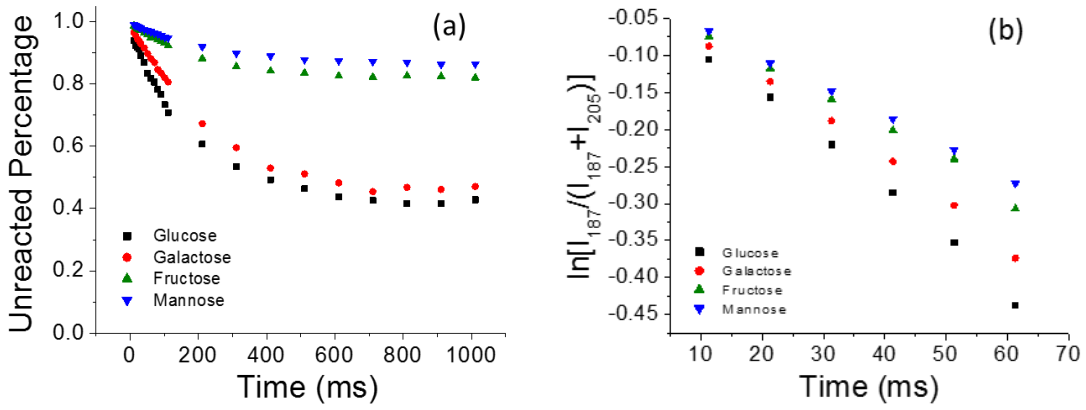

Figure 3.3. (a) Decay curves for all four hexoses studied, and (b) the linear plots are observed when plotting natural log of signal intensity versus time

As discussed previously, each decay curve in Figure 3.3 (a) asymptotes before all of the lithiated hexose reacts. When calculating the reaction rate, only reactive (capable of water adduction) species should be considered in the equation, and the unreactive species should be subtracted from the total I_{187} observed in the mass spectrum. The proportion of unreactive species, R_U, was determined by finding the ratio of $\frac{I_{187}}{I_{187}+I_{205}}$ after a reaction time of 1000 ms. Equation 2.1 was used to find the proportion of reactive species remaining at given delay time, R_R, for the determination of the corrected reaction rate.

Plotting $\ln(R_R)$ vs. time yields a linear trend as expected, and provides the true reaction rate i.e. the rate constant times the unknown concentration of water in the ion trap. Using R_R is preferred to simply using I_{187} because the ratio is unaffected by fluctuations in absolute signal intensity across many scans. Using these corrected reaction rates, the four biologically relevant isomers can still be distinguished, with the two most similar being Gal and Glc (p = 0.02). Neither the unreactive fraction nor the corrected reaction rate was conclusively more useful for

discriminating between isomers. Both demonstrate small relative standard deviations (less than 8%) for all the hexoses studied (Table 3.1). The most significant difference between the two methods is the time it takes to acquire the data necessary to generate the reaction rate versus the unreactive fraction. The unreactive fraction is a single data point whereas measuring a reaction rate requires measurements be made at multiple timepoints, i.e. multiple mass spectra must be obtained. For this reason measuring the unreactive fraction may be preferred in an experiment with limited sample or in an experiment where analysis time is limited such as a peak eluting in a chromatographic experiment.

Table 3.1: Reaction rates and final unreactive ratios of four hexoses

Hexose	Reaction Rate, k' ($x10^{-4}$)	Unreactive Fraction
Glucose	63.4 (2.3)[a]	0.35 (0.01)
Galactose	56.7 (3.8)	0.44 (0.03)
Fructose	44.9 (1.9)	0.77 (0.02)
Mannose	39.9 (2.1)	0.83 (0.01)

[a]The average is reported followed by one standard deviation in parenthesis (N = 4).

It was verified that the unreactive fraction and reaction rate are not a function of hexose or lithium concentrations. The concentration of lithium acetate was varied from 10 µM to 1000 µM (with 10 µM glucose), and the only observed difference was the appearance of $[Li + (LiOAc)_n]^+$ clusters (where n = 2, 3, and 4) prior to isolation of $[M+Li]^+$ at high concentrations of lithium acetate. Additionally, several different concentrations of glucose ranging from 20 nM to 500 µM (all with 100 µM lithium acetate) were analyzed. The unreactive fraction and two reaction rates remained constant within experimental error, and the RSD for each measurement

never exceeded 10%. A negative control was performed with a reagent blank to ensure that the results were not caused by contamination in the instrument.

At higher hexose concentrations dimer species, $[2M+Li]^+$, are observed. The dimer species do not adduct water for all of the hexoses studied. This supports the hypothesis that a reactive species requires the lithium cation to be coordinated to a minimal number of oxygens, because a dimer would be expected to have a greater number of oxygen-lithium bonds than the monomer. Across all concentrations studied the reaction rates and final unreactive ratios remain constant within experimental error. Previous methods for distinguishing hexoses using either CID, ion mobility, or the fixed ligand kinetic method do not report limits of detection; however, both use 100 µM or higher concentrations of hexose, orders of magnitude more sample than is necessary for the water adduction method[4,5].

Experiments were conducted to determine the origin of the water in the quadrupole ion trap. If the water originates from the electrosprayed solvent, then this method would not be as robust because the concentration of water in the solvent as well as ESI flow rate would play a factor in the resulting reaction rate. When the flow rate was changed from 1 µL/min to 10 µL/min, there was no difference in the measured reaction rate or unreactive fraction within experimental error (though signal intensity increased by over a factor of 20 from 1 to 10 µL/min). Analogously, as stated previously, changing the concentration of glucose from 20nM to 500 µM only resulted in changing the signal intensity but not the reaction rates or the unreactive fraction.

To further ensure that the water that adducts does not come from the ESI solvent, a solution of 10 µM glucose and 100 µM lithium acetate in 50/50 D_2O/CD_3OD was

electrosprayed. The Bruker Esquire and HCTultra are equipped with a heated dry gas that is flowed directly opposite the inlet to the mass spectrometer to keep solvents and other neutrals from entering the mass spectrometer. This experiment resulted in the glucose exchanging all five hydroxyl protons with deuterons (after no more than an hour of being in solution) prior to electrospray. After isolating the new $[M+Li]^+$ peak at *m/z* 192 the same corrected/uncorrected reaction rates and unreactive fraction were measured as those from solutions of glucose in H_2O/CH_3OH. More importantly, only the adduction of 18 to form *m/z* 210 was observed; therefore, the water in the ion trap is not a result of water from the electrospray.

Because the water does not come from the electrospray solvent, it most likely originates from water vapor in the atmosphere. Based on this hypothesis a simple calculation was performed to provide some means of estimating the true rate constant. When the valve which allows in helium (used to collisionally cool ions in the ion trap) is shut, the pressure in the trapping region is measured to be 3.7×10^{-6} torr. The relative humidity in the laboratory is measured to be about 50% most days of the year (+/- 10%). At room temperature (about 21°C) this relative humidity corresponds to the water vapor being 1.5% of the atmosphere. Therefore, the partial pressure of water in the trap would be about 1.5% of the 3.7×10^{-6} torr, or 5×10^{-8} torr. Assuming the trap is at room temperature, the number density of water is calculated to be about 2×10^{9} molecules/cm^3. Dividing the k' calculated earlier for each hexose by this concentration yields a rate constant of 3.2×10^{-12} cm^3 $molecule^{-1}$ s^{-1} for glucose, 2.8×10^{-12} cm^3 $molecule^{-1}$ s^{-1} for galactose, 2.2×10^{-12} cm^3 $molecule^{-1}$ s^{-1} for fructose, and 2.0×10^{-12} cm^3 $molecule^{-1}$ s^{-1} for mannose.

3.2. Distinguishing Pentoses with Water Adduction

Pentoses are especially difficult to discriminate compared to larger monosaccharides because their structures differ only by the equatorial or axial placement of two hydroxyl groups. Unlike hexoses where the pyranose structure is almost always preferred, pentoses form both furanose and pyranose structures in solution. Each ring structure also has two anomeric configurations, and these different conformations produce multiple peaks for a single pentose during chromatographic separation, complicating quantitative data analysis[6]. Only one example using ion mobility to separate pentose isomers exists in the literature, and that method was only used to separate D-arabinose and D-xylose[7]. The water adduction reaction just described for distinguishing hexoses was applied to an exhaustive list of D-pentoses (Figure 3.4).

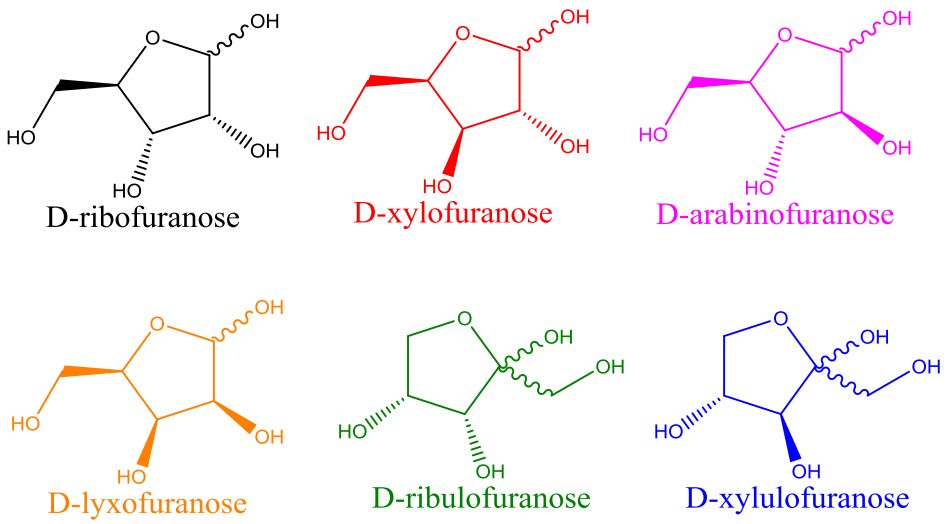

Figure 3.4: Structures for all D-pentoses studied shown in their furanose conformation

Similarly to the hexoses, the pentoses show an exponential decay without all $[M+Li]^+$ ions adducting water. The reaction rates of the pentoses (Figure 3.5) exhibit much greater similarity than reaction rates for the hexoses, and likewise, there is a much smaller range in the unreactive fractions for the pentoses than the hexoses.

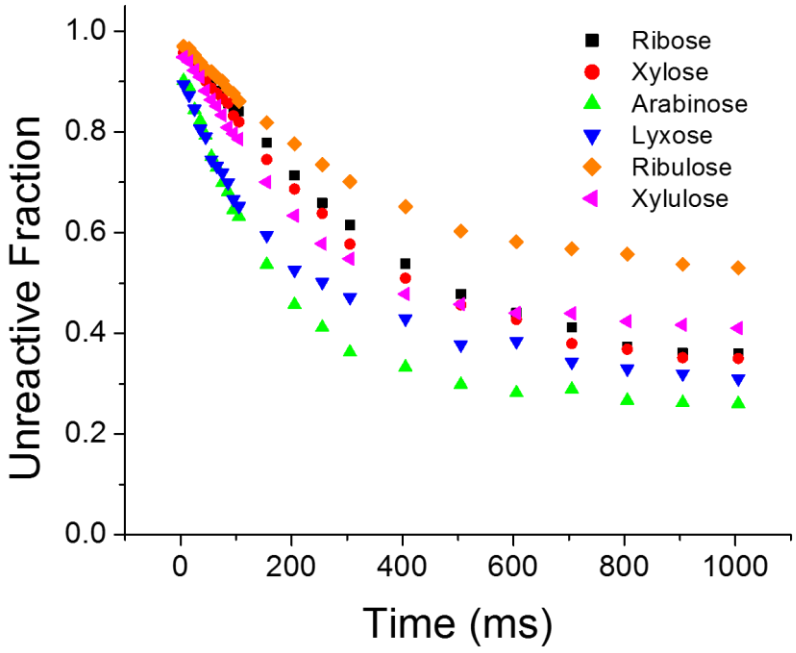

Figure 3.5. Exponential decay curves for the reaction of $[M+Li]^+ + H_2O$ in a quadrupole ion trap

While the hexoses could be distinguished based on either the reaction rate or the unreactive fraction, distinguishing all pentoses required both parameters to be measured. The unreactive fraction of lithiated pentose ($\frac{I_{157}}{I_{157}+I_{175}}$) produced during ESI is very reproducible (with RSD's ≤ 8.0%). This fraction can be used to distinguish ribulose, xylulose, and arabinose from all other pentoses (with $p \leq 0.027$ using Student's t-test). However, ribose, lyxose, and xylose are not able to be distinguished from each other using only the unreactive fraction. The

reaction rate measured was found to be unique for all of the pentoses studied (with $p \leq 0.025$ using Student's t-test), with the exception of Ara and Lyx. However, Ara and Lyx can be confidently distinguished from one another using the unreactive fraction as discussed previously. Therefore, when both unreactive fraction and reaction rate are used all six pentoses can be readily distinguished. This is shown in Figure 3.6 where the unreactive fraction is plotted versus the reaction rate, separating all the isomers in a two-dimensional space.

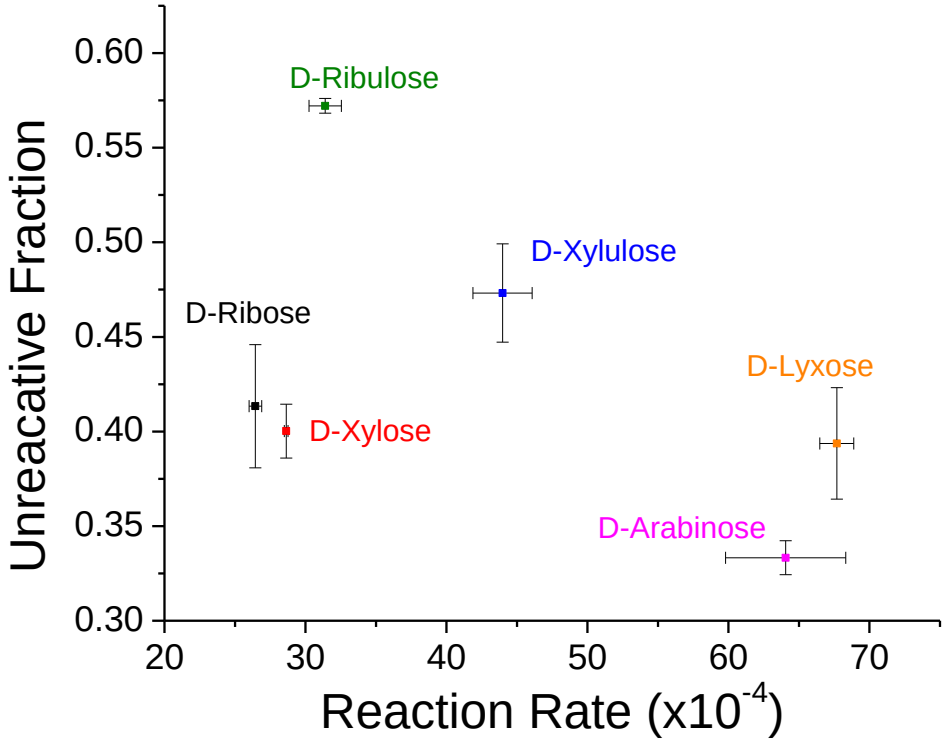

Figure 3.6. Unreactive fraction versus reaction rate for all of the D-pentoses studied. All pentoses can be distinguished after measuring both parameters

This method was also used to compare distinguishing the absolute configuration of two pentoses, D-arabinose and L-arabinose. The reaction rates and unreactive fractions were

measured for each as previously explained. The enantiomers were unable to be distinguished within experimental error. The reaction rates for D-Ara and L-Ara were 64.1 +/- 4.2 and 63.9 +/- 3.9, respectively, and the unreactive fraction for D-Ara and L-Ara were 0.333 +/- 0.009 and 0.336 +/- 0.005, respectively. This result is expected as the two enantiomers would have identical binding sites for Li^+, i.e. the distances and angles between all oxygen atoms in the pentose are same in each enantiomer.

The effect of pentose concentration on the unreactive fraction and the reaction rate was tested with ribose. Experiments were performed with 100 μM lithium acetate and different concentrations of ribose ranging from 500 μM to 250 nM. The reaction rate remained unchanged (within one standard deviation) throughout the entire range of concentrations tested. However, at 250 nM the relative standard deviation was greater than 10% (compared to less than 5% for all other concentrations). The unreactive fraction remains constant (within one standard deviation) at all concentrations tested, and the relative standard deviation of all measurements remains below 10%.

3.3 Distinguishing Hexosamines and N-acetylhexosamines

The water adduction method was further applied to derivatized monosaccharides. In biological systems the individual monosaccharide units found in larger carbohydrate chains or individually can have modifications including *O*-acetylation, *O*-methylation, *O*-sulfation, amination, and *N*-acetylation[8]. One of the most common modifications is amination and N-acetylation, and these modifications can occur on several different hexoses. The three hexosamines and three N-acetylhexosamines are shown in Figure 3.7.

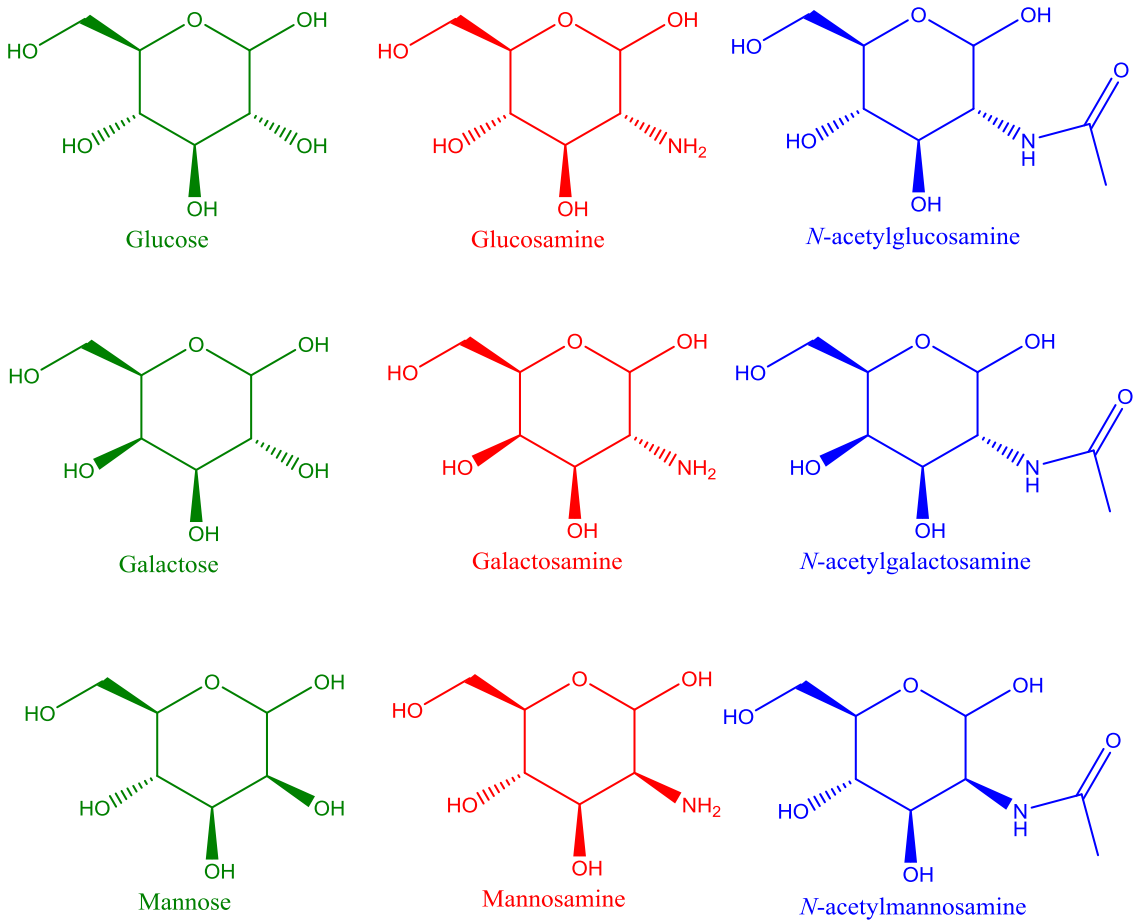

Figure 3.7: The hexoses (green), hexosamines (red), and N-acetylhexosamines (blue) studied. All substitutions occur at the 2-hydroxyl.

The water adduction reaction rates and unreactive fractions were measured for three isomeric hexosamines (glucosamine, galactosamine, and mannosamine) and three isomeric N-acetylhexosamines (N-acetylglucosamine, N-acetylgalactosamine, and N-acetylmannosamine). These nitrogen containing monosaccharides have a much higher proton affinity than their non-modified counterparts. Therefore, some $[M+H]^+$ is observed in the mass spectrum after ESI, but the signal intensity of the protonated molecule is less than 10% the signal of the lithium

cationized molecule. All three hexosamines and N-acetylhexosamines can be distinguished using either the unreactive fraction or the reaction rate (Figure 3.8).

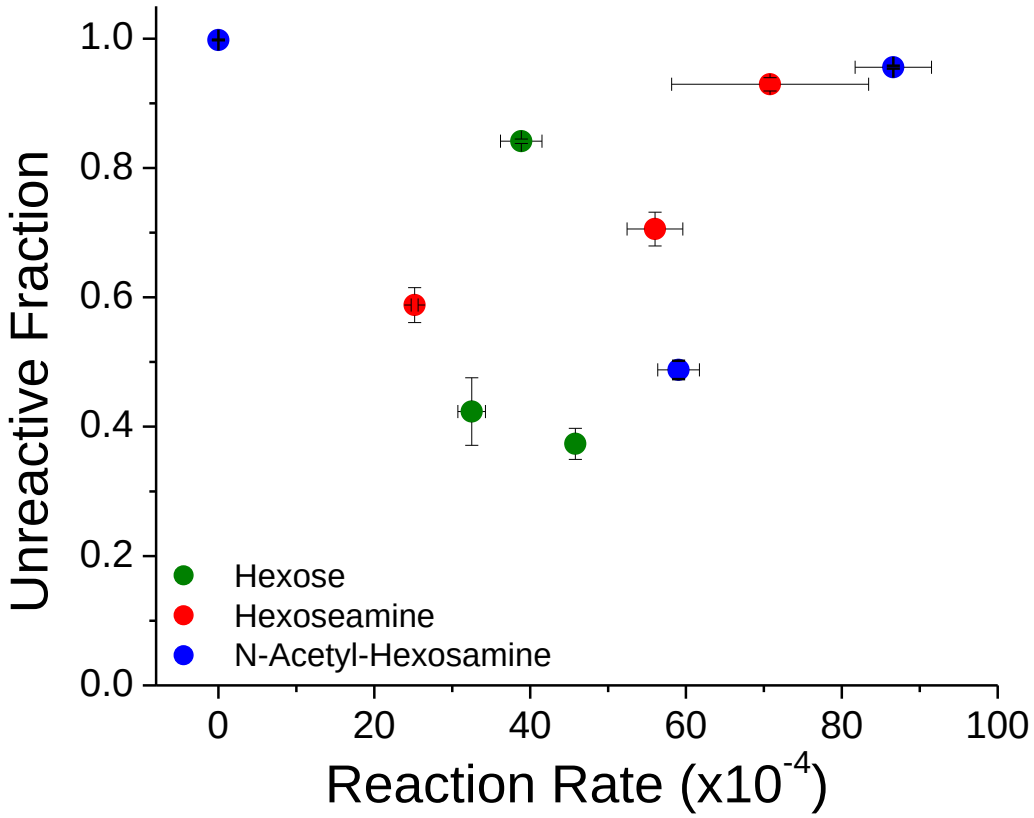

Figure 3.8: Unreactive fraction versus reaction rate for glucose, galactose, mannose (green) and their amine (red) and N-acetylamine derivatives (blue). All isomeric species can be distinguished using either the unreactive fraction or the reaction rate, with the exception of two hexosamine species.

The underivatized hexoses were also studied to compare them to their derivatized analogs. It is important to note that the unreactive fractions and reaction rates do not match those given in the previous discussion for distinguishing hexoses. This is because samples in this

section were analyzed from completely aqueous solutions, while samples in the previous sections were analyzed from solution of 50:50 methanol:water. A discussion of the effect of solvent on unreactive fraction and rate can be found in chapter 6 of this dissertation. Some trends can be observed by comparing the unreactive fractions for a given hexose and its derivatives. For example, all hexosamines and N-acetyl hexosamines have a greater unreactive fraction compared their respective hexosamines and hexose, and with the exception of glucose, all N-acetylhexosamines have a greater unreactive fraction than the hexosamines. These differences are almost certainly caused by new coordinations to either the nitrogen in the case of hexosamines or the nitrogen and/or the carbonyl oxygen in the case of the N-acetylhexosamines. N-acetylgalactosamine is almost completely unreactive, and N-acetylmannosamine has no reactive structure at all (Figure 3.9).

There are little differences in reaction rate comparing across glucose and its two other derivatives. Similarly, galactose and galactosamine have very similar reaction rates; however, the reaction rate of N-acteylgalactosamine is almost three times as fast as its counterparts. The reaction rate also increases drastically when comparing mannose and mannosamine.

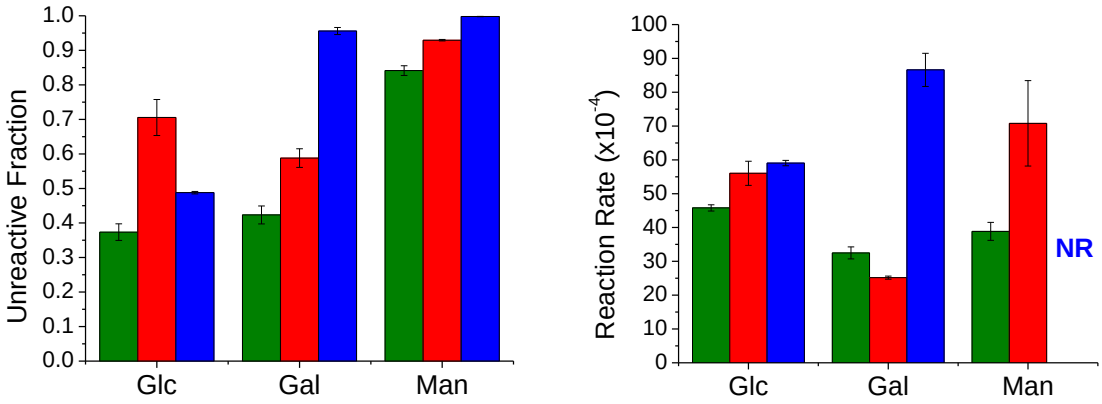

Figure 3.9: The measured unreactive fraction (a) and reaction rates (b) for each of the three sets of isomers from aqueous solutions. N-acetylmannosamine is completely unreactive and has no reaction rate. Green represents the hexose, red represents the hexosamine, and blue represents the N-acetyl hexosamine. This is the same data shown in Figure 3.8

3.4 Summary

ESI of monosaccharides and a lithium salt produces $[M+Li]^+$, which adduct water in a quadrupole ion trap. The water adduction reaction rate can be measured and used to distinguish isomeric hexoses. Furthermore, not all lithium cationized molecules will adduct water, and the unreactive fraction of ions is very reproducible (RSDs typically less than 5%) and can be used to distinguish isomers. Together the reaction rate and unreactive fraction were able to distinguish four biologically relevant hexoses and an exhaustive list of D-pentoses. A conservative lower limit on the concentration of hexose necessary in solution for the water adduction method was estimated to be around 20 nM for the hexoses and below 250 nM for the pentoses. These limits are based on an increase in the relative standard deviation for the reaction rate and unreactive

fraction at low concentrations making it difficult to distinguish isomers. This is a significant improvement from previous methods, which typically only report using concentrations of 100 μM or greater. Experiments using D_2O as the solvent showed that water in the ion trap does not originate from the electrospray solvent. A more exact reaction rate for each of the hexoses was calculated based on the relative humidity in the room and the base pressure in the ion trap. The water adduction method was also applied to the three most biologically significant hexosamines and N-acetylhexosamines to demonstrate the applicability of this method beyond underivatized hexoses. Both sets of isomeric hexose derivatives could be distinguished using either the unreactive fraction or the reaction rate. The hexosamines and N-acetylamines generally have higher unreactive fractions and reaction rates compared to their hexose derivative.

REFERENCES

1 G. E. Hofmeister, Z. Zhou and L. J.A., Linkage position determination in lithium-cationized disaccharides: Tandem mass spectrometry and semiempirical calculations, *J. Am. Chem. Soc.*, 1991, **113**, 5964–5970.

2 M. R. Asam and G. L. Glish, Tandem mass spectrometry of alkali cationized polysaccharides in a quadrupole ion trap, *J. Am. Soc. Mass Spectrom.*, 1997, **8**, 987–995.

3 M. T. Rodgers and P. B. Armentrout, Collision-Induced Dissociation Measurements on Li+(H2O)n, n = 1-6: The First Direct Measurement of the Li+-OH2 Bond Energy, *J. Phys. Chem. A*, 1997, **101**, 1238–1249.

4 G. Nagy and N. L. B. Pohl, Monosaccharide Identifcation as a First Step toward de Novo Carbohydrate sequencing: Mass Spectrometry Strategy for the Identifcation and Differentiation of Diastereomic and Enantiomeric Pentose Isomers, *Anal Chem*, 2015, **87**, 4566–4571.

5 G. Nagy and N. L. B. Pohl, Complete Hexose Isomer Identifcation with Mass Spectrometry, *J Am Soc Mass Spectrom*, 2015, **26**, 677–685.

6 K. E. Mutenda and R. Matthiesen, in *Mass Spectrometry Data Analysis in Proteomics*, ed. R. Matthiesen, Humana Press, Totowa, 2007, vol. 1, p. 289.

7 X. Zheng, X. Zhang, N. S. Schocker, R. S. Renslow, D. J. Orton, J. Khamsi, R. A. Ashmus, I. C. Almeida, K. Tang, C. E. Costello, R. D. Smith, K. Michael and E. S. Baker, Enhancing glycan isomer separations with metal ions and positive and negative polarity ion mobility spectrometry-mass spectrometry analyses, *Anal. Bioanal. Chem.*, 2017, **409**, 467–476.

8 H. Yu and X. Chen, Carbohydrate post-glycosylational modifications, *Org. Biomol. Chem.*, 2007, **5**, 865.

CHAPTER 4: COMPUATIONAL AND EXPERIMENTAL INVESTIGATION OF THE CHEMISTRY DICTATING THE UNREACTIVE FRACTION

4.1. The Mechanism of Electrospray Ionization

Electrospray ionization (ESI)[1] revolutionized the types of analytes that could be studied with mass spectrometry, allowing for everything from small molecules to proteins to be easily transferred from solution phase to the gas phase. ESI can produce multiply charged ions, reducing the mass-to-charge ratio for large molecular weight proteins or polymers and allowing these ions to be analyzed with mass analyzers that have a maximum mass-to-charge limitation[2].

ESI is performed by passing the analyte solution through a metal or glass capillary (inner diameter typically < 200 μm) with a potential difference applied between the emitter and the MS inlet a few mm away[3–5]. A Taylor Cone forms at the tip of the emitter where small droplets with excess charge are produced that are around 100 nm in diameter[6]. As these charged droplets are drawn towards the inlet of the mass spectrometer by the electric potential, solvent molecules are lost, desolvating the ions and leaving behind a positive charge. Several studies have been published on the final stages of these droplets[1,7–14]. It is believed that these final steps towards desolvation dictate the mechanism for adduction of protons or metal cations as the molecule is transferred into the gas phase.

One particularly interesting question these studies aimed to answer is the final structure of the gas phase ion. Does the protontated/metal cationized molecule retain its solution phase structure, or does it convert to a conformation more energetically favorable for the gas phase?

This question has been studied extensively for ESI of proteins, where it is well known that solvent and pH dictate the structure and function of the large molecule[11]. These studies typically electrospray the proteins from aqueous solvent buffered around pH 7 with appropriate salt concentrations aimed to match physiological conditions as closely as possible. Ion mobility experiments are then used to measure the collisional cross-section of the gas phase protein, a measurement which provides the relative size of the protein or macromolecular complex[15–17]. These cross-sections can then be compared to crystal structures or cross-sections calculated with molecular mechanics to determine if the gas phase structure has the same collision cross-section as the expected solution phase structure.

The mechanism for desolvation of a protein or macromolecular complex is by predicted by experimental and molecular modeling results to follow the Charged Residue Model (CRM)[18,19], where solvent molecules are ejected from the droplet until the protein and charges are the only remaining species[7,8,16,20,21]. However, small molecules are predicted to transfer into the gas phase via the Ion Evaporation Model (IEM)[22], where ions at the surface of very small droplets are forced out of the droplet by columbic repulsion[7,8,23]. The structure of small protonated/metal cationized molecules produced via the IEM has also been studied, though not as thoroughly as with proteins. While it is the prevailing opinion that proteins can retain their solution phase conformation after transferring into the gas phase[8,17], different mechanisms for desolvation warrant separate studies of small molecules. Most of what is known about these mechanisms are studied with molecular dynamics, and experimental results are needed to confirm theories developed from molecular dynamics[16,20].

The knowledge gained from experiments in Chapters 3 and 4 are used to form hypotheses about the structure of small, lithium cationized molecules after electrospray ionization. When

these lithium cationized molecules are isolated in a quadrupole ion trap (QIT), some ions will then adduct a single water molecule. Quadrupole ion trap mass spectrometers can be used to monitor the kinetics of gas phase reactions of the ions before subsequent mass analysis because ions can be held for a specified amount of time, allowing the reaction time to be controlled.

Controlling the reaction time allows for the lithium cationized molecules to be distinguished in one of two ways. First, the reaction rate of the water adduction reaction can be used to distinguish several isomers. A second, more original method can be used to distinguish isomers. For all the lithium cationized monosaccharides and disaccharides studied, there exist some reactive ions that will adduct water, and some ions that will not adduct water. The ratio of unreacted to reacted (non-water adducted to water adducted) ions is unique for a given lithium cationized species, and this unreactive fraction can be used to distinguish isomeric monosaccharides and disaccharides as described in Chapters 3 and 4. Both the reaction rates and unreactive fractions are very reproducible, allowing for the isomers to easily be distinguished.

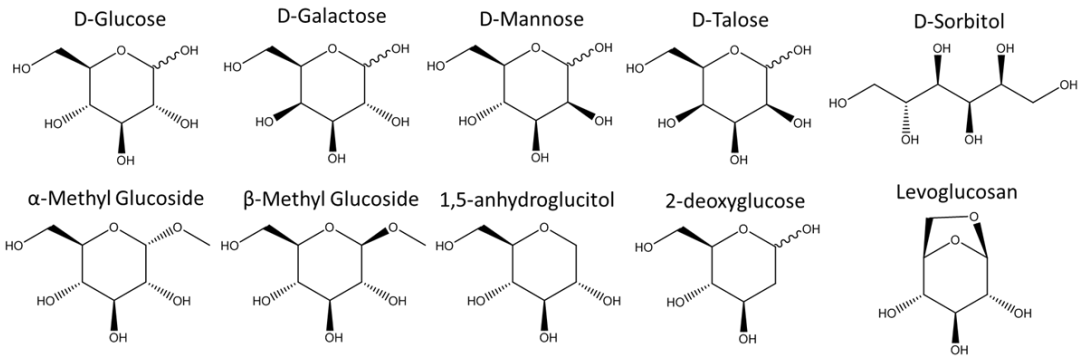

Figure 4.1: Molecular structures for the molecules studied

The chemistry dictating the unreactive fraction is studied here using both experimental data with density functional theory calculations. ESI typically produces protonated molecules, where the proton is typically bound to single electronegative atom on the molecule. However,

with metal cationization, the cation can be coordinated to multiple electronegative atoms. These monosaccharides contain many oxygen atoms, allowing for numerous different coordination sites for metal cations. A lithium cation coordinates to at least two oxygen atoms (bidentate), but three or four coordinations (tridentate or tetradentate, respectively) are also possible. Typically, a greater number of coordinated oxygen atoms decreases the energy of the overall gas phase complex, making tridentate and tetradentate structures often the most energetically favorable. However, density functional theory (DFT) calculations suggest that while in the dissolved in water, the lithium cation prefers coordinations to water, minimizing the number of coordinations to the hexose. It's believed that the number of coordination bonds to the lithium cation determines if a water molecule can adduct in the quadrupole ion trap.

Density functional theory calculations were used to determine the number of cooridnations a lithium cation is likely to form between several different hexoses, methyl glucosides, and other poly-hydroxylated compounds. Water adduction experiments were performed on these same lithium cationized molecules if their reactivity with water. The structures calculated to be energetically favored in the gas phase are typically tri/tetradentate, and therefore, would not likely adduct water. Conversely, the calculations suggested the thermodynamically preferred aqueous phase conformations prefer bidentate interactions. If the bidentate conformations are transferred into the gas phase, they will be able to adduct water. The fraction of ions that are able to adduct water would therefore provide some indication of the number of ions that retained their solution phase conformation after transferring into the gas phase.

4.2. Introduction to Density Functional Theory Calculations

Density functional theory uses quantum mechanical calculations to determine electronic energies of a molecule or complex. Single-point energy calculations are used to determine the electronic energy based upon the coordinates of the atoms involved, the overall charge and multiplicity of the system being studied, and the level of theory desired for the calculation. Optimization calculations can be used to systematically change the coordinates of the atoms in the system to minimize electronic energy, ultimately producing structures for the global minimum or a local minima. Vibrational calculations determine the vibrational frequencies of optimized structures, and can also be used to calculate the free energies of different structures. The Gibbs free energies of systems composed of the same atoms but in a different arrangement can be compared to determine the more energetically favorable structure. Density functional theory is used in this study to determine likely binding sites for the lithium cation to bind and the relative Gibbs free energy for each unique structure. Additionally, the change in Gibbs Free Energy of water adduction ($\Delta G_{WaterAdduction}$) was calculated for each unique structure.

The lowest energy structures of the alpha and beta anomers for D-glucose, D-galactose, D-mannose, and D-talose were previously calculated in vacuo at the 6-311++G(d,p) level of theory[27–29]. These structures for the global minimum were reproduced here, and the energies matched (within 0.01%) at the same level of theory, and these global minimum structures for each anomer was used for all subsequent calculations. Each optimized anomer was lithiated systemically by adding a single lithium cation to each of four locations around all oxygen atoms. These four locations were the vertices of an imaginary tetrahedron such that the lithium was always 1.4 Å from the targeted oxygen, the typical bond distance after optimization. Adding a single lithium cation in four locations around each of six oxygens results in 24 unique structures. If the added lithium cation was greater than 0.6 Å from all other atoms in the structure, the

structures were optimized using B3LYP at the 3-21G level of theory with an implicit solvent (conductor-like polarization continuum model, cpcm) where water was chosen as the solvent. Optimizations with the lithium cation 0.6 Å or closer to another atom rarely converge. The resulting optimized structures are again optimized and vibrational calculations are performed with B3LYP functional at the 6-311++G(d,p) level of theory with the implicit solvation model.

The structures previously optimized at the 6-311++G(d,p) level of theory with an implicit aqueous solvent were again optimized at the 6-311++G(d,p) level of theory in vacuo to make the computational modelling process as similar as possible to the electrospray process, where ions are transferred from solution phase to gas phase. This allows the energies for lithiation to be compared in both the aqueous phase as well as the gas phase. After optimization of $[M+Li]^+$ in the gas phases, a single water molecule is then added to each optimized gas phase structure, and each structure is then optimized at the 3-21G level of theory before a subsequent optimization and subsequent vibrational calculations were performed at the 6-311++G(d,p) level of theory. Additionally, all structures also had vibrational calculations performed at the M06-2X/cc-pTZV level of theory. The M06-2X functional[30] was previously shown to provide more accurate vibrational calculations compared to the B3LYP functional[31,32], and values calculated with each functional are compared below. Vibrational calculations were also performed at the MP2/6-311++G(d,p) level of theory for several structures to ensure maximum accuracy possible.

4.3. Calculations and Experimental Results of Hexoses

Lithium cationized molecules are generated by electrospraying a solution with a dissolved lithium salt and the analyte. All analytes were electrosprayed from completely aqueous solutions. Though greater sensitivity is attainable using mixtures of methanol and water, purely

aqueous solvent was used to keep the parameters used in calculations and experiments as similar as possible. For all analytes the lithiated species was first isolated in the QIT, and a subsequent delay was applied before detection of the resulting ions. The delay allows time for water adduction reaction to occur. The ratio of hydrated lithium cationized molecule to total lithium cationized molecules ($[M+Li]^+$ / ($[M+Li+H_2O]^+$ + $[M+Li]^+$) exponentially decays as expected (Figure 5.1).

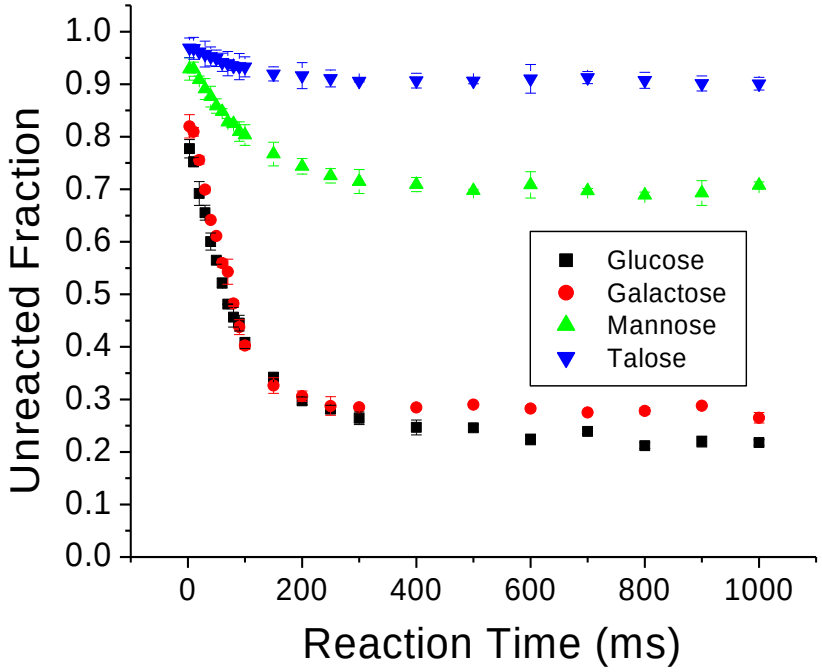

Figure 4.2: Decay curves for the four hexoses studied. The y-axis represents the fraction that have not adducted water as a function of the delay time.

These decay curves all asymptote before reaching zero, demonstrating that for the hexoses studied not all lithium cationized molecules produced during ESI are able to adduct water. This is in agreement with previous experiments involving hexoses, pentoses, and

disaccharides where this final ratio of unreacted ions to total ions, herein referred to as R_U, could be used to distinguish the epimers. A likely cause for both reactive and unreactive $[M+Li]^+$ is that there are multiple different locations for the lithium cation to bind to each of the molecules – a minimum of one that will adduct water and at least one that is unreactive.

The final ratios of unreacted lithium cationized hexose to total lithium cationized hexose are reported in Table 1. The measured values of R_U for glucose, galactose, and mannose are the most biologically relevant aldohexoses, and talose was also studied because in the most favorable aqueous phase conformation (the $^4C_1$ chair), all hydroxyl groups are on the same side of the ring. This is expected to provide a very different environment for coordination of the lithium cation, especially compared to glucose where all hydroxyls are equatorial on alternating sides of the ring structure.

Table 4.1: Unreactive fractions and reaction rates for several molecules studied

Molecule	*m/z* of $[M+Li]^+$	R_U
Glucose	187	0.213 ± 0.004
Galactose	187	0.308 ± 0.018
Mannose	187	0.685 ± 0.012
Talose	187	0.904 ± 0.005
1,5-Anhydroglucitol	171	0.049 ± 0.006
2-Deoxyglucose	171	0.695 ± 0.007
Methyl α-glucose	201	0.045 ± 0.004
Methyl β-glucose	201	0.261 ± 0.005

Density functional theory calculations were used to determine the number of oxygen atoms coordinated to the lithium cation and the relative free energy for each structure in vacuo and with an implicit aqueous solvent. Optimizing first with a solvation model and subsequently optimizing in vacuo was done to match the desolvation process of ESI, where the lithiated

molecules are passed from solution to the gas phase, as closely as possible. The first step was to optimize molecular structures in vacuum for each of the four hexoses studied experimentally. Because each of the hexoses have two anomers that can freely mutarotate in solution, each of the anomers was first optimized without a lithium cation to find a global minimum for each of the eight anomers.

Several local minima were expected for each anomer, because there are six oxygens that can coordinate to the lithium cation. Local minima are often found with molecular dynamics calculations, where the energy of the structure is calculated as the atoms in the system move freely. Classical molecular dynamics calculations are somewhat analogous to classical physics, where calculations are based on only Newtonian physics, while ignoring electronic energies, which must be calculated using quantum mechanical calculations. Quantum molecular dynamics such as Born-Oppenheimer molecular dynamics (BOMD), which consider electronic structure, should be more accurate than traditional molecular dynamics. During BOMD calculations performed here, the lithium cation did not move from the oxygen atoms to which it was originally bound. Increasing the temperature used in the BOMD calculation can be used to explore a larger conformational space. Increasing the temperature led to greater amplitudes in the vibrations of the lithium-oxygen coordinations, but never to the lithium cation moving to a new binding site. Further increases in temperature ultimately results in breaking covalent bonds (around 900 K) while the lithium cation remains coordinated at the same site.

Because molecular dynamics were unable to provide different lithiation sites, a “shotgun” method was used where several different starting structures were built, each composed of the optimized anomer and a lithium cation in a new location as described in section 4.2 above. The resulting structures were then optimized and subsequent vibrational energies were calculated at

the B3LYP/6-311++G(d,p) level of theory while still using the solvation model. The newly optimized structures were then used for a further optimization at the B3LYP/6-311++G(d,p) level of theory without the solvation model (in vacuo). This allows each of the in vacuo structures to be matched to a corresponding solution phase structure, and the implications of these successive optimizations and vibrational calculations are discussed below. Optimizing with an implicit solvation model did not limit the number of vacuum phase structures that were found. An analogous set of successive optimization calculations, which did not involve the implicit solvation model, produced the same vacuum phase structures as the successive optimizations with the solvation model.

When starting from the $^4C_1$ chair conformation, 4 – 8 unique lithium binding sites were optimized for each of the studied anomers. All in vacuo energies are shown (Figure 5.2) relative to the lowest energy for that respective hexose. The number of oxygen atoms coordinated to the lithium cation as well as the relative energy for each structure are compared in Figure 5.2. All of the structures with only 2 oxygen atoms coordinated (bidentate) are designated with green markers, 3 oxygen atoms coordinated (tridentate) are designated with yellow markers, and 4 oxygen atoms coordinated (tetradentate) are designated with red markers. The differences in the number of bound oxygens for the lowest energy structures in vacuo becomes very obvious when comparing glucose and talose. A quick observation of the $^4C_1$ structure of glucose shows all hydroxyls are on alternating sides of the pyranose ring, compared to talose, whose oxygen atoms are near one another (refer to Figure 4.1). It is not surprising that talose is able to form significantly more structures that are tridentate and tetradentate compared to glucose. More importantly, glucose has the lowest experimentally measured R_U and talose has the highest. It was therefore hypothesized that coordination to a greater number of oxygen atoms lowers the

affinity for water adduction by reducing the charge on the lithium cation making it less Lewis acidic. Galactose and mannose, which have intermediate R_U relative to glucose and talose, have tridentate structures as their most favorable gas phase structures followed by higher energy bidentate structures, which would be reactive.

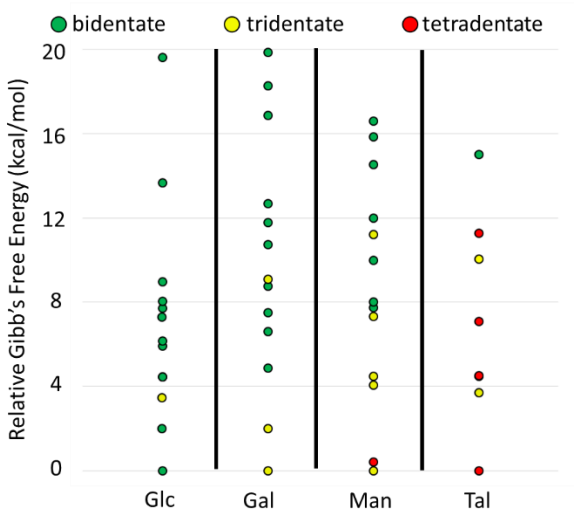

Figure 4.3. Each dot represents a unique structure for each of the hexoses and the gas phase Gibb's Free energy relative to structure with the lowest energy of that same hexose. Both alpha and beta anomers are shown together in the plot. Green, yellow, and red dots represent structures where the lithium cation is bound in a bidentate, tridentate, and tetradentate coordination, respectively.

This theory was tested computationally by adding an explicit water molecule to the structures optimized in vacuo. The water molecule is expected to coordinate to the lithium cation, hydrogen bond with a hexose hydroxyl, or both. Originally, water molecules were added to each structure in a manner similar to the addition of the lithium cation: a water molecule was added in several positions around each oxygen at as well as the lithium cation. Because the water could be oriented in different directions, 8 different "hydrated" structures were produced for each previously optimized lithium-hexose complex. The eight structures differed by the location and orientation of the water molecule relative to the lithium cation. A water was added at each of the four vertices of a tetrahedron, analogous to adding the lithium cation to each oxygen atom previously. The final four structures added water in the same locations, but with the orientation

of the water molecules mirrored, relative to the previously generated structures. Initial calculations with the alpha anomer of glucose showed that water binding to the lithium cation was more than 16 kcal/mol more favorable than hydrogen bonding to a glucose hydroxyl. For this reason, future optimizations only considered structures where the water coordinates to the lithium cation or coordinates to both the lithium cation and nearby hydroxyls. Optimizations for all structures was first performed at the B3LYP/3-21G level of theory, and a subsequent optimization was performed at the B3LYP/6-311++G(d,p) level of theory. The final optimized structures were used for vibrational calculations at both the B3LYP/6-311++G(d,p) and M06-2X/cc-pTZV level of theory. The $\Delta G_{WaterAdduction}$ is calculated as $\Delta G_{WaterAdduction} = G_{Hydrated} - (G_{Lithiated\ Hexose} + G_{Water})$.

For all structures the $\Delta G_{WaterAdduction}$ was calculated to be a negative value, suggesting water adduction should be favorable for all structures. However, grouping the measured $\Delta G_{WaterAdduction}$ by number of bound oxygens show there is a statistical difference between the calculated $\Delta G_{WaterAdduction}$ of bidentate structures and tri/tetradentate structures. $\Delta G_{WaterAdduction}$ is more negative for bidentate structures, suggesting that water binding to these structures would be more favorable than to tri/tetradentate structures. It is possible that there is a systematic error in the calculated $\Delta G_{WaterAdduction}$, though -14 kcal/mol would be much larger than expected. Often DFT calculations overestimate the energy of non-covalent bonds. This overestimate can be measured with a counterpoise calculation which measures the basis-set superposition error, determining the error in the calculated noncovalent interaction. The counterpoise calculations performed at B3LYP/6-311++G(d,p) determined the error to be about 1 kcal/mol for bidentate, tridentate, and tetradentate structures. This suggests that the basis-set superposition error was not sufficiently large to explain the possible systematic error.

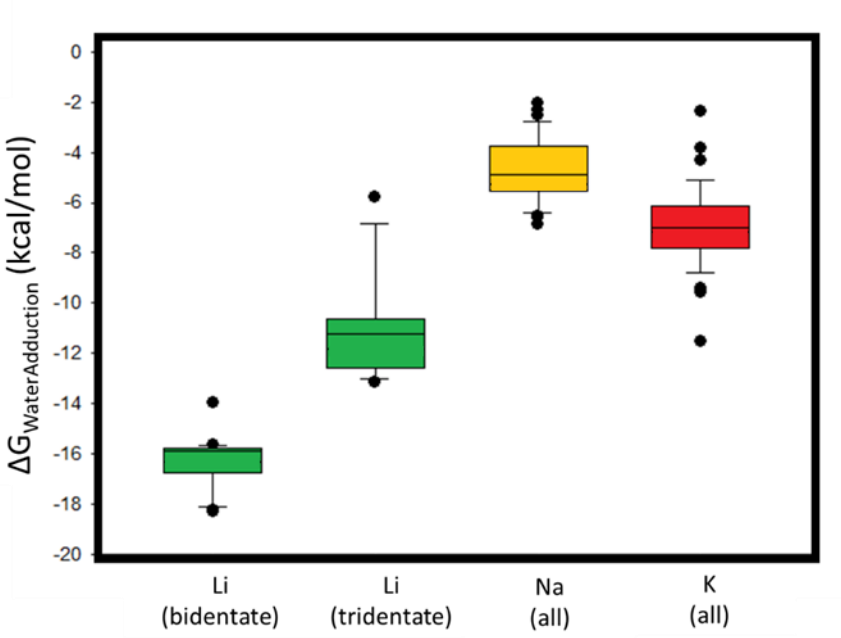

Figure 4.4. A box-and-whisker plot of the calculated $\Delta G_{WaterAdduction}$ grouped based on the metal cation and number of coordinations. The inner-quartile range is shown in color and outliers are shown as black dots. $\Delta G_{WaterAdduction}$ is significantly more negative for a bidentate lithium cationized molecule. The $\Delta G_{WaterAdduction}$ was also calculated to be negative for sodium and potassium cationized molecules, which are shown experimentally to be 100% unreactive.

To further investigate this possible error, calculations were repeated with sodium and potassium cations with the same method previously described for lithium cations. Experiments were conducted where a sodium salt or potassium salt was added to a hexose solution to produce either $[M+Na]^+$ or $[M+K]^+$, respectively. Water adduction was not observed to either of these cations in the quadrupole ion trap for any of the hexoses studied. The calculated $\Delta G_{WaterAdduction}$ for the new cations was also found to be negative for all structures. However, the values were less negative than the calculated $\Delta G_{WaterAdduction}$ for bidentate lithium structures. The sodiated

structures showed more positive $\Delta G_{WaterAdduction}$ than the tridentate lithiated structures, suggesting that a value that more positive than -14 kcal/mol will not be able to adduct water.

4.4. Comparing Solvated and Vacuum Phase Structures

If all tri/tetradentate structures are unreactive, it would seem unlikely that galactose, mannose, and talose would form any reactive ions considering the lowest energy bidentate structures are much higher in energy than the lowest energy tri/tetradentate structures. This is especially true for talose, where the gas phase Gibb's free energy of the only bidentate structure was calculated 16 kcal/mol higher than the lowest energy, tetradentate structure. However, it is important to consider that these in vacuo calculations, and during the electrospray process, these ions are first solvated in aqueous droplets prior to being transferred into the gas phase. Therefore, it is possible that aqueous phase thermodynamics may determine which structures are formed. The lithium cationized molecule whose structure is dictated by solution phase thermodynamics could become kinetically trapped in that same orientation after being desolvated into the gas phase, even if that structure is not favorable in the gas phase.

As stated previously, all structures were first optimized (followed by a vibrational calculation) in the aqueous phase, and the resulting structures were subsequently optimized (followed by a vibrational calculation) in vacuo. This allowed a solution phase structure (and energy) to be linked to a resulting vacuum phase structure (and energy). The solution phase energies are shown in Figure 4.4, where an arrow is drawn to the resulting vacuum phase structure. The solution phase calculations show that bidentate structures are the lowest energy solvated structures for glucose, galactose, and mannose. Even more interesting, the only

bidentate structure for talose is the third most favorable in the solution phase, suggesting how lithium cationized talose may have some reactive fraction.

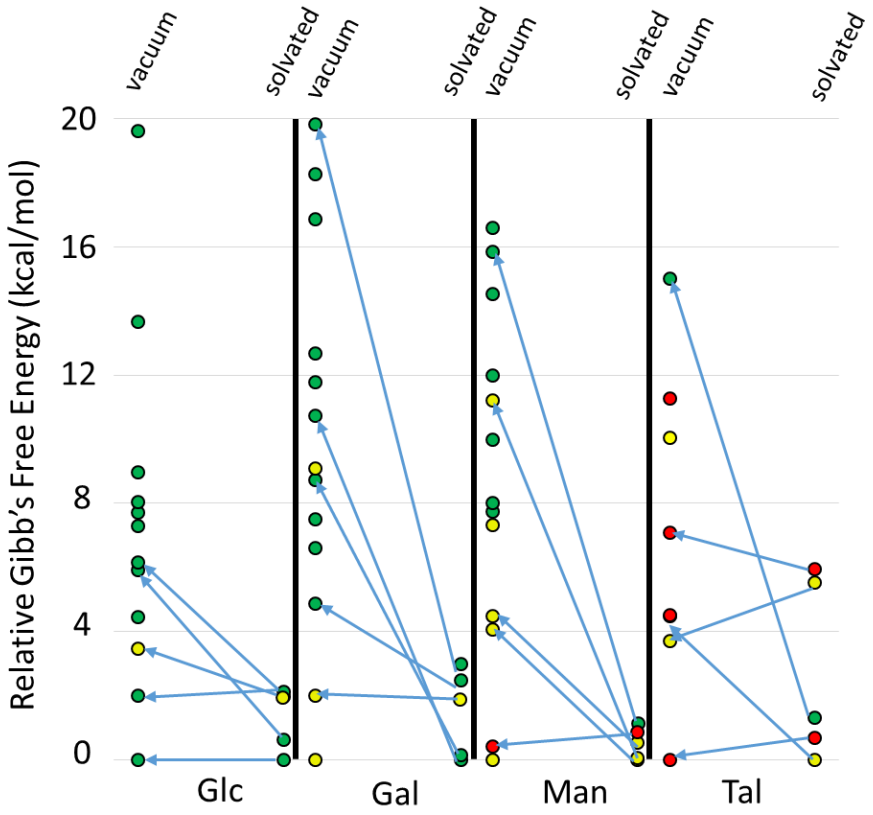

Figure 4.5. Each dot represents an optimized structure, and the vertical axis measures the relative Gibb's free energies from vibrational calculations (M06-2X/cc-pTVZ) after optimization (B3LYP/6-311++g(d,p)) in both solution phase and the gas phase. Energies for structures in the vacuum (left of each column) are relative to the lowest energy structure in vacuum for a given hexose, and solution phase energies (right of each column) are relative to lowest energy in solution phase for a given hexose. An arrow points connects the solution phase structure to the vacuum phase structure where the lithium cation is coordinated to the same oxygens i.e. for glucose the lowest energy structure in solution phase is also the lowest energy in vacuum; however, the second lowest energy structure is solution phase is

the fourth lowest in vacuum. Green, yellow, and red dots represent bidentate, tridentate, and tetradentate coordination's to the lithium cation, respectively.

The theory that bidentate structures are reactive while tri- and tetradentate are unable to adduct water is was further tested by experiments with lithium cationized 1,2-propandiol, 1,3-propandiol, and 1,2,3-propantriol. The decay curves for all three lithium cationized molecules can be seen in Figure 4.5. Though they react at different rates, both the dihydroxy compounds react to completion as expected when only bidentate structures can be formed. However, the 1,2,3-propantriol can form both bidentate and tridentate structures, allowing for some reactive species and some unreactive species. Thus, the decay curve asymptotes before all of the lithium cationized molecules adduct water because only 78% of the lithium cationized molecules are reactive (Figure 4.6).

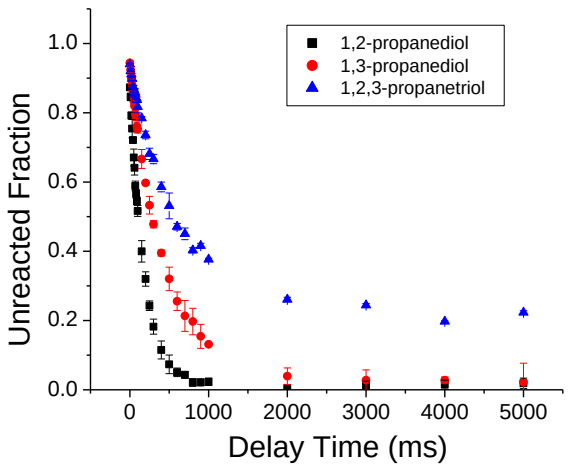

Figure 4.6: Exponential decay curves for the compounds with either 2 or 3 hydroxyl groups. Compounds with only two hydroxyl groups can only form bidentate interactions and are 100% reactive given a long enough time to react. The 1,2,3-propantriol can form tridentate interactions causing some ions to be unreactive, and the unreactive fraction is measured to be 0.22.

The theory that only bidentate structures are reactive was used to predict the relative unreactive fractions of α-methyl-glucoside and β-methyl-glucoside. These two species are easier to model computationally because only one anomer is present, and mutarotation between anomers is not possible with the methyl group bound to the anomeric oxygen (refer to Figure 4.1). Additionally, because there is only a small difference between the two structures at the anomeric carbon, differences in R_U can be easily assigned to a specific binding site. The previously described method for determining lithium cationized structures was used for both methyl glucosides (Figure 4.6). When starting from the $^4C_1$ conformation of both methyl glucosides, only bidentate structures were found for the α-anomer, and only a single structure for

the β-anomer was tridentate (Figure 4.6, structure b5). Based on these calculated structures for both anomers, it was determined that only the β-anomer should have a non-zero R_U, and the α-anomer should be completely reactive.

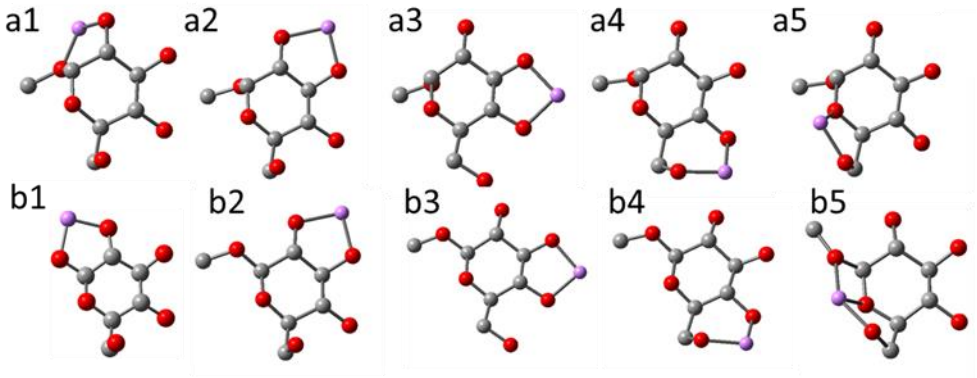

Figure 4.7: Optimized gas phase lithium cationized structures for alpha (a) and beta (b) methyl glucopyranoses when starting from the optimized $^4C_1$ chair conformation. All conformations remained in the $^4C_1$ chair after optimization. Structure b5 is the only tridentate structure for either anomer

Experimental results showed that this prediction was only partially true. The β-anomer did show a greater unreactive fraction than the α-anomer. However, the R_U for the α-anomer was non-zero (about 0.05) suggesting either some tridentate structure was able to form or there was a significant amount of noise at *m/z* 187. This seems unlikely because the only optimized tridentate structure was a boat conformation that is much less favorable in aqueous phase, and also not favorable in the gas phase. While the solution phase thermodynamics seem to dictate the conformation of ions transferred into the gas phase after electrospray ionization, the lithium cationized molecules could change conformation in the gas phase with enough added energy. An increase in internal energy can result from collisions with neutrals in the source of the mass spectrometer as the ions enter the beginning stages of the differential pumping region. The

pressure regime is high enough in this region of the mass spectrometer that collisions are still likely, but also low enough that ions have a long mean free path giving them time to accelerate and increase kinetic energy before collisions.

As ions are transferred from atmospheric pressure into differentially pumped regions of the mass spectrometer, their kinetic energy can be increased by increasing the voltages on the ion optics. The voltage difference between the exit of the inlet capillary and the first skimmer used to block neutral molecules from entering the high vacuum region of the mass spectrometer was systematically changed from 10 V to 100 V in 10 V increments, and the R_U of the ions passed through this region were subsequently measured (Figure 4.7). The β-anomer shows only a slight change in R_U as the voltage was increased; however, the α-anomer showed a drastic increase in the unreactive fraction as the voltage was increased. This is believed to be caused by an increase in the isomerization to a tridentate boat conformation as the amount of internal energy added to the gas phase ions is increased.

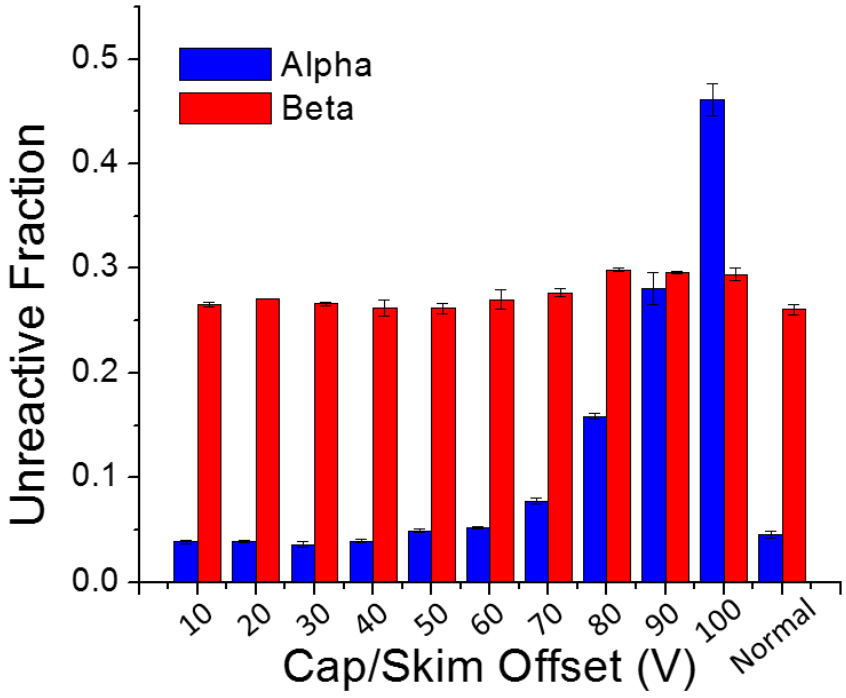

Figure 4.8. Experimental unreactive fractions and reaction rates for alpha and beta methyl glucopyranoses as a function of the voltage between the capillary and skimmer. The unreactive fraction of the alpha anomer increases as the lithiated molecule isomerizes from a bidentate chair conformation to a tridentate boat conformation in the gas phase. The bars labeled "Normal" refer to the voltages applied to the optics for maximum ion transmission of $[M+Li]^+$ (in these experiments 62 V).

Previous optimizations to determine likely lithiation sites were performed only considering the energetically favorable $^4C_1$ chair ring conformation. Based upon Crème-Pople parameters for pyranose rings there are two possible chair conformations, six unique boat conformations, and six unique skewboat ring conformations. Further calculations were performed starting from at least 6 different boat/skewboat conformations as well as the $^1C_4$ chair

conformation for both methyl glucosides as well as the four hexoses previously discussed to ensure that the entire conformational space of each of the molecules was thoroughly considered. These 6 or 7 boat/skewboat structures for each molecule (Figure 4.8) were chosen to represent as wide a range of conformations as possible (in contrast to selecting only boat/skewboat conformations from one portion of the possible conformational space). After performing the same method for determining likely lithiation sites and optimization of at B3LYP/6-311++G(d,p) level of theory, each of the molecules studied produced lithiated structures that were not previously found starting from the $^4C_1$ structure. Vibrational calculations of these structures showed that some of the vacuum phase boat structures were lower in Gibbs free energy than the most favorable chair conformations. These structures were always tri- or tetradentate structures, suggesting that increasing the number of coordination bonds to the lithium cation provides more than enough energy to offset the increased energy caused by the newly induced ring strain.

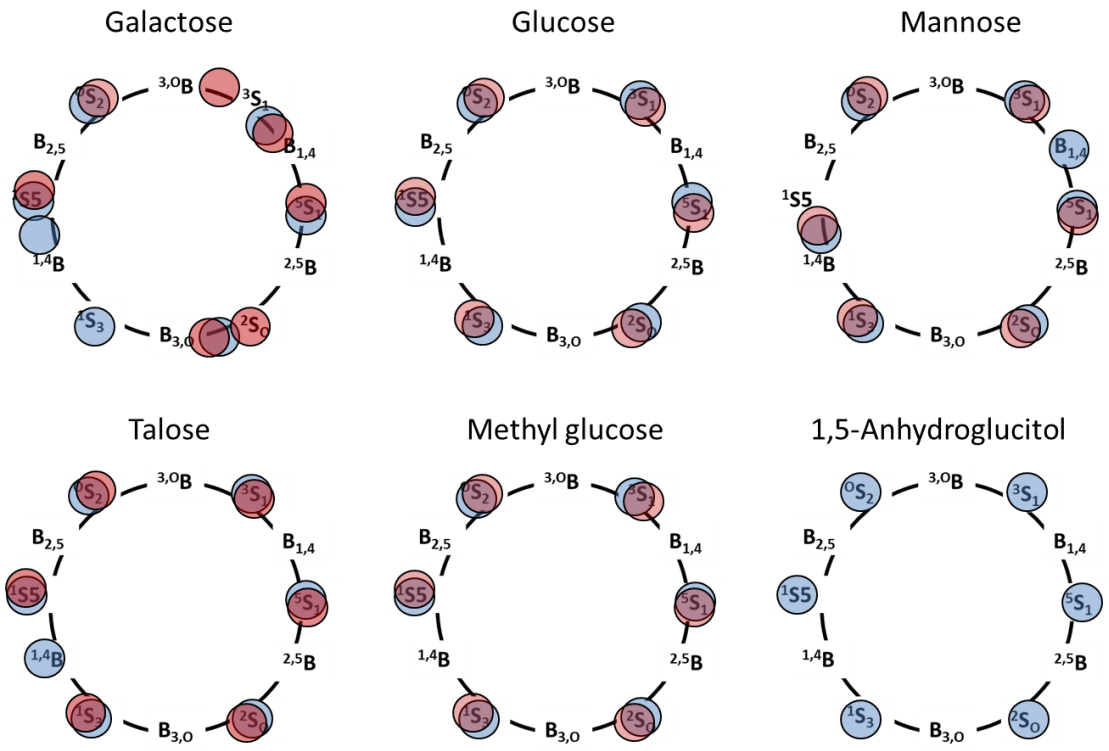

Figure 4.8: Each circle represents the ring conformation of the optimized starting structures used for subsequent calculations (addition of a lithium cation). Blue circles represent an alpha anomer, and red circles indicate a beta anomer, except for 1,5-anhydroglucitol where the anomeric hydroxyl is replaced by a hydrogen.

When comparing the methyl glucosides, both anomers optimize to a boat structure that is more favorable in the vacuum phase than the previously discussed chair conformations. This structure involves coordination of the lithium cation to the 4-hydroxyl, 6-hydroxyl, and ring hydroxyl. However, this boat structure is not favorable in solution phase and unlikely to form prior to collisional activation of the ions in the ion optics of the mass spectrometer based on the relatively high energy of the boat structure with an implicit aqueous solvent. Considering the structures that are likely to be produced based on aqueous phase calculations, the most likely structures to produce this boat structure are those where the lithium cation is already bound to at least one of the oxygen atoms coordinated in the tridentate boat. For the alpha anomer it seems the most energetically favorable to start from the chair structure where the lithium cation is already bound to the 6-hydroxy and ring oxygen, so that the transition state will not require the breaking of any coordination bonds. The tridentate boat for the β-anomer could likely be formed from the analogous structure where the lithium cation is coordinated to the 1-hydroxy, 6-hydroxy, and the ring oxygen. This would require breaking the coordination between the 1-hydroxy and the lithium cation, and because the chair and the boat conformation are tridentate, no difference would be observed on the R_U even if the conformation change occurs. This demonstrates that the theoretical model helps explain why R_U can be changed for alpha anomer and not the beta anomer based on small differences in their structures.

Further confirmation of the differences in R_U of the anomers was tested by removing the oxygens completely (deoxyglucose molecules). Two more glucose analogs, each with a single oxygen removed from the system were studied with calculations and experimentally. The first molecule, 1,5-andydroglucitol, is structurally identical to the methyl glucoside compounds except with a hydrogen in place of the anomeric methoxide (refer to Figure 4.1). Because the anomeric carbon is no longer present, the tridentate structure that was likely to form in solution between the 1-hydroxy, 6-hydroxy, and ring oxygen for the β-anomer is no longer a possibility. Therefore the R_U of 1,5-anhydroglucitol should be much more similar to α-methyl-glucoside than β-methyl-glucoside. Calculations were performed starting from both the $^4C_1$ and $^1C_4$ structures as well as 6 other skew boat conformations. These showed that the likely aqueous phase structures are similar to those for the α-methyl-glucoside, and that the lowest energy gas phase structures are tridentate boats. This suggests not only that R_U should be very small, but also that R_U should increase as the voltage between the exit capillary and skimmer is increased. The second deoxyglucose studied, 2-deoxyglucose, was used as a control, ensuring that simply removing one oxygen from the methyl glucoside molecules does not guarantee a small R_U. Calculations show that the β-anomer of 2-deoxyglucose exists and tridentate structures can be formed in the energetically favorable $^4C_1$ conformation.

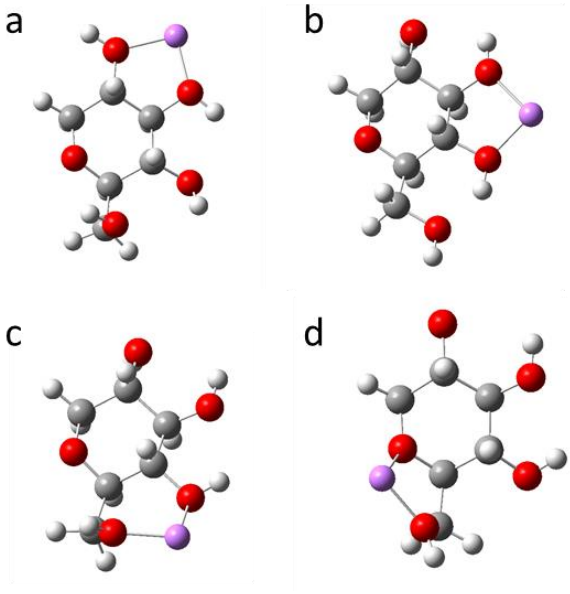

Figure 4.10. Lithiated structures for the $^4C_1$ ring conformation of 1,5-anhydroglucitol. All structures in the $^4C_1$ conformation are bidentate.

Experimental results with 1,5-andydroglucitol showed that the R_U is exceptionally low (less than 5% was unreactive) as expected, because no tridentate structures are predicted when limited to the $^4C_1$ chair conformation. The 2-deoxyglucose has a relatively large R_U (0.695 +/- 0.007), further demonstrating the small R_U measured for 1,5-anhydrosorbitol is caused specifically by the removal of the anomeric oxygen and not caused by simply having fewer total oxygens. As the voltages in the ion optics of the source were increased, the measured R_U for 1,5-anhydrosoribitol also increases, believed to be caused by isomerization to a tridentate structure in the gas phase. These observations demonstrate that the water adduction characteristics, including R_U and how R_U will change as internal energy is added to the gas phase ions can be approximated based upon theoretical calculations. Ideally, the relative difference in Gibb's free energy between the likely aqueous phase structures could be used to calculate R_U based on the fraction of species that are expected to be bidentate versus tri- and tetradentate. However, this

calculation becomes convoluted by the fraction of ions that will isomerize because of increased internal energy added during the electrospray process by collisions occurring in the electric field or subsequently by collisions while passing through the source region into the mass spectrometer. If not for these processes which alter the expected solution phase structures to structures more favored in the gas phase, the fraction of bidentate structures should be easily calculated.

Levoglucosan (1,6-anhydro-β-glucose) is a carbohydrate molecule derived from glucose (Figure 4.1). Its bicyclic ring structure and single anomer restrict the conformational space of the molecule, making it significantly easier to model than the previously discussed molecules. This rigid structure also allows the presumption that the lithium cation will not change from a bidentate coordination to a tridentate coordination during electrospray or after desolvation.

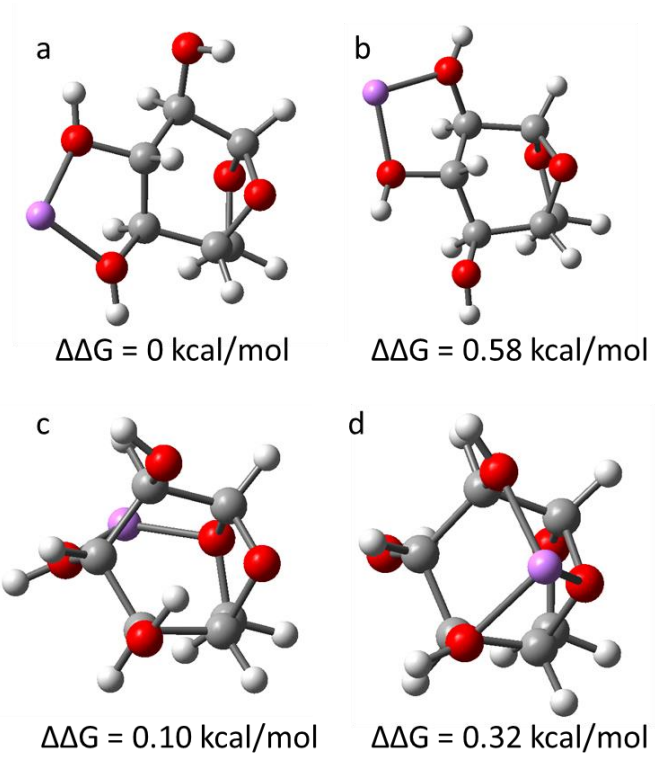

Figure 4.11. The only four lithium cationized structures for levoglucosan. Energies shown are calculated with an implicit aqueous solvent and relative to the lowest energy structure (a). The only tridentate structure is shown as structure d.

Only four different locations for the lithium cation to coordinate were found. Vibrational calculations were performed on both the aqueous and gas phase theoretical structures. The relative percentage of tridentate structures can be calculated from the relative Gibbs free energies with the following equation which assumes a Boltzmann distribution,

$$K_{eq} = e^{\frac{-\Delta G}{kT}} \qquad \text{Equation 4.1}$$

where T is the absolute temperature and k is the Boltzmann constant. The temperature in this calculation would be based on the effective temperature of the electrospray process, which is not well known and will vary slightly between different mass spectrometers and ionization sources. Recently, experimental and theoretical data predicted the effective temperature around 650 K for the electrospray source studied[33]. Because of this uncertainty, the same calculation is performed at a variety of realistic temperatures. Calculations with temperature between 300 and 750 K provide a R_U (shown in Table 5.2) that very closely match the experimental R_U measured for levoglucosan (0.22 +/- 0.02, shown in Figure 5.11). This prediction is made easier because of the relatively small conformation space of levoglucosan compared to other carbohydrate and carbohydrate like molecules.

Table 4.2: **The calculated unreactive fraction at different temperatures for levoglucosan**

Temp (K)	Unreactive percentage
300	20.9
350	21.6

400	22.1
450	22.5
500	22.8
550	23.0
600	23.2
650	23.4
700	23.5
750	23.6

Experimental evidence demonstrates that increasing the voltages in the ion optics does have an effect on the measured R_U, but this effect is relatively small compared to α-methyl glucoside. The R_U could potentially be calculated for other molecules if the conformational space is very restricted such as for levoglucosan, and if the process of transferring of ions into mass spectrometer be as gentle as possible so that solution phase structures are conserved.

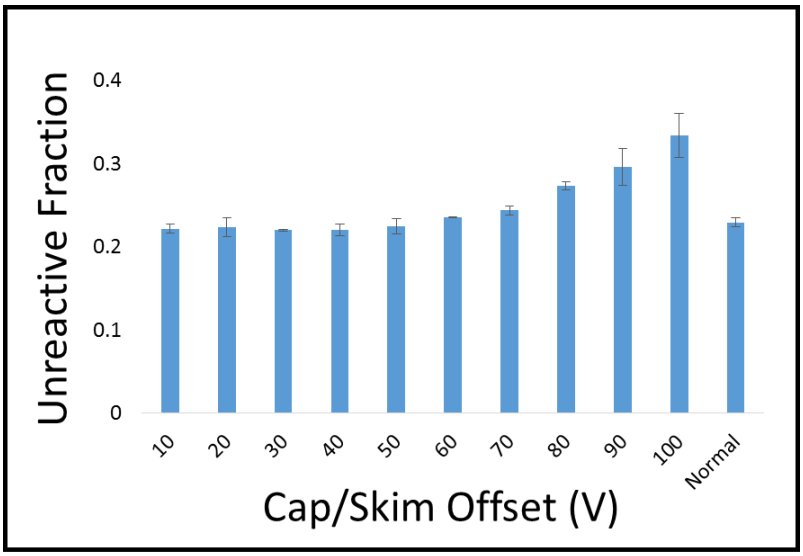

Figure 4.12. Experimental unreactive fractions and reaction rates for levoglucosan as a function of the voltage between the capillary and skimmer. The unreactive fraction only increases slightly as the voltage difference is increased. The bar labeled "Normal" refers to

the voltages applied to the optics for maximum ion transmission of $[M+Li]^+$ (in these experiments 55.5 V).

4.5. Summary

Water adduction can be observed to metal cationized molecules while they are trapped in a quadrupole ion trap mass spectrometer[34,35]. Using a quadrupole ion trap allows for the water adduction reaction time to be easily controlled, allowing for easy measurements of reaction rates. In the case of carbohydrates, some portion of the ions are unreactive, and the fraction of both reactive ions and unreactive ions can be measured. The chemistry dictating the unreactive fraction was investigated both experimentally and computationally, and these results show that a lithium cation bound to three or more oxygen atoms is not able to bind water in the quadrupole ion trap. Only bidentate structures are reactive. By calculating the relative Gibbs free energy of the solution phase ions and determining the number of coordination bonds after desolvation, the unreactive fraction can be predicted, given the ions are unable to isomerize being transferred into the gas phase. This suggests that solution phase structures are retained during the transfer of ions from solution to the gas phase during ESI. This subject is highly debated area in the field of mass spectrometry[8-10].

When modelling metal adducted carbohydrates in the gas phase, the entire conformational space must be analyzed including both chair and boat/skewboat structures. Previous studies have made the assumption that only structures with the pyranose ring in the most stable chair conformation are sufficient for modeling; however, this is likely inadequate because increased number of coordination bonds is more favorable than the increase in energy caused by ring strain. Calculations were performed on levoglucosan with an implicit aqueous

solvent. The Gibbs free energies were used to calculate the abundance of each structure assuming a Boltzmann distribution at temperatures ranging from 300 to 750 K. Previous experiments have shown the effective temperature of ESI could reach temperatures of 650 K during some point in the electrospray process. The calculations show that from 300 K to 750 K the unreactive fraction would be expected to increase from 0.209 to 0.236. These calculated unreactive fractions are very close to the experimental value of 0.22 +/- 0.02.

REFERENCES

1 J. B. Fenn, M. Mann, C. K. Meng, S. F. Wong and C. M. Whitehouse, Electrospray ionization for mass spectrometry of large biomolecules, *Science (80-.).*, 1989, **246**, 64.

2 A. J. R. Heck and R. H. H. van den Heuvel, Investigation of intact protein complexes by mass spectrometry, *Mass Spectrom. Rev.*, 2004, **23**, 368–389.

3 T. R. Covey, B. A. Thomson and B. B. Schneider, Atmospheric pressure ion sources, *Mass Spectrom. Rev.*, 2009, **28**, 870–897.

4 G. J. V. B. and V. Kertesz, G. J. Van Berkel and V. Kertesz, Using the electrochemistry of the electrospray ion source, *Anal. Chem.*, 2007, **79**, 5510–5520.

5 N. B. Cech and C. G. Enke, Practical implications of some recent studies in electrospray ionization fundamentals, *Mass Spectrom. Rev.*, 2002, **20**, 362–387.

6 X. Wu, R. D. Oleschuk and N. M. Cann, Characterization of microstructured fibre emitters: in pursuit of improved nano electrospray ionization performance, *Analyst*, 2012, **137**, 4150.

7 P. P. Kebarle and U. H. Verkerk, Electrospray: from ions in solution to ions in the gas phase, what we know now., *Mass Spec. Rev.*, 2009, **28**, 898–917.

8 L. Konermann, E. Ahadi, A. D. Rodriguez and S. Vahidi, Unraveling the mechanism of electrospray ionization, *Anal. Chem.*, 2013, **85**, 2–9.

9 E. Ahadi and L. Konermann, Surface charge of electrosprayed water nanodroplets: A molecular dynamics study, *J. Am. Chem. Soc.*, 2010, **132**, 11270–11277.

10 E. Ahadi Konermann,L., Modeling the Behavior of Coarse-Grained Polymer Chains in Charged Water Droplets: Implications for the Mechanism of Electrospray Ionization, *J. Phys. Chem. B*, 2012, **116**, 104–112.

11 D. N. Mortensen and E. R. Williams, Investigating Protein Folding and Unfolding in Electrospray Nanodrops Upon Rapid Mixing Using Theta-Glass Emitters, *Anal. Chem.*, 2015, **87**, 1281–1287.

12 C. J. Hogan, J. A. Carroll, H. W. Rohrs, P. Biswas and M. L. Gross, Combined charged residue-field emission model of macromolecular electrospray ionization, *Anal. Chem.*, 2009, **81**, 369–377.

13 J. A. Loo, Electrospray ionization mass spectrometry: A technology for studying noncovalent macromolecular complexes, *Int. J. Mass Spectrom.*, 2000, **200**, 175–186.

14 J. A. Loo, Studying noncovalent protein complexes by electrospray ionization mass spectrometry, *Mass Spectrom. Rev.*, 1998, **16**, 1–23.

15 H. Higashi, T. Tokumi, C. J. Hogan, H. Suda, T. Seto and Y. Otani, Simultaneous ion and neutral evaporation in aqueous nanodrops: experiment, theory, and molecular dynamics

simulations, *Phys. Chem. Chem. Phys.*, 2015, **17**, 15746–15755.

16 D. Kim, N. Wagner, K. Wooding, D. E. Clemmer and D. H. Russell, Ions from Solution to the Gas Phase: A Molecular Dynamics Simulation of the Structural Evolution of Substance P during Desolvation of Charged Nanodroplets Generated by Electrospray Ionization, *J. Am. Chem. Soc.*, 2017, **139**, 2981–2988.

17 T. Wyttenbach and M. T. Bowers, Structural stability from solution to the gas phase: Native solution structure of ubiquitin survives analysis in a solvent-free ion mobility-mass spectrometry environment, *J. Phys. Chem. B*, 2011, **115**, 12266–12275.

18 A. T. Iavarone and E. R. Williams, Mechanism of charging and supercharging molecules in electrospray ionization, *J. Am. Chem. Soc.*, 2003, **125**, 2319–2327.

19 L. L. MACK, P. KRALIK, A. RHEUDE and M. DOLE, Molecular Beams of Macroions .2., *J. Chem. Phys.*, 1970, **52**, 4977-.

20 R. G. McAllister, H. Metwally, Y. Sun and L. Konermann, Release of Native-like Gaseous Proteins from Electrospray Droplets via the Charged Residue Mechanism: Insights from Molecular Dynamics Simulations, *J. Am. Chem. Soc.*, 2015, **137**, 12667–12676.

21 J. Fernandez De La Mora, Electrospray ionization of large multiply charged species proceeds via Dole's charged residue mechanism, *Anal. Chim. Acta*, 2000, **406**, 93–104.

22 J. V. Iribarne, On the evaporation of small ions from charged droplets, *J. Chem. Phys.*, 1976, **64**, 2287.

23 P. Kebarle and M. Peschke, On the mechanisms by which the charged droplets produced by electrospray lead to gas phase ions, *Anal. Chim. Acta*, 2000, **406**, 11–35.

24 M. T. Campbell, D. Chen, N. J. Wallbillich and G. L. Glish, Distinguishing Biologically Relevant Hexoses by Water Adduction to the Lithium Cationized Molecule, *Anal. Chem.*, 2017, acs.analchem.7b02647.

25 M. T. Campbell, D. Chen and G. L. Glish, Identifying the D-Pentoses Using Water Adduction to Lithium Cationized Molecule, *J. Am. Soc. Mass Spectrom.*, 2017, **28**, 1420–1424.

26 M. T. Campbell, D. Chen and G. L. Glish, Distinguishing Linkage Position and Anomeric Configuration of Glucose–Glucose Disaccharides by Water Adduction to Lithiated Molecules, *Anal. Chem.*, 2018, acs.analchem.7b04162.

27 F. A. Momany, M. Appell, J. L. Willett, U. Schnupf and W. B. Bosma, DFT study of α- and β-d-galactopyranose at the B3LYP/6-311++G** level of theory, *Carbohydr. Res.*, 2006, **341**, 525–537.

28 M. Appell, G. Strati, J. L. Willett and F. A. Momany, B3LYP/6-311++G** study of α- and β-d-glucopyranose and 1,5-anhydro-d-glucitol: 4C1 and 1C4 chairs, 3,OB and B3,O boats, and skew-boat conformations, *Carbohydr. Res.*, 2004, **339**, 537–551.

29 U. Schnupf, J. L. Willett and F. Momany, DFTMD studies of glucose and epimers: anomeric ratios, rotamer populations, and hydration energies, *Carbohydr. Res.*, 2010, **345**, 503–511.

30 Y. Zhao and D. G. Truhlar, The M06 suite of density functionals for main group thermochemistry, thermochemical kinetics, noncovalent interactions, excited states, and transition elements: Two new functionals and systematic testing of four M06-class functionals and 12 other function, *Theor. Chem. Acc.*, 2008, **120**, 215–241.

31 G. I. Csonka, A. D. French, G. P. Johnson and C. a Stortz, Evaluation of Density Functionals and Basis Sets for Carbohydrates, *J. Chem. Theory Comput.*, 2009, **5**, 679–692.

32 W. M. C. Sameera and D. A. Pantazis, A Hierarchy of Methods for the Energetically Accurate Modeling of Isomerism in Monosaccharides, *J. Chem. Theory Comput.*, 2012, **8**, 2630–2645.

33 J. E. Carpenter, C. P. McNary, A. Furin, A. F. Sweeney and P. B. Armentrout, How Hot are Your Ions Really? A Threshold Collision-Induced Dissociation Study of Substituted Benzylpyridinium 'Thermometer' Ions, *J. Am. Soc. Mass Spectrom.*, 2017, **28**, 1876–1888.

34 O. Hernandez, S. Isenberg, V. Steinmetz, G. L. Glish and P. Maitre, Probing Mobility-Selected Saccharide Isomers: Selective Ion–Molecule Reactions and Wavelength-Specific IR Activation, *J. Phys. Chem. A*, 2015, **119**, 6057–6064.

35 Y. Zhu, H. A. Roy, N. A. Cunningham, S. F. Strobehn, J. Gao, M. U. Munshi, G. Berden, J. Oomens and M. T. Rodgers, IRMPD Action Spectroscopy, ER-CID Experiments, and Theoretical Studies of Sodium Cationized Thymidine and 5-Methyluridine: Kinetic Trapping During the ESI Desolvation Process Preserves the Solution Structure of [Thd+Na]+, *J. Am. Soc. Mass Spectrom.*, 2017, 1–15.

CHAPTER 5: DISTINGUISHING DISACCHARIDE ISOMERS INCLUDINGANOMERIC CONFIGURATION AND LINKAGE POSITION

5.1 Overview of Techniques for Distinguishing Disaccharides

Dissociative techniques are often used to differentiate isomeric compounds and have been used to distinguish some linkage positions and anomeric configurations of disaccharides. The viability of these dissociative techniques is often proven by analyzing and distinguishing an array of glucosyl-glucose disaccharides varying in linkage position and anomericity. Previously, collision induced dissociation (CID) has been used to distinguish the linkage position for several disaccharides.[1,2] CID was then used to determine the anomericity of several disaccharides that were derivatized with Zn(II)-diethylenetriamine chloride prior to mass spectral analysis.[3] Since then other methods have been developed to determine linkage position and the anomericity of some linkages which do not require a prior derivatization step[4–11]. Most of these methods report relatively high concentrations (typically ≥ 100 μM) to provide sufficient signal intensity to confidently distinguish isomers. Large concentrations are necessary for determining the anomericity of the linkage because there are only very small differences in product ions ratios. However, these methods did not demonstrate the ability to distinguish linkage position and anomericity for both reducing and non-reducing disaccharides. Infrared multi-photon dissociation has also been used to determine some linkage position and anomericity of some disaccharides but requires separate MS/MS experiments and the additional cost and complexity of a tunable CO_2 laser.[12,13] Recently, a method was reported that was capable of distinguishing linkage position and anomeric configuration for both reducing and non-reducing disaccharides

by measuring collisional cross-section of the MS^2 product.[14] However, this method requires the extra cost/complexity of the Traveling Wave Ion Mobility Cell.

Here, a method was developed using just a quadrupole ion trap mass spectrometer to distinguish both the linkage position and anomeric conformation of an exhaustive list of reducing glucosyl-α/β(1→x)-glucose compounds (where x = 2, 3, 4, 6) as well as two non-reducing glucosyl-glucose compounds (α1→α1 and α1→β1) as illustrated in Figure 4.1. Three other disaccharides which contain monomers other than glucose were also distinguished including two of the most common naturally occurring disaccharides, lactose and sucrose, and one synthetic disaccharide, lactulose.

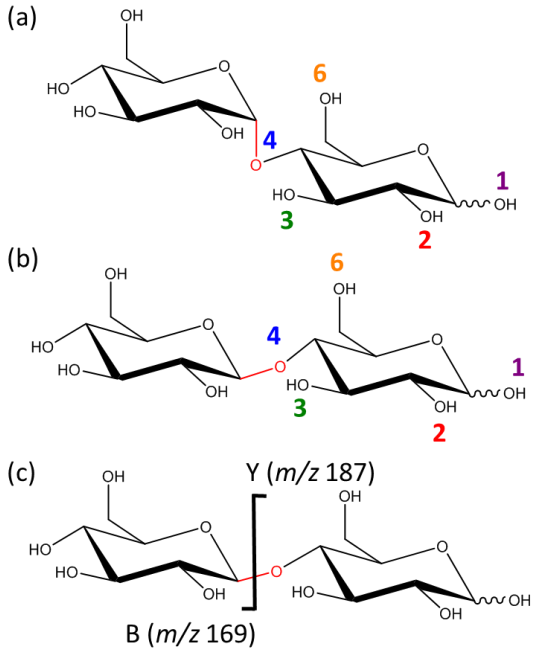

Figure 5.1. Disaccharides studied differ by the linkage position 1, 2, 3, 4, or 6 and anomeric configuration shown as (a) alpha and (b) beta. Part (c) shows Domon-Costello nomenclature for the product ions used in experiments after CID.

Electrospray ionization of disaccharides with standard solvents (e.g. MeOH, ACN, or H_2O) usually produces $[M+Na]^+$. During CID of $[M+Na]^+$ the sodium cation is the primary product ion formed, providing no structural information about the molecule.[15] Addition of a lithium salt to the solution results in $[M+Li]^+$ being formed. Research over the past couple of decades has shown that CID of lithium cationized disaccharides results in some cross-ring cleavages providing information about the linkage position of the disaccharides.[1,2,16] However, the most abundant product ions result from cleavage of the glycosidic bond, denoted as B and Y type ions (Figure 5.1, part c).

The product ions *m/z* 187 and *m/z* 169 formed from CID of the disaccharide were found to adduct water while in the quadrupole ion trap similarly to lithium cationized monosaccharides which undergo the same reaction.[17] The water adduction reaction between a lithiated carbohydrate and water in a quadrupole ion trap has previously been used to distinguish pentose epimers[18] and hexose epimers[19] (Chapter 3). Here, the water adduction reaction is first studied individually for the product ions *m/z* 187 and *m/z* 169 to demonstrate that two product ions each provide unique information about the disaccharide. For example, the water adduction reaction used with only the *m/z* 187 product ion is sufficient for distinguishing all disaccharides studied, but using the *m/z* 169 product ion can help increase the confidence of assigning structures to the parent disaccharide. The water adduction reaction can also be monitored for both product ions simultaneously to determine both linkage position and anomericity in a single experiment.

5.2 Water Adduction to Disaccharide Standards

Previous experiments using water adduction to distinguish monosaccharides began with isolation of the monosaccharide of interest. A delay time was added between isolation and detection for the water adduction reaction to occur, and this reaction was used to distinguish

epimers. The same procedure was applied to disaccharides. However, after isolation of the lithiated disaccharide (*m/z* 349), no water adduction is observed. Previous studies using Density Functional Theory calculations show the most likely binding site for metal cations to disaccharides is between the two monomer hexoses, maximizing the number of bonds coordinated to oxygen atoms.[1,20] Experimental and theoretical results have shown for a hydrated lithium cation the bond energy decreases as each subsequent water is added.[21] A similar effect is expected here. That is, if the lithium cation is coordinated to several oxygen atoms of the disaccharide, water adduction will not be favorable (more details in Chapter 5). The only way to enable water adduction would be to break some coordination bonds, which can be achieved by CID. After CID the product ions will likely have fewer bonds to the lithium cation compared to the larger parent ion, enabling the water adduction reaction.

CID of the disaccharides produces several peaks, including peaks corresponding to cleavage of the glycosidic bond linking the two monomers at *m/z* 187 and *m/z* 169. These product ions were chosen for water adduction experiments because they are present after CID of all disaccharides studied. Previously, CID of lithiated disaccharides with an O^{18} labeled anomeric oxygen (labeled 1 in Figure 4.1) were used to determine if the each product ions *m/z* 187 and *m/z* 169 consisted of reducing end, non-reducing end, or a mixture of both. Cleavage occurs only on the non-reducing side of the glycosydic bond, producing only B and Y type ions.[1,2] Experiments with product ion *m/z* 187 are discussed first, and the same experiments with *m/z* 169 are subsequently discussed.

After CID of the parent disaccharide ion at *m/z* 349, the product ion of *m/z* 187 was isolated in the quadrupole ion trap where it adducted water. Isolation of *m/z* 187 serves as time = 0 for the water adduction reaction. After isolation, a delay time is used to control the reaction

time before mass analysis. Peaks are observed for the water adducted species (*m/z* 205) and the non-adducted species (*m/z* 187). Two parameters of the water adduction reaction are measured. First, just as with the monosaccharides in Chapter 3, some of the product ions (for both *m/z* 169 or *m/z* 187) will adduct water and others will not. The maximum reaction time needed to hydrate all of the reactive (water binding) product ions is about 700 ms for the species with the slowest reaction rates. The number of ions that are unable to adduct water can be measured by the signal intensity of *m/z* 187 (I_{187}), and the number of reactive ions can be measured by the signal intensity at *m/z* 205 (I_{205}). The unreactive fraction of ions, R_U, was measured as $(\frac{I_{187}}{I_{187} + I_{205}})$ after 1,000 ms delay time. The unreactive fractions of the *m/z* 187 product ions were measured for each disaccharide after dissociation at several different CID voltages. The unreactive fractions were found to be very reproducible at all CID voltages used (RSD typically less than 2%).

The reaction rate of water adduction was also measured for the product ions. As previously stated, only a fraction of the ions are reactive, and the unreactive ions should be excluded from the reaction rate calculation. The equation shown in Chapter 3 was used to calculate the reaction rate while excluding the unreactive fraction. Plotting $\ln(R_R)$ versus time results in linear plots as expected for pseudo-first order kinetics (Figure 4.2).

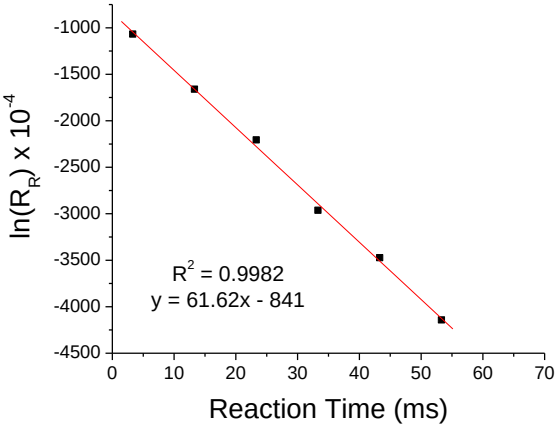

Figure 5.2: ln(R_R) versus reaction time for water adduction to the m/z 187 product ion of maltose (α1→4) after using a CID amplitude of 0.45 V

When measuring the water adduction reaction rate, pseudo-first order kinetics were assumed because the concentration of water in the quadrupole ion trap is expected to greatly exceed concentration of ions.[19] The generic first order kinetics equation for a reactant, A, $\frac{A_t}{A_0} = -k't$, was therefore used to measure the water adduction reaction kinetics. In our system A_t, the concentration of reactant at any time, t, can be represented by I_{187}, and A_0, the initial concentration of reactant, can be represented by the sum of $I_{187} + I_{205}$, assuming negligible ion loss during trapping and ejection. Finally, the measured rate constant is k', where $k' = k[H_2O]$. The concentration of water in the quadrupole ion trap is unknown; however, experiments have very reproducible reaction rates even over several months, suggesting that the water concentration remains quite constant.

Analogous experiments from solutions prepared in D_2O and CD_3OD demonstrated that the water in the QIT does not come from the electrospray solvent. The water adduct still showed a mass shift of 18 and not 20 as would be expected for D_2O adduction. Additionally, a moisture trap (Agilent Technologies, part num. BMT-4) was added to the nitrogen gas line prior to the inlet for the dry gas. The dry gas in the Bruker QIT instruments is heated and delivered coaxially to the inlet capillary. The delivered dry gas should be the only gas which is pulled into the inlet capillary of the mass spectrometer.

CID fragmentation amplitude settings of 0.45, 0.65, 0.85, 1.05, and 1.25 V were used to determine the effect of increased collision energy on the subsequent water adduction reaction (Figure 5.3). The unreactive fraction remains relatively constant as the CID voltage is increased for each of the disaccharides containing a β-glycosydic linkage. However, there is a statistically

significant increase in the unreactive fraction when comparing adduction after CID at 0.45 V to 0.65 V for disaccharides with an α-glycosydic linkage. The change in unreactive fraction is likely attributed to the excess energy imparted by CID rearranging one of many reactive lithium-glucose structures to a more energetically favorable unreactive structure. Using fragmentation amplitudes lower than 0.45 V provides insufficient collision energy to provide enough signal intensity of the product ions to measure the reaction rate and unreactive fraction with high precision. There is little effect observed on the reaction rate of disaccharides containing a β-glycosidic linkage as the CID voltage is increased. The disaccharides with α-glycosidic linkages exhibit a statistically significant decrease ($p < 0.01$) in reaction rate as the CID voltage is increased from 0.45 V to higher CID voltages. As discussed previously, the excess internal energy likely enables rearrangement of the lithium-glucose complex after CID, and some reactive structures may isomerize to form unreactive structures (studied in greater detail in Chapter 5). This data suggests that there are multiple reactive structures, and these reactive structures that are isomerized to unreactive structures likely have faster kinetics than other reactive structures that are retained.

Combining both the unreactive fraction and reaction rate (Figure 4.4) allows all thirteen of the disaccharides studied to be distinguished at all CID voltages used (0.85 V shown in Figure 4.3). The most difficult disaccharides to distinguish using only *m/z* 187 were maltose (α1→4) from cellobiose (β1→4), and nigerose (α1→3) from laminarbiose (β1→3) with p-values of 0.001 and 0.028, respectively, using Student's t-test. Linkage positions were found to be easier to distinguish than the anomeric conformation, as the two anomers for each linkage position cluster together with the exception of two (1→1) disaccharides. The differences in the unreactive ratio and water adduction reaction rate likely results from differences in favorable binding sites after

CID. As noted, previous experiments have shown that the product ion *m/z* 187 of reducing disaccharides is solely comprised of non-reducing end of the disaccharide.[2,16] Before CID the lithium cation likely binds between the two hexose monomers. Therefore, after CID the lithium is most likely bound to oxygen atoms close to the oxygen that previously served as the glycosidic linkage, and these unique binding sites lead to unique water adduction properties.

The same experiments previously described for the *m/z* 187 product ion (Y type ion) were used to measure reaction rate and the unreactive fraction were applied to the *m/z* 169 product ion (B type ion). The unreactive fraction and adduction rate measured for *m/z* 169 were found to differ greatly from the *m/z* 187 for all the disaccharides studied (Figure 4.4, bottom). The *m/z* 169 peak yields drastic differences in unreactive ratio and reaction rate when comparing anomeric configuration, but the differences in linkage positions are not as pronounced. Therefore, results obtained for *m/z* 187 are better for determining differences in linkage position, and results for *m/z* 169 are better for determining anomeric configuration. The tendency for each product ion to more easily distinguish different properties of the disaccharide is likely a result of the lithium coordination between the two monomer units prior to CID. If the lithium cation remains with the non-reducing end (product ion *m/z* 169), the lithium cation will likely still be coordinated to oxygens near the anomeric oxygen that was used to form the glycosidic linkage prior to dissociation. Therefore, the lithium cation is limited to the 2-hydroxyl, ring oxygen, and hydroxymethyl for all disaccharides regardless of linkage position of the reducing end. The only difference between the disaccharides dictating where the lithium is likely to bind is the anomericity of the glycosidic linkage before CID. Thus, anomericity is confidently distinguished by water adduction to *m/z* 169 and linkage position is not. Conversely, if the lithium remains with the reducing end (and thus the product ion will be *m/z* 187), the lithium cation will likely

remain coordinated to oxygens that were used in the glycosidic linkage. Therefore, as the linkage position changes, the lithium will be in chemically different environments, changing the kinetics and thermodynamics of the water adduction reaction. Thus, with product ion *m/z* 187 linkage position can be more confidently distinguished than anomericity.

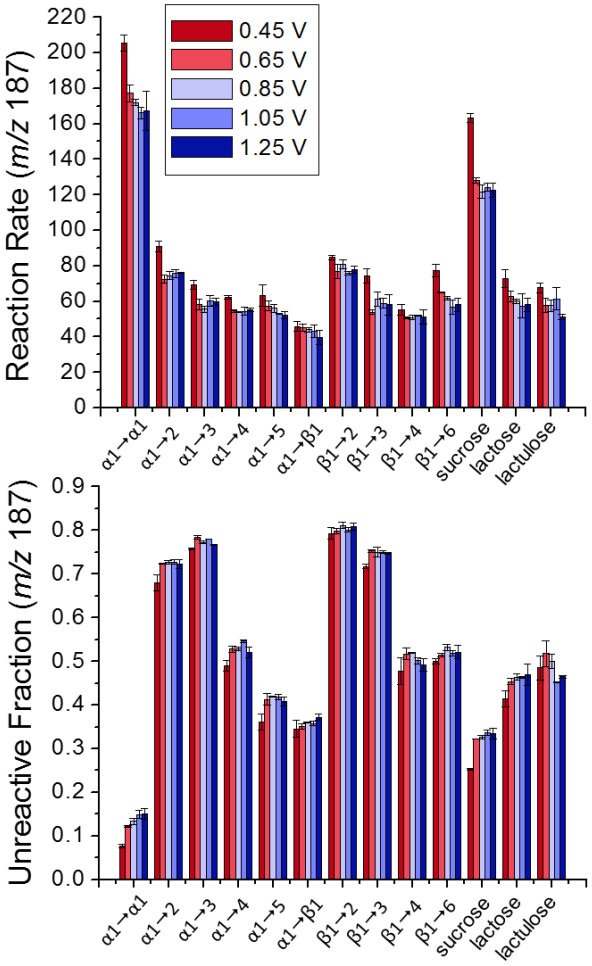

Figure 5.3. Reaction rates (top) and unreactive fractions (bottom) for each of the 10 Glc-Glc disaccharides studied as a function of CID fragmentation amplitude

These results demonstrate that using multiple product ions provide complementary information for identification of the disaccharide. Measuring the reaction rate and the unreactive fraction for both *m/z* 187 and *m/z* 169 allows all disaccharides to be distinguished with $p < 0.001$.

Using other product ions beyond *m/z* 187 and *m/z* 169 could provide further information to increase the confidence when assigning structures to disaccharides. Using other product ions besides *m/z* 187 is unnecessary for the subset of disaccharides studied here, but other product ions such as cross-ring cleavages could be useful when studying a significantly larger array of different disaccharides.

The water adduction reaction was applied to other biologically relevant disaccharides, sucrose, lactose, and lactulose, containing hexoses other than glucose. Sucrose (glucosyl-α(1→2)β-fructose) is a non-reducing disaccharide containing glucose and fructose. Lactose (galactosyl-β(1→4)-glucose)and lactulose (galactosyl-β(1→4)-fructose) are reducing disaccharides. The unreactive ratio and water adduction reaction rates were measured with same method previously described at each CID voltage. All three are able to be distinguished from the previous ten disaccharides studied (Figure 4.4). These experiments show that the water adduction method could be extended beyond disaccharides that contain solely glucose.

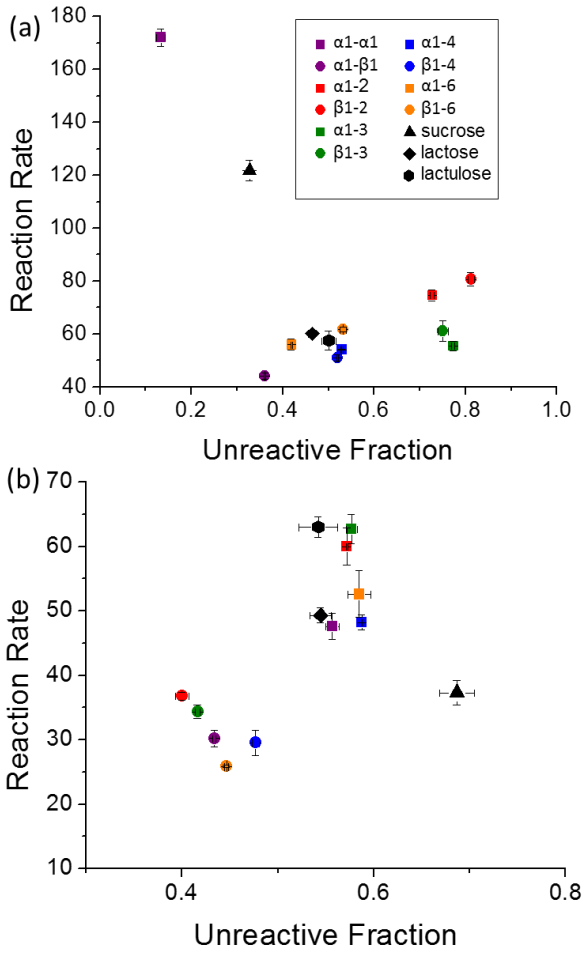

Figure 5.4: Plot of reaction rate versus unreactive fraction for each of the 10 Glc-Glc Disaccharides studied for the product ions m/z 187 (top) and m/z 169 (bottom) after CID with 0.85 V

The effect of analyte concentration on the water adduction reaction was studied using maltose. Several solutions were prepared in 50:50 methanol:water with different concentrations of maltose and 100 μM lithium acetate. Maltose was chosen because it is one of the most common disaccharides found in biological systems that was used in this study. The unreactive

fraction and reaction rate were measured for *m/z* 187 after CID of *m/z* 349 at 0.85 V. This CID voltage was selected because it provides the highest absolute signal intensity for the product ion at *m/z* 187 of the voltages used in this study. Solutions with concentrations ranging from 500 μM to 10 nM were analyzed (Table 5.1). Analysis of solutions at concentrations of 500, 50, 10, 1, and 0.1 μM all provided similar reaction rates and unreactive ratios with RSD's less than 10%. Solutions with 50 and 10 nM maltose also provided accurate reaction rates and unreactive fractions; however, the RSD of each measurement increased to greater than 30% for the reaction rate. This much uncertainty in the measurement does not allow for all disaccharides to be confidently distinguished, and therefore, 100 nM (or less than picomole amounts of sample based on the rate of sample infusion) is estimated as a conservative lower concentration limit required. This error is attributed to a lack of signal intensity at lower concentrations not because the kinetics or thermodynamics of the water adduction reaction are changing with concentration. Measuring the reaction rate and unreactive fraction of the *m/z* 169 product ion would help regain some confidence in the assignment, further lowering the concentration necessary to distinguish isomers. Additionally, there is no reason to believe that results would be any less accurate at concentrations higher than 500 μM.

Table 5.1. Measuremetns of unreactive fraction and reaction rate at several different

concentrations of maltose (CID fragmentation amplitude = 0.85 V)

	500 µM	50 µM	10 µM	1 µM	500 nM	100 nM	50 nM	10 nM
Unreactive Fraction	0.521 (0.011)	0.529 (0.003)	0.524 (0.011)	0.508 (0.007)	0.512 (0.009)	0.524 (0.018)	0.584 (0.241)	0.539 (0.080)
Reaction Rate	54.2 (1.1)	54.9 (0.8)	53.3 (1.8)	53.8 (1.1)	57.2 (4.6)	51.7 (7.1)	54.3 (17.1)	54.0 (14.7)

An even simpler experiment can be used to distinguish all thirteen of the disaccharides by first performing CID of the lithium cationized disaccharide and adding a 1000 ms delay without the prior isolation step described in previous experiments. In the resulting MS/MS spectrum all product ions are still present along with a new peak at *m/z* 205 from water adducted species previously at *m/z* 187. The peak at *m/z* 187 consists of both hydrated ions that previously had a mass-to-charge ratio of 169 and the unreactive ions at *m/z* 187, while the peak at *m/z* 169 is only unreactive species at *m/z* 169. The relative intensities of *m/z* 169, 187, and 205 can be used to be distinguished quickly in a single experiment ($p < 0.01$, Figure 4.4). Eliminating the second isolation step makes this method much more similar to typical CID experiments, where product ion ratios are used to distinguish the disaccharides. Eliminating the isolation removesthe need to measure the reaction rate for this particular set of isomers which requires multiple time points to be measured but also requires that there are no background ions at *m/z* 187 or *m/z* 169.

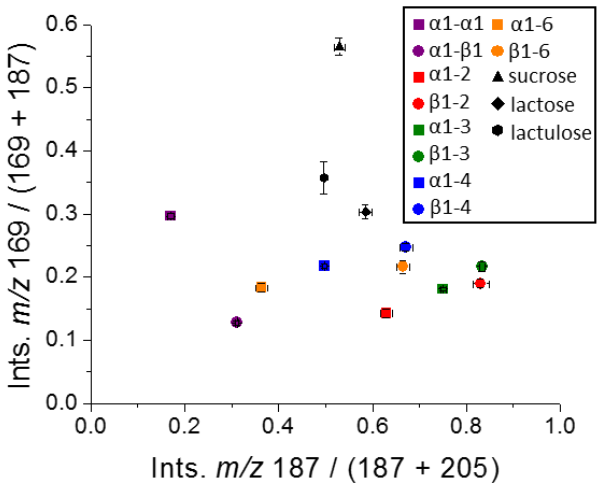

Figure 5.5. The ratio of the signal intensity of m/z 169 to the sum of m/z 169 and m/z 187 versus the ratio of the signal intensity of m/z 187 to the sum of m/z 187 and m/z 205 after CID and 1000 ms of reaction time

5.3 Applications to Real-World Samples

The water adduction method was applied to samples that naturally contain disaccharides (Table 1). Maltose is leftover after barley malt is cooked in the brewing process of malt beverages. ESI of a sample containing 1,000-fold diluted Yuengling and lithium acetate yielded an ion at *m/z* 349. Water adduction experiments conclusively identified the peak as maltose. Mushrooms and other fungi are well known to use trehalose as their major form of energy[22]. Shiitake mushrooms were ground and an aqueous extract was diluted 2000-fold and analyzed by ESI (Figure 4.6). After isolation of *m/z* 349 the peak was identified as trehalose (Table 4.2).

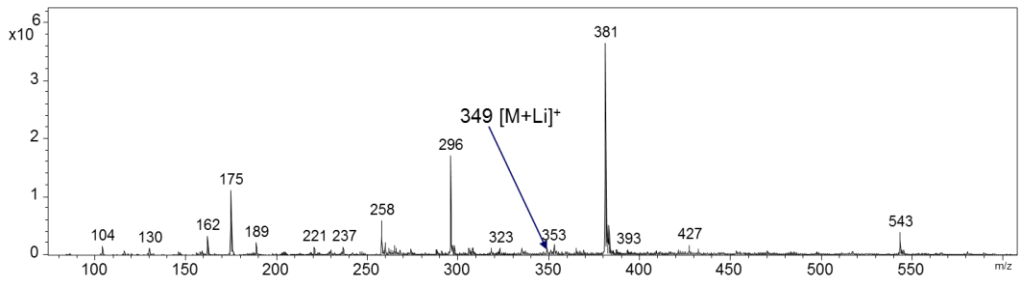

Figure 5.6. Mass spectrum of diluted supernatant of the ground shiitake mushroom. The lithium cationized disaccharide is highlighted at *m/z* 349.

Finally, the liquid medium used for vaping in electronic cigarettes was analyzed. Electronic cigarettes are becoming a very popular alternative for tobacco smokers. The vaping liquid is placed into the electronic cigarette and heated by a coil while the user inhales. These liquids consist primarily of propylene glycol and glycerol, but numerous flavorings are added to these liquids to give the user unique tastes. The vaping liquids (and their additives) are largely concocted by small businesses, and the full list of flavorings, as well as the health effects upon vaping, are not very well studied. The vaping liquid was analyzed by diluting (~2,000-fold) in 50:50 water:methanol and electrosprayed without further purification. Two vaping liquids both named “methanol tobacco” (one advertised as containing nicotine and the other nicotine free) showed a peak at *m/z* 349. After CID the water adduction reaction was studied for both product ions, *m/z* 169 and *m/z* 187. Water adduction experiments with either product ion determined with great confidence that the peak was from lithiated sucrose. This is the first report of sugars being used as sweeteners in the vaping liquids. Both the liquid containing nicotine and without nicotine gave very similar results, so only the results for the liquid with nicotine are shown for the most intense product ion, *m/z* 169 (Table 5.2).

Table 5.2: Unreactive Fraction and Reaction Rates (product ion *m/z* 187 for beer and mushroom and *m/z* 169 for Vaping liquid) for Standards and Complex Matricies with a CID Fragmentation Amplitude of 0.85 V

	Maltose	Beer
Unr. Frc.	0.529 (0.004)	0.541 (0.003)
Rxn. Rate	54.1 (0.2)	50.2 (0.8)
	Trehalose	Mushroom
Unr. Frc.	0.133 (0.008)	0.156 (0.023)
Rxn. Rate	172.1 (1.7)	169.6 (12.1)
	Sucrose	Vaping Liquid
Unr. Frc.	0.655 (0.010)	0.663 (0.006)
Rxn. Rate	38.0 (0.9)	38.1 (1.0)

5.4 Summary

A method was developed for fast identification of linkage position and anomericity between glucose-glucose disaccharides, as well as other disaccharides containing other monosaccharides. Monitoring the water adduction reaction to the product ions after CID can be used to distinguish the linkage position and anomericity of the parent disaccharide. This indicates that product ions retain some memory of their anomeric and linkage configuration after CID, in agreement with other recent report that had similar findings.[14,23] Measuring the reaction rate of the water adduction reaction and unreactive fraction for both the *m/z* 187 and the *m/z* 169 product ions provides complementary information to further elucidate structure. Using the water

adduction method to distinguish disaccharides avoids the long times necessary for sample cleanup, sample derivatization, or chromatographic separation prior to analysis. No other method has been able to distinguish this many different types of glucosyl-glucose linkages using only mass spectrometry. Using water adduction is significantly simpler compared to previously reported methods that can distinguish both linkage position and anomericity for reducing and non-reducing disaccharides. Our method requires only the addition of a lithium salt to the analyte solution and a quadrupole ion trap for the reaction. The precision in the measurements of the reaction rate and unreactive ratio are very constant across concentration ranging from 100 nM (less than a picomole of sample) to 500 μM. Water adduction can be used to confidently identify disaccharides from complex matrices based on the water adduction reaction rate and unreactive ratios to the product ion m/z 187, or an even simpler method can be used which requires only CID and a subsequent delay before comparing the ratios of the product ions m/z 169, 187, and 205 measured simultaneously in a single experiment.

REFERNCES

1 J. B. Fenn, M. Mann, C. K. Meng, S. F. Wong and C. M. Whitehouse, Electrospray ionization for mass spectrometry of large biomolecules, *Science (80-.).*, 1989, **246**, 64.

2 A. J. R. Heck and R. H. H. van den Heuvel, Investigation of intact protein complexes by mass spectrometry, *Mass Spectrom. Rev.*, 2004, **23**, 368–389.

3 T. R. Covey, B. A. Thomson and B. B. Schneider, Atmospheric pressure ion sources, *Mass Spectrom. Rev.*, 2009, **28**, 870–897.

4 G. J. V. B. and V. Kertesz, G. J. Van Berkel and V. Kertesz, Using the electrochemistry of the electrospray ion source, *Anal. Chem.*, 2007, **79**, 5510–5520.

5 N. B. Cech and C. G. Enke, Practical implications of some recent studies in electrospray ionization fundamentals, *Mass Spectrom. Rev.*, 2002, **20**, 362–387.

6 X. Wu, R. D. Oleschuk and N. M. Cann, Characterization of microstructured fibre emitters: in pursuit of improved nano electrospray ionization performance, *Analyst*, 2012, **137**, 4150.

7 P. P. Kebarle and U. H. Verkerk, Electrospray: from ions in solution to ions in the gas phase, what we know now., *Mass Spec. Rev.*, 2009, **28**, 898–917.

8 L. Konermann, E. Ahadi, A. D. Rodriguez and S. Vahidi, Unraveling the mechanism of electrospray ionization, *Anal. Chem.*, 2013, **85**, 2–9.

9 E. Ahadi and L. Konermann, Surface charge of electrosprayed water nanodroplets: A molecular dynamics study, *J. Am. Chem. Soc.*, 2010, **132**, 11270–11277.

10 E. Ahadi Konermann,L., Modeling the Behavior of Coarse-Grained Polymer Chains in Charged Water Droplets: Implications for the Mechanism of Electrospray Ionization, *J. Phys. Chem. B*, 2012, **116**, 104–112.

11 D. N. Mortensen and E. R. Williams, Investigating Protein Folding and Unfolding in Electrospray Nanodrops Upon Rapid Mixing Using Theta-Glass Emitters, *Anal. Chem.*, 2015, **87**, 1281–1287.

12 C. J. Hogan, J. A. Carroll, H. W. Rohrs, P. Biswas and M. L. Gross, Combined charged residue-field emission model of macromolecular electrospray ionization, *Anal. Chem.*, 2009, **81**, 369–377.

13 J. A. Loo, Electrospray ionization mass spectrometry: A technology for studying noncovalent macromolecular complexes, *Int. J. Mass Spectrom.*, 2000, **200**, 175–186.

14 J. A. Loo, Studying noncovalent protein complexes by electrospray ionization mass spectrometry, *Mass Spectrom. Rev.*, 1998, **16**, 1–23.

15 H. Higashi, T. Tokumi, C. J. Hogan, H. Suda, T. Seto and Y. Otani, Simultaneous ion and neutral evaporation in aqueous nanodrops: experiment, theory, and molecular dynamics

simulations, *Phys. Chem. Chem. Phys.*, 2015, **17**, 15746–15755.

16 D. Kim, N. Wagner, K. Wooding, D. E. Clemmer and D. H. Russell, Ions from Solution to the Gas Phase: A Molecular Dynamics Simulation of the Structural Evolution of Substance P during Desolvation of Charged Nanodroplets Generated by Electrospray Ionization, *J. Am. Chem. Soc.*, 2017, **139**, 2981–2988.

17 T. Wyttenbach and M. T. Bowers, Structural stability from solution to the gas phase: Native solution structure of ubiquitin survives analysis in a solvent-free ion mobility-mass spectrometry environment, *J. Phys. Chem. B*, 2011, **115**, 12266–12275.

18 A. T. Iavarone and E. R. Williams, Mechanism of charging and supercharging molecules in electrospray ionization, *J. Am. Chem. Soc.*, 2003, **125**, 2319–2327.

19 L. L. MACK, P. KRALIK, A. RHEUDE and M. DOLE, Molecular Beams of Macroions .2., *J. Chem. Phys.*, 1970, **52**, 4977-.

20 R. G. McAllister, H. Metwally, Y. Sun and L. Konermann, Release of Native-like Gaseous Proteins from Electrospray Droplets via the Charged Residue Mechanism: Insights from Molecular Dynamics Simulations, *J. Am. Chem. Soc.*, 2015, **137**, 12667–12676.

21 J. Fernandez De La Mora, Electrospray ionization of large multiply charged species proceeds via Dole's charged residue mechanism, *Anal. Chim. Acta*, 2000, **406**, 93–104.

22 J. V. Iribarne, On the evaporation of small ions from charged droplets, *J. Chem. Phys.*, 1976, **64**, 2287.

23 P. Kebarle and M. Peschke, On the mechanisms by which the charged droplets produced by electrospray lead to gas phase ions, *Anal. Chim. Acta*, 2000, **406**, 11–35.

24 M. T. Campbell, D. Chen, N. J. Wallbillich and G. L. Glish, Distinguishing Biologically Relevant Hexoses by Water Adduction to the Lithium Cationized Molecule, *Anal. Chem.*, 2017, acs.analchem.7b02647.

25 M. T. Campbell, D. Chen and G. L. Glish, Identifying the D-Pentoses Using Water Adduction to Lithium Cationized Molecule, *J. Am. Soc. Mass Spectrom.*, 2017, **28**, 1420–1424.

26 M. T. Campbell, D. Chen and G. L. Glish, Distinguishing Linkage Position and Anomeric Configuration of Glucose–Glucose Disaccharides by Water Adduction to Lithiated Molecules, *Anal. Chem.*, 2018, acs.analchem.7b04162.

27 F. A. Momany, M. Appell, J. L. Willett, U. Schnupf and W. B. Bosma, DFT study of α- and β-d-galactopyranose at the B3LYP/6-311++G** level of theory, *Carbohydr. Res.*, 2006, **341**, 525–537.

28 M. Appell, G. Strati, J. L. Willett and F. A. Momany, B3LYP/6-311++G** study of α- and β-d-glucopyranose and 1,5-anhydro-d-glucitol: 4C1 and 1C4 chairs, 3,OB and B3,O boats, and skew-boat conformations, *Carbohydr. Res.*, 2004, **339**, 537–551.

29 U. Schnupf, J. L. Willett and F. Momany, DFTMD studies of glucose and epimers: anomeric ratios, rotamer populations, and hydration energies, *Carbohydr. Res.*, 2010, **345**, 503–511.

30 Y. Zhao and D. G. Truhlar, The M06 suite of density functionals for main group thermochemistry, thermochemical kinetics, noncovalent interactions, excited states, and transition elements: Two new functionals and systematic testing of four M06-class functionals and 12 other function, *Theor. Chem. Acc.*, 2008, **120**, 215–241.

31 G. I. Csonka, A. D. French, G. P. Johnson and C. a Stortz, Evaluation of Density Functionals and Basis Sets for Carbohydrates, *J. Chem. Theory Comput.*, 2009, **5**, 679–692.

32 W. M. C. Sameera and D. A. Pantazis, A Hierarchy of Methods for the Energetically Accurate Modeling of Isomerism in Monosaccharides, *J. Chem. Theory Comput.*, 2012, **8**, 2630–2645.

33 J. E. Carpenter, C. P. McNary, A. Furin, A. F. Sweeney and P. B. Armentrout, How Hot are Your Ions Really? A Threshold Collision-Induced Dissociation Study of Substituted Benzylpyridinium 'Thermometer' Ions, *J. Am. Soc. Mass Spectrom.*, 2017, **28**, 1876–1888.

34 O. Hernandez, S. Isenberg, V. Steinmetz, G. L. Glish and P. Maitre, Probing Mobility-Selected Saccharide Isomers: Selective Ion–Molecule Reactions and Wavelength-Specific IR Activation, *J. Phys. Chem. A*, 2015, **119**, 6057–6064.

35 Y. Zhu, H. A. Roy, N. A. Cunningham, S. F. Strobehn, J. Gao, M. U. Munshi, G. Berden, J. Oomens and M. T. Rodgers, IRMPD Action Spectroscopy, ER-CID Experiments, and Theoretical Studies of Sodium Cationized Thymidine and 5-Methyluridine: Kinetic Trapping During the ESI Desolvation Process Preserves the Solution Structure of [Thd+Na]+, *J. Am. Soc. Mass Spectrom.*, 2017, 1–15.

Chapter 6: USING WATER ADDUCTION TO DETERMINE THE RELATIVE RATIOS IN MIXTURES AND DETERMINING ANOMERIC RATIOS WITH MASS SPECTROMETRY

6.1 Introduction to Water Adduction to Mixture of Isomers

Chapters 3 and 4 focused on distinguishing pentose, hexose, hexosamine, N-acetylhexosamines or disaccharide stereoisomers based on water adduction to the lithiated molecule. The reaction rate or the unreactive fraction of ions could be used to distinguish the isomers, and in some cases both the reaction rate and the unreactive fraction were needed to distinguish stereoisomers. Until this point only solutions containing a single isomer have been analyzed, limiting the analytical utility of the water adduction method. This chapter focuses on analyzing samples with multiple hexoses as well as multiple disaccharides.

Mixtures with various ratios of fructose and glucose were analyzed to determine if the water adduction reaction could be used to accurately determine the relative concentration of each hexose. Two calibration curves were generated: one measuring the unreactive fraction versus percentage of fructose in the mixture and another measuring reaction rate versus percentage of fructose in the mixture. Eleven different mixtures that contained a total of 10 μM hexose were used in the calibration curve ranging from 0% fructose to 100% fructose in 10% increments (where the remaining percentage would be glucose).

A linear calibration curve is obtained when reaction rate is plotted versus percentage of fructose (Figure 3a). This was used to determine the concentration of fructose in samples of high fructose corn syrup. High fructose corn syrup (HFCS) is the most common sweetener currently

used. It is produced by first hydrolyzing the glucose polysaccharide chains from corn into glucose monomer. Then the glucose is enzymatically catalyzed to fructose, and this reaction continues until the desired ratio of fructose to glucose is reached. Three samples of HFCS were analyzed: 45-HFCS, 52-HFCS, and 90-HFCS. The number preceding HFCS is indicative of the percentage of fructose in each type of HFCS. Using the calibration curve of reaction rate versus percent fructose (Figure 6.1a), the percentage of fructose in the 42-HFCS, 55-HFCS, and 90-HFCS were measured to be 41.5%, 57.1%, and 86.7 %, respectively. The percent error in these measurements are 0.5%, 2.1%, and 3.3%. This is comparable to the accuracy of this method is compared to GC-MS results presented below.

The calibration curve generated by plotting the unreactive fraction versus the percentage of fructose yields a curved plot, where the slope of the curve (and thus the sensitivity) decreases as the percentage of fructose increases (Figure 6.1b). The curve can be fitted with a fourth-order polynomial to calculate the percentage of fructose in each sample of HFCS; the polynomial is only used to calculate the expected percentage of fructose and provides no meaningful description of the underlying chemistry. This curve provides poorer accuracy (> 10% error) compared to the calibration curve generated based on reaction rate. This is largely due to the decrease in sensitivity at high percentages of fructose. The sensitivity is so low at very high percentages of fructose that the measured unreactive fraction for the 90-HCFS is greater than the unreactive fraction for 100% fructose sample, even though the residual between the 90-HFCS and the calibration curve is very small. The unreactive fraction is consistently greater for the samples of HFCS than the calibration standards. This could be caused by a background ion in the HFCS at *m/z* 187 that does not adduct water. This would not affect the reaction rate because only the reactive ions are used to calculate the reaction rate; however, the unreactive fraction would

be skewed. The calibration curve based on the unreactive fraction is therefore much better suited for samples with high percentages of glucose than high percentages of fructose.

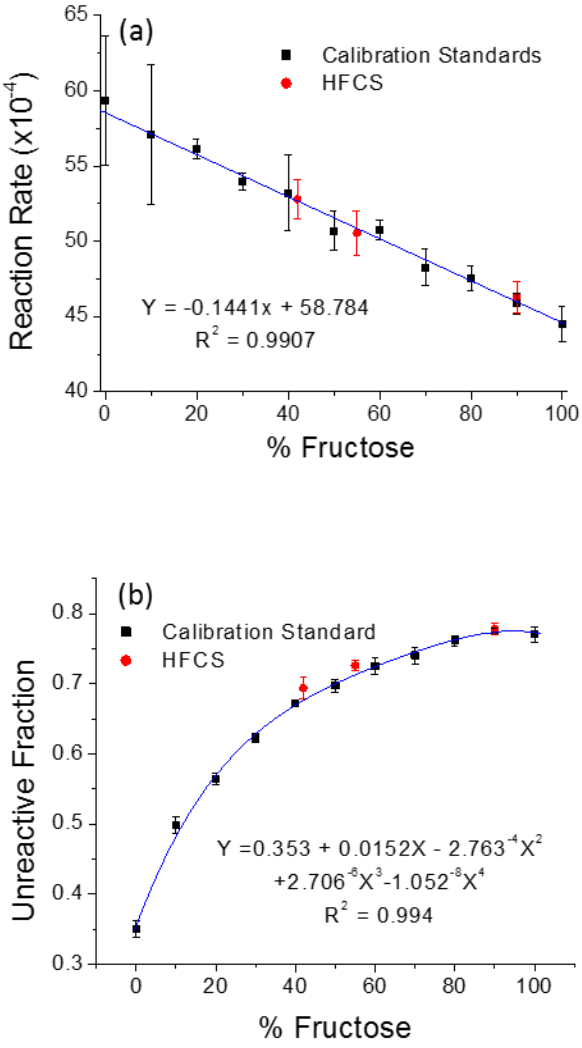

Figure 6.1: Calibration curve for percent fructose as a function of reaction rate (a) and as a function of unreactive fraction (b). In both cases the remaining percentage would be glucose.

GC-MS analysis was also performed to compare the water adduction method to a more conventional form of analysis. Analysis by GC first requires trimethyl silanating the hydroxyl

groups prior to the chromatographic separation to increase the volatility of the analytes. The derivatization reaction combined with the time required for chromatographic separation greatly lengthen the time required for analysis. The derivatization requires 30 minutes and the chromatographic separation requires about 10 minutes per sample, compared to tens of seconds required to measure the reaction rate or unreactive fraction.

Multiple peaks are observed in the GC chromatogram for both glucose and fructose because of different anomeric configurations as well as furanose and pyranose ring conformations[1]. Therefore, standards were necessary to determine which peaks originate from glucose and which originate from fructose. The glucose standard results in two peaks that are caused by separation of the two pyranose anomers, while fructose splits into multiple peaks caused by both anomers in the pyranose and furanose forms that are not completely resolved (Figure 6.2). Multiple peaks on the chromatogram of the fructose standard could be caused by incomplete derivatization of the analyte.

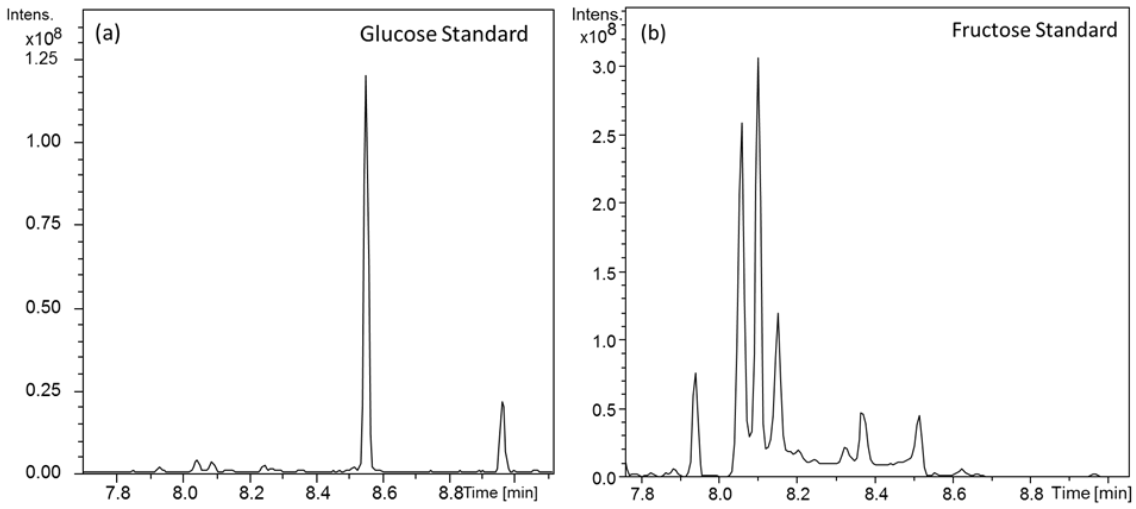

Figure 6.2. Total ion current of chromatograms of either glucose or fructose standards. Multiple peaks are observed for both species.

Chromatograms for all three derivatized HFCS samples are provided in Figure 6.3. The relative concentration of fructose and glucose were determined using a three point standard addition curve where intensities were measured by summing the area under both peaks for glucose and all five peaks for fructose. The relative concentration of each hexose can then be calculated. The percentage of fructose in the 42-HFCS, 55-HFCS, and 90-HFCS were measured as 44.2%, 56.6%, and 85.5%, respectively. Assuming that the HFCS samples contain the stated values of fructose and glucose the GC-MS method gives percent errors of 2.2%, 1.6%, and 4.5%, similar to the accuracy of method using the reaction rate of water adduction. However, the water adduction method does not require the derivatization step nor the chromatographic separation.

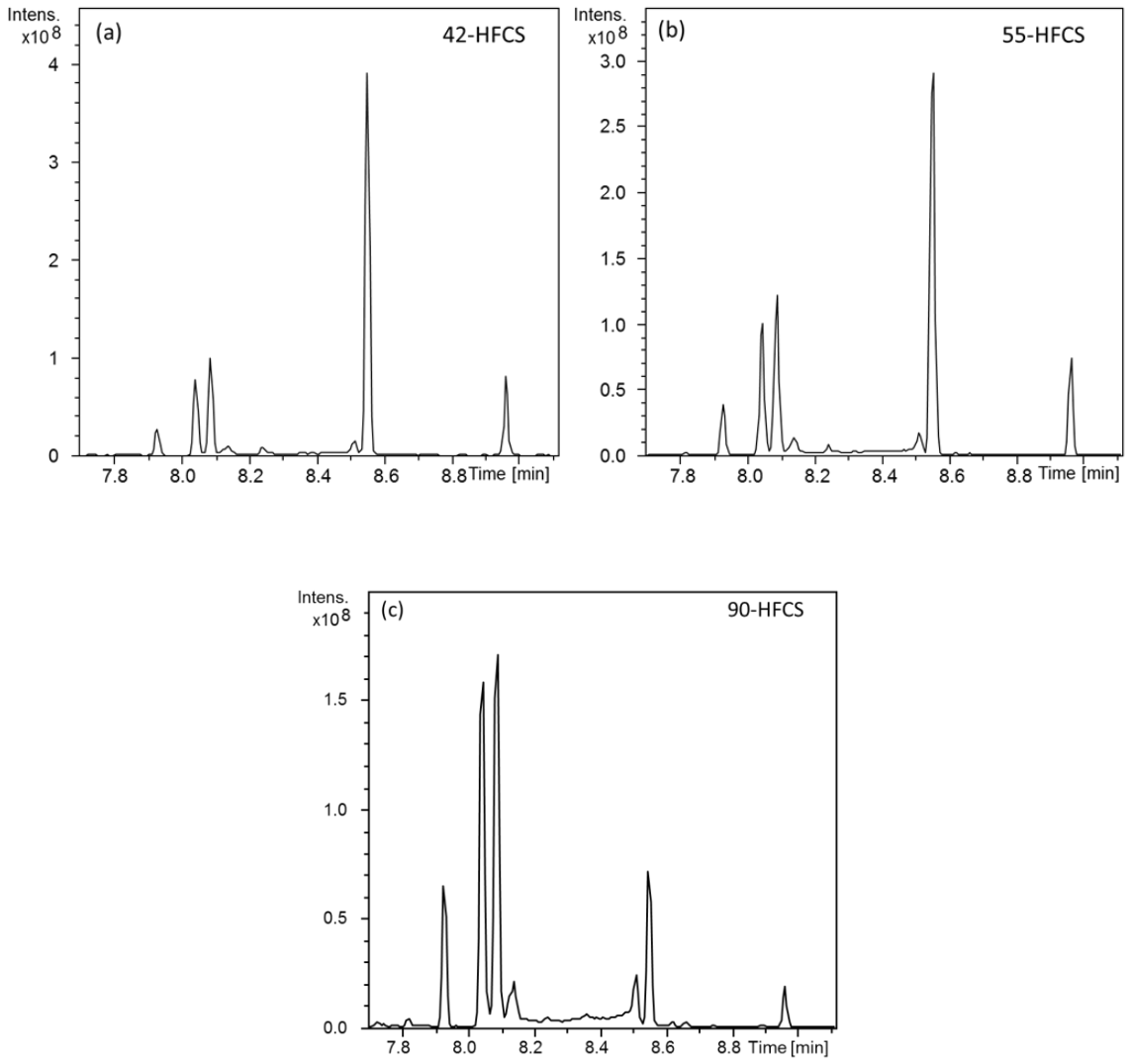

Figure 6.3. Chromatograms three samples of HFCS: (a) 42-HFCS, (b) 55-HFCS, and (c) 90-HFCS

6.2. Dimers Produce Non-linearity in Calibration Curves

The results from using mixtures of fructose and glucose were used to measure the relative concentration of analytes in other binary mixtures including mixtures of α-methyl glucoside and β-methyl glucoside. The reaction rate and unreactive fraction were measured for several standards with various rations of α- and β-methyl glucoside. Using total hexose concentrations of

100 μM, the calibration curve of reaction rate versus relative concentration of β-methyl glucoside was found to be linear. However, the calibration curve of R_U versus relative concentration of β-methyl glucoside was found to be non-linear, similar to the previously reported curve measuring the unreactive faction of mixtures of glucose and fructose. The plot of unreactive fraction versus the relative concentration of β-methyl glucoside appears to be curved (Figure 6.4). This is similar to experiments just described measuring the relative concentration of fructose in binary mixtures of fructose and glucose. Calibration curves with the unreactive fraction plotted versus relative concentration of fructose showed much higher sensitivity when small amounts of fructose were added to solutions of glucose (Figure 6.1).

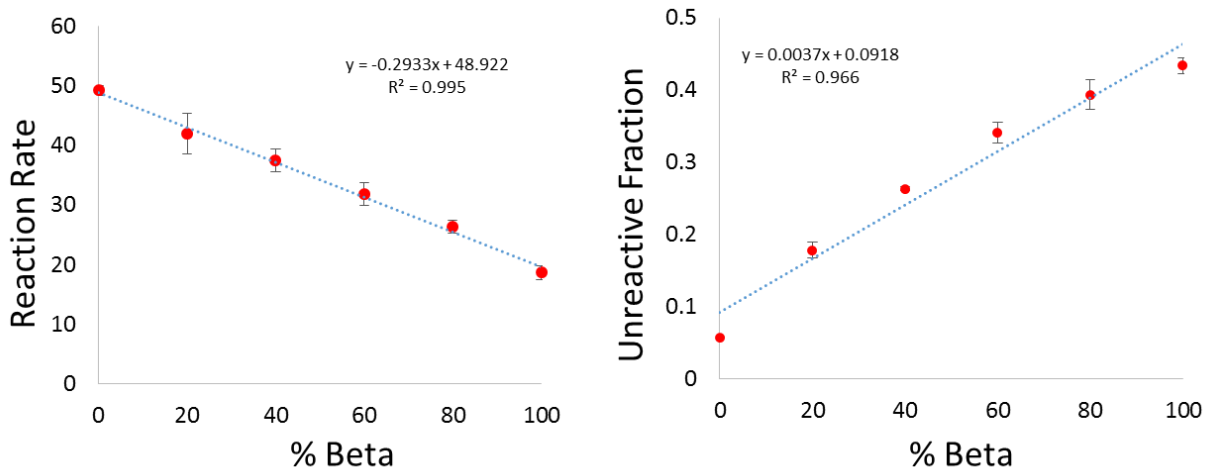

Figure 6.4. Calibration curves used to calculate the percentage of α- or β-methyl glucoside in solution based on either the reaction rate (left) or the unreactive fraction (right) of the sample. The summed concentration of α- or β-methyl glucoside in solution is always 100 μM. A nonlinear response is observed when plotting the unreactive fraction versus percentage of β-methyl glucoside. The trendline is placed on the graph so the curved shape of the data is easier to visualize.

For both mixtures of fructose and glucose and mixtures of the methyl glucosides, the calibration curve was more sensitive when samples contained large percentages of the species with a smaller unreactive fraction. For example, the unreactive fraction for fructose is 0.85, much greater than 0.34 for glucose. The unreactive fraction for β-methyl glucoside is 0.44, and the unreactive fraction for α-methyl glucoside is 0.05. This issue could be caused by any number of factors. First, ionization efficiency for the molecules could be significantly different. If fructose is more likely to adduct a lithium cation than glucose, there would be a larger fraction of fructose ions in the quadrupole ion trap than would be expected based on the concentration in solution. However, this does not seem to be the case for either the hexoses of the methyl glucosides. Solutions containing only glucose or fructose showed nearly identical signal intensities for the lithium cationized molecule. Analogous results were observed with solutions containing only one methyl glucoside.

Another possible reason for the curved calibration curves could be a competitive reaction in the ion trap. This is unlikely considering the number of water molecules is significantly greater than the number of ions in the quadrupole ion trap. Additionally, for both mixtures, the calibration curve is more sensitive to the lithium cationized molecule that has a slower reaction rate. Nevertheless, this hypothesis was tested by electrospraying mixtures of fructose and isotopically labeled glucose-$^{13}C_6$. Using the isotopically labeled glucose allowed the reaction rate and unreactive fraction of glucose and fructose to be measured independently from the mixture. These metrics first measured by conventional isolation of only a single mass-to-charge ratio, e.g. isolating fructose and allowing water adduction to occur, then isolating glucose and allowing water adduction to occur. Alternatively, the isolation width could be increased from the conventional 1 – 2 mass-to-charge units centered around the desired peak to 10 mass-to-charge

units centered at *m/z* 190. This allows both fructose and glucose to be isolated simultaneously, more similar to experiments with fructose and non-isotopically labeled glucose.

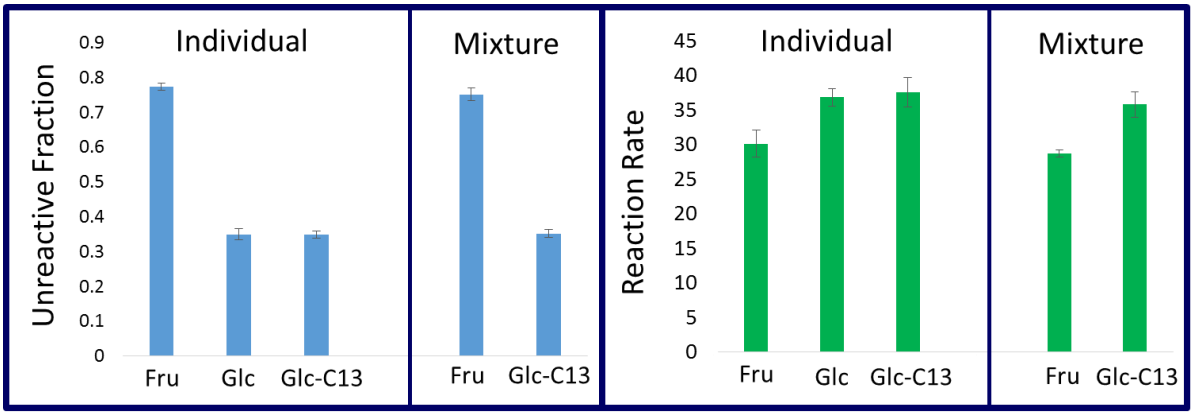

Figure 6.5. The unreactive fraction and reaction rates measured individually for fructose, glucose and glucose-$^{13}C_6$. The unreactive fraction and reaction rates were also measured for fructose and glucose-$^{13}C_6$ simultaneously, and these measured values matched the unreactive fractions and reaction rates when measured individually

Regardless of the isolation scheme used, both the reaction rate and unreactive fraction for the isotopically labeled mixture was identical to measuring either fructose or glucose individually. Varying the ratio of fructose and glucose-$^{13}C_6$ in the mixture also had no effect on either reaction rate or the unreactive fraction. This demonstrated that having both fructose and glucose ions in the quadrupole ion trap simultaneously was not the cause for the deviation from linearity in the calibration curve of unreactive fraction of versus percentage of fructose.

Thus far, standards were prepared with the fructose and glucose concentration summing to 100 µM, and the high fructose corn syrup samples were prepared such that they give similar signal intensities for the standards. This is a relatively high concentration considering very low concentrations are needed to from dimers, especially when using lithium as a cation. When using

100 µM hexose, the intensity of the dimer peak is roughly 50% to 75% the intensity of the monomer peak. Therefore, if unequal amounts of fructose and glucose are forming dimers, it would shift the measured ratio of fructose to glucose to that of the species which is less likely to form dimer.

Weakly bound dimers, $[2M+Li]^+$, are commonly formed during electrospray. Often mass spectrometers equipped with electrospray ionization have an array of ion optics, which are responsible for guiding ions into the high vacuum and dissociating non-covalent complexes formed during ESI. In the Bruker Esquire, dimers are usually fragmented from collisions between the exit of the ion transfer capillary and a subsequent skimmer. The voltage between the capillary exit and the skimmer, called the capillary offset voltage, can be increased to fragment clusters or decreased to keep clusters intact. Mixtures of fructose and glucose-$^{13}C_6$ produce three different lithium bound dimer peaks: a fructose homodimer (*m/z* 367), a glucose homodimer (*m/z* 379), and a heterodimer with fructose and glucose (*m/z* 373). If glucose more readily forms dimers, then the signal intensity for the homodimer at *m/z* 379 would be greater than the signal intensity for the homodimer at *m/z* 367. For the following experiments, the voltages on the ion optics were set to relatively low (20 V compared to the previously used 60 V) reduce fragmentation of dimers passing from atmosphere into the ion trap.

When a mixture of fructose and glucose-$^{13}C_6$ was analyzed with the capillary offset voltage set to 20 V, the ratio of fructose homodimer:heterodimer: glucose-$^{13}C_6$ homodimer is measured to be 1:2:1 (Figure 6.6). This ratio suggest that formation of dimer is equally favorable for both hexoses. However, increasing the voltage to those used in previous experiments shows a different ratio. The signal intensity for the fructose homodimer is lower than that for the glucose

homodimer. Likewise, increasing the voltages further shows the fructose homodimer has fragmented almost completely, while some glucose homodimer still remains.

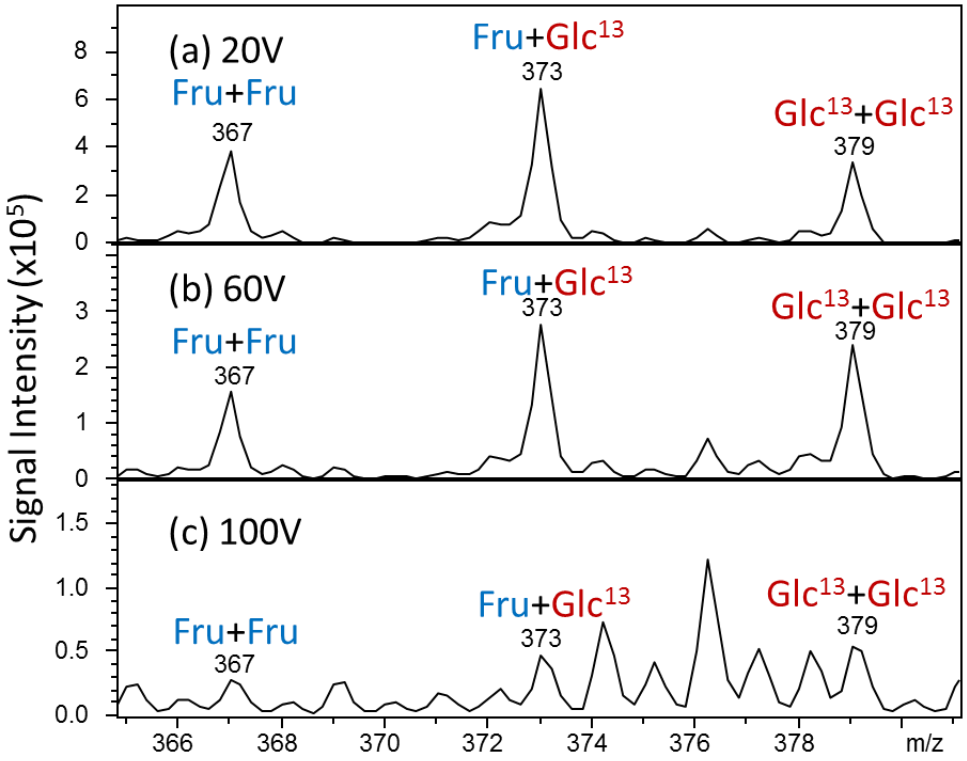

Figure 6.6. The mass spectra of the dimers shown from a 50:50 mixture of fructose and glucose-$^{13}C_6$. As the capillary skimmer voltage increases from part a to part c, the ratio of heavy homodimer (*m/z* 379) to light homodimer (*m/z* 367) increases. This is caused by an increased voltage in the ion optics more readily fragmenting the fructose homodimer than the glucose-$^{13}C_6$ homodimer. Part c has very little signal intensity for the dimers because the majority of the ions are being fragmented in the optics

The homodimers were studied more systematically by applying a low capillary offset voltage (20 V) to ensure minimal fragmentation of each dimer. Each dimer was isolated in the ion trap, and CID experiments were performed at various fragmentation amplitudes to create a

survival yield curve for each dimer. The onset of fragmentation occurs at a much lower amplitude for the fructose homodimer than the glucose homodimer (Figure 6.6). Fragmentation is more likely for the fructose homodimer than the glucose homodimer, thereby increasing the ratio of fructose to glucose monomer in the ion trap (Figure 6.7a). CID of the heterodimer provides another interesting observation. At fragmentation amplitudes sufficient for complete dissociation of the heterodimer, fructose is 9 times more likely to retain the lithium cation than the isotopically labeled glucose (Figure 6.7b). This demonstrates that fragmentation of the heterodimer also increases the ratio of fructose to glucose in the ion trap.

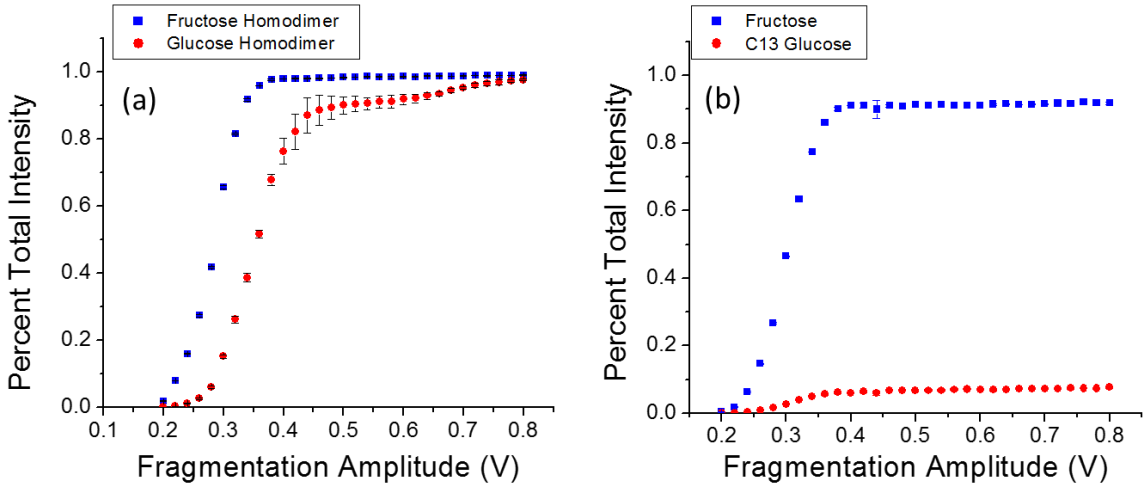

Figure 6.7. (a) fragmentation curves of the homodimers of fructose and glucose generated with CID at various amplitudes. Fructose homodimers fragment more readily than glucose homodimers at the same fragmentation amplitude. (b) the relative intensity of product ions of fructose and glucose-$^{13}C_6$ generated with CID at various fragmentation amplitudes. Fructose retains the lithium cation after 90% of the dissociations.

The results of the experiments studying dimers could provide an explanation for the non-linear shape of the calibration curve observed when plotting unreactive fraciton versus the relative concentration of fructose. Adding small amounts of glucose to fructose does not dramatically change the unreactive fraction, because glucose homodimers require more energy to fragment than fructose homodimers. Likewise, fructose is more likely to retain the lithium cation upon fragmentation of a fructose-glucose heterodimer. This idea is in agreement with results from Chapter 5, which suggested that lithium cationized molecules with a greater unreactive fraction are more likely to form tri- and tetradentate interactions with lithium than bidentate interactions with lithium. If the average heterodimer involves a fructose with more coordination bonds to the lithium cation than glucose, fructose will be more likely to retain the lithium cation after dissociation of the heterodimer.

β-methyl glucoside has a greater unreactive fraction than α-methyl glucoside. Therefore, the β-anomer likely retains the lithium cation upon fragmentation of a heterodimer. This was tested by analysis of solutions containing fructose and β-methyl glucoside and solutions of fructose and α-methyl glucoside. The lithiated heterodimer of fructose and the methyl glucoside was isolated, and CID was performed with various fragmentation amplitudes. The ratio of the product ions after CID demonstrates that fructose retains the lithium cation much more than either methyl glucoside; however, the β-methyl glucoside is three times as likely to retain the lithium cation than the α-methyl glucoside. This result suggests that fragmentation of a heterodimer consisting of each anomer would likely favor the β-methyl glucoside retaining the lithium cation.

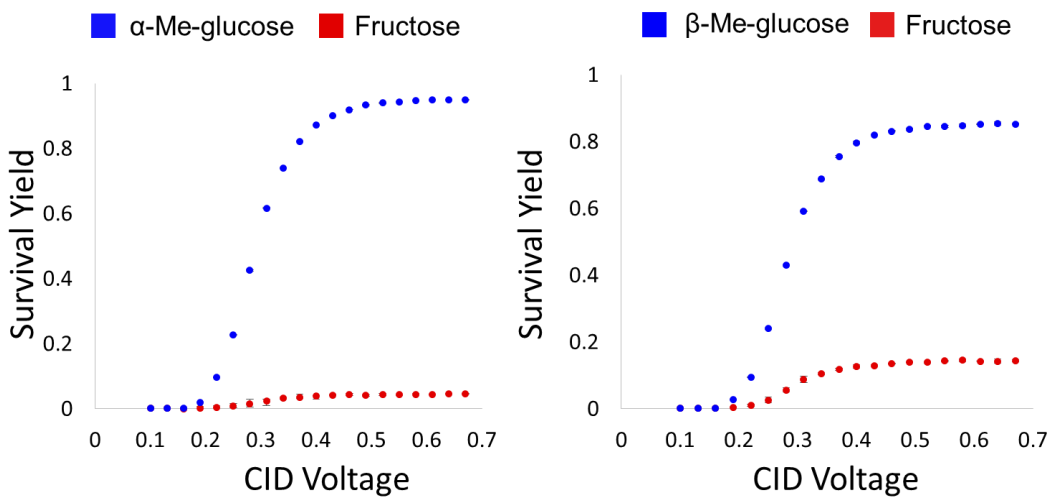

Figure 6.8 Plots showing the relative intensity for the two product ions after dissociation of the heterodimer formed between fructose and either α- or β- methyl glucoside generated with CID. The α-methyl glucoside only retains the lithium cation after 5% of dissociations from fructose, and the β- methyl glucoside retains the lithium cation after 15% of the dissociations from fructose.

There are two changes that could be made to the previously presented method to prevent the formation and fragmentation of dimers from making the calibration curve non-linear. The first is reducing the concentration of analyte in solution to avoid dimer formation, and the second is minimizing the voltages on the ion optics to prevent fragmentation should ensure that the ratio of fructose to glucose in the ion trap is representative of that in solution. The same calibration curves were constructed using standards with varying concentrations of total methyl glucosides (100, 50, 10, and 5 µM) and the capillary offset voltage set to 20 V and 60 V. Decreasing the concentration provides a linear calibration curves. The resulting calibration curve was significantly more linear than the previous with higher concentrations and harsher capillary offset voltages (Figure 6.9). Decreasing the concentration improved the linearity for the calibration curves measured using either capillary offset voltages. Decreasing the capillary offset

voltage from 20 V to 60 V has much more profound effect on increasing the linearity than decreasing concentration. This is because fragmentation of the homo- and heterodimers in the ion optics is greatly reduced.

6.3. Measuring the anomeric ratio of Glucose in Water

Using the information learned from previous experiments, linear calibration curves were produced with either reaction rate or unreactive fraction versus differing ratios of α- and β-methyl glucoside. The reaction rate and unreactive fraction of glucose was then measured to determine if the calibration curves could be used to determine anomeric ratio of glucose in solution. The anomeric configuration that is energetically preferred changes after glucose is transferred from solution phase to the gas phase; however, mutarotation between anomers has been shown to be a solvent assisted reaction, and it is therefore safe to assume that the ions produced from electrospray represent the solution phase thermodynamics. Using the calibration curves shown in Figure 6.9, the anomeric ratio of glucose was determined to be 66.0% β-methyl glucoside with the calibration curve based on unreactive fraction and 66.3% % β-methyl glucoside with the calibration curve based on reaction rate. This is very close to the widely accepted literature value of 36:64 $(\alpha{:}\beta)$[2].

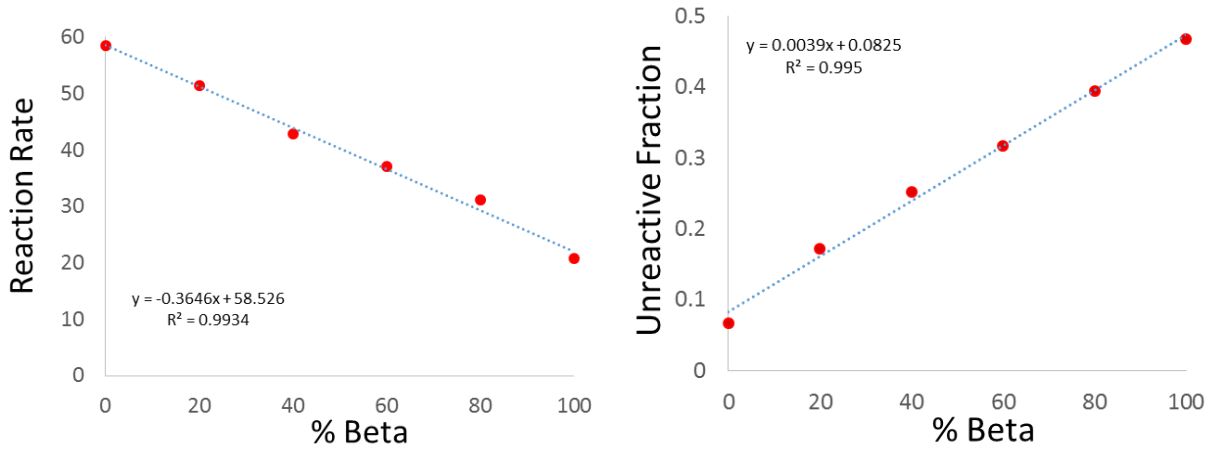

Figure 6.9. Calibration curves used to calculate the percentage of α- or β-methyl glucoside in solution based on either the reaction rate (left) or the unreactive fraction (right) of the sample. The summed concentration of α- or β-methyl glucoside in solution is always 10 µM, and capillary skimmer offset is set to 20 V.

The accuracy in measuring the anomeric ratio would also require that the addition of the substituted methyl group on the methyl glucosides not significantly contribute to thermodynamics dictating the binding site of the lithium cation or water adduction, thereby affecting reaction rate and unreactive fraction. Plotting the reaction rate versus unreactive fraction for the calibration standards should create a curve of possible combinations of reaction rate and unreactive fractions that could be found when analyzing glucose, and the reaction rate and unreactive fraction for glucose did lie on the curve (Figure 6.10).

Glucose is commercially available in the solid form as the α-anomer (96% purity). Because mutarotation is a solvent assisted reaction, the solid remains as the α-anomer until dissolved in solution. Upon being dissolved in water, the glucose will begin to mutarotate until equilibrium is reached a few hours later. Immediately after being dissolved, the sample of α-

glucose was diluted to the 10 µM and analyzed. The unreactive fraction and reaction rate were measured over the next 10 minutes. The combination of reaction rate and unreactive fraction also matched the line of expected values shown in Figure 6.10 based on the methyl glucosides.

Figure 6.10. Plotting the unreactive fraction versus reaction rate for the methyl glucoside standards (red) combinations of values that would be expected for samples of actual glucose. A sample of glucose falls on this line (green), as well as a sample of α-glucose that has yet mutarotated to equilibrium.

The fast analysis times possible with mass spectrometry allow the anomeric ratio to be measured as mutarotation occurs with excellent temporal resolution. The unreactive fraction was measured continuously just after dissolving solid α-glucose in water. The calibration curve based on unreactive fraction was used to calculate the concentration of the alpha anomer as a function of time. The purity of the solid α-glucose stock was measured as 96% by the manufacturer, but the highest concentration of α-glucose ever observed was 8.4 µM. This lower concentration than expected indicates that even the 5 – 10 minutes required to dissolve the sample, dilute to 10 µM, and begin direct infusion at the mass spectrometer, is enough time a significant amount of

mutarotation to occur. The sample asymptotes at around 3.0 μM α-glucose, demonstrating that equilibrium was achieved at 70% β-glucose and 30% α-glucose.

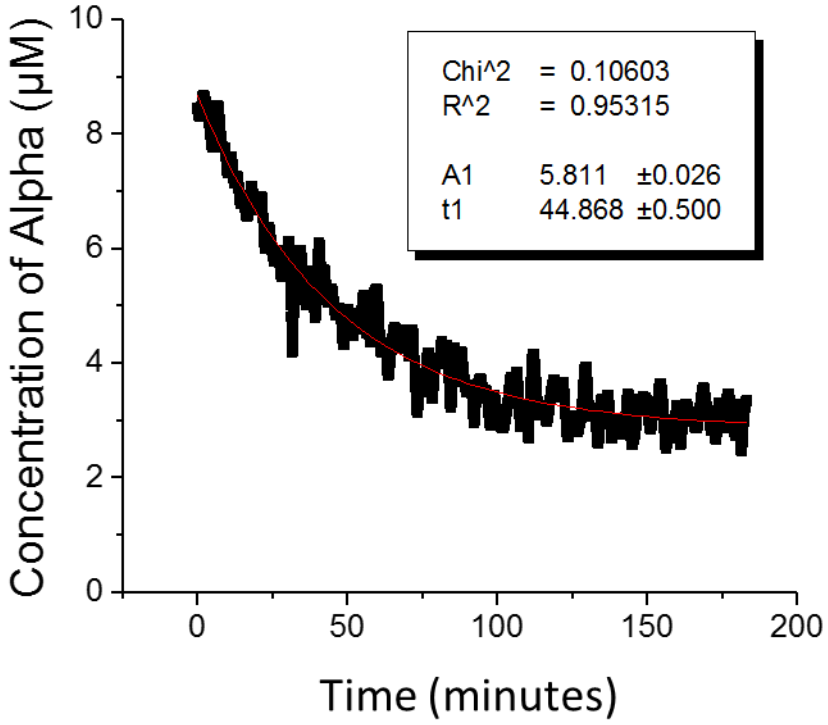

Figure 6.11. The concentration of α-glucose is monitored by measuring the unreactive fraction of the sample for 3 hours. Analysis began 5 – 10 minutes after the α-glucose was dissolved in solution.

6.4. Water Adduction to Cross-Ring Cleavage Product Ions

As discussed in Chapter 4, lithium cationized disaccharides do not adduct water in a quadrupole ion trap. This is likely because the lithium cation coordinates near the glycosidic bond, between the two monosaccharide residues, hindering the water molecule from adducting.

CID can be used to dissociate the disaccharide into smaller pieces, creating space for the water molecule to adduct. Cleavage most commonly occurs at the glycosidic bond, resulting in a product ion that contains only the reducing end monosaccharide (Y type ion at *m/z* 187) or the dehydrated non-reducing monosaccharide (B type ion at *m/z* 169). Previously, the B and Y product ions were used to distinguish the disaccharide isomers. These product ions were chosen because they are ubiquitous to all disaccharides after CID.

Other product ions are also observed for reducing disaccharides as a result from cross ring cleavages. The dissociation mechanism has been studied elsewhere[3], and these results showed that cross ring cleavages occur upon ring opening of reducing end monosaccharide, followed by cleavage of the newly opened tail. The resulting cross-ring cleavages are different for ions with different linkage positions. A list of the cross linkages observed for each linkage position is shown in Tables 6.1 and 6.2.

The cross ring cleavages are still unable to adduct water, supporting the hypothesis that the lithium cation is sequestered between the two monosaccharide subunits. Isolation of the cross-ring cleavage product ions followed by CID (an MS^3 experiment) results in cleavage of the glycosidic bond, leaving behind only the dehydrated reducing end monosaccharide. This is the same ion that would originally be considered the B type ion after the first CID step. Isolating the cross ring cleavage product ion and using CID adds extra selectivity to the analysis. For example, CID of Kojibiose gives product ions at m/z 331 and a cross-ring cleavage at *m/z* 229. Both of these product ions can be further dissociatied in an MS3 experiment to produce *m/z* 169. The reaction rate and unreactive fraction of *m/z* 169 can be measured and used to distinguish ions (Table 6.1).

Table 6.1. Reaction rates for all observed cross-ring cleavages.

Disaccharide	*m/z* 331	*m/z* 289	*m/z* 259	*m/z* 229	*m/z* 169[a]
Kojibiose (α1→2)	57.8 (6.7)			61.0 (2.2)	57.6 (4.4)
Sophorose (β1→2)	45.1 (8.8)			43.4 (0.9)	39.0 (1.5)
Nigerose (α1→3)	70.8 (1.0)		68.0 (1.0)		61.6 (2.5)
Laminarbiose(β1→3)	37.5 (2.5)		43.7 (3.8)		37.3 (2.9)
Maltose (α1→4)	53.2 (3.1)	58.2 (2.7)			53.4 (1.9)
Cellobiose (β1→4)	37.3 (0.5)	35.2 (2.5)			33.4 (2.4)
Isomaltose (α1→6)	65.6 (9.3)	73.7 (3.7)	57.9 (13.2)	54.9 (9.4)	60.0 (3.3)
Gentibiose (β1→6)	33.1 (2.4)	28.3 (1.0)	29.5 (1.0)	30.7 (2.4)	26.6 (0.9)
Lactose[b]	55.5 (3.8)	56.4 (3.3)			48.3 (3.7)
Palitunose[c]	53.5 (3.3)	63.7 (6.5)	67.7 (0.3)	72.8 (4.5)	69.4 (1.7)

[a]m/z 169 refers to the B type ion after MS^2

[b]lactose is a galactose-(β1→4)-glucose

[c]palitunose is glucose-(α1→6)-fructose

Table 6.2. Unreactive fraction for all observed cross-ring cleavages.

Disaccharide	*m/z* 331	*m/z* 289	*m/z* 259	*m/z* 229	*m/z* 169[a]
Kojibiose (α1→2)	0.803 (0.014)			0.419 (0.005)	0.512 (0.014)
Sophorose (β1→2)	0.741 (0.052)			0.318 (0.008)	0.359 (0.024)
Nigerose (α1→3)	0.471 (0.008)		0.381 (0.027)		0.534 (0.004)
Laminarbiose(β1→3)	0.374 (0.006)		0.290 (0.033)		0.381 (0.010)
Maltose (α1→4)	0.529 (0.015)	0.400 (0.039)			0.531 (0.013)
Cellobiose (β1→4)	0.458 (0.007)	0.306 (0.028)			0.424 (0.008)
Isomaltose (α1→6)	0.676 (0.019)	0.435 (0.040)	0.406 (0.051)	0.451 (0.068)	0.555 (0.010)
Gentibiose (β1→6)	0.682 (0.016)	0.356 (0.015)	0.391 (0.015)	0.347 (0.023)	0.424 (0.020)
Lactose[b]	0.530 (0.004)	0.445 (0.011)			0.537 (0.005)
Palitunose[c]	0.872 (0.005)	0.454 (0.038)	0.423 (0.009)	0.433 (0.024)	0.724 (0.014)

[a]m/z 169 refers to the B type ion after MS^2

[b]lactose is a galactose-(β1→4)-glucose

[c]palitunose is glucose-(α1→6)-fructose

The reaction rate and unreactive fraction were measured for the MS^3 product ions of all cross-ring cleavages for an exhaustive list of glucose-glucose reducing disaccharides. Interestingly, when comparing the B type ion (*m/z* 169) after an MS^2 experiment and an MS^3 experiment, the reaction rate remains relatively constant. Conversely, the unreactive fraction changes quite significantly for some disaccharides. The constant rate suggests that the MS^3 experiment does not produce any new locations for the lithium cation to coordinate. Thus, the same reactive sites are still occupied, and the rate remains constant. However, a number of these

reactive sites could be converted to unreactive sites, which would increase the unreactive fraction while leaving the rate unchanged.

A particularly large change in unreactive fraction is observed for 1→2 linked disaccharides, especially when comparing the B type after and MS^2 experiment and after an MS^3 experiment using *m/z* 331 as the precursor ion. The product ion *m/z* 331 corresponds to losing the anomeric hydroxyl of the reducing end as water. Considering the proximity of the anomeric hydroxyl to the glycosydic linkage at position 2, the anomeric hydroxyl of the reducing end monosaccharide likely coordinates the lithium cation in some structures, while the 3-hydroxyl coordinates the lithium in others. Dissociation of the 1-hydroxyl as water ensures that it was not bound to the lithium cation, and therefore the ions remaining at *m/z* 331 likely all have the 3-hydroxyl bound the lithium cation. This is a possible explanation for the drastic change in unreactive fraction observed for the 1→2 linked disaccharides.

Until this point only reducing disaccharides could be disaccharides in mixtures, because non-reducing disaccharides such as sucrose do not produce cross-ring cleavages. Because both anomeric centers are used in the glycosidic linkage, neither ring can open to produce a cross-ring cleavage. The only product ions observed are B and Y type ions resulting from cleavage of the glycosidic bond, and these two product ions are observed for all disaccharides.

One difference between reducing disaccharides and non-reducing disaccharides is that non-reducing disaccharides have a lower critical energy for dissociation. That means if a CID experiment is performed on a mixture of reducing disaccharide and a non-reducing disaccharide ions, a greater percentage of the non-reducing disaccharide ions will fragment than the reducing disaccharide. This assumes that the CID fragmentation amplitude is high enough such that

dissociation of some ions occurs yet low enough that not all ions dissociate. Survival yield curves are shown in Figure 6.12 for sucrose and isomaltose. It was found that increasing the fragmentation time increases the slope of the sigmoidal survival yield curves. Steeper curves are beneficial because they provide greater selectivity between the sucrose and isomaltose at a given fragmentation amplitude. Therefore, greater fragmentation times provide greater selectivity, but also increase the length time needed to complete the experiment. A fragmentation time of 250 ms was selected for experiments containing mixtures to compromise for both selectivity and speed of analysis.

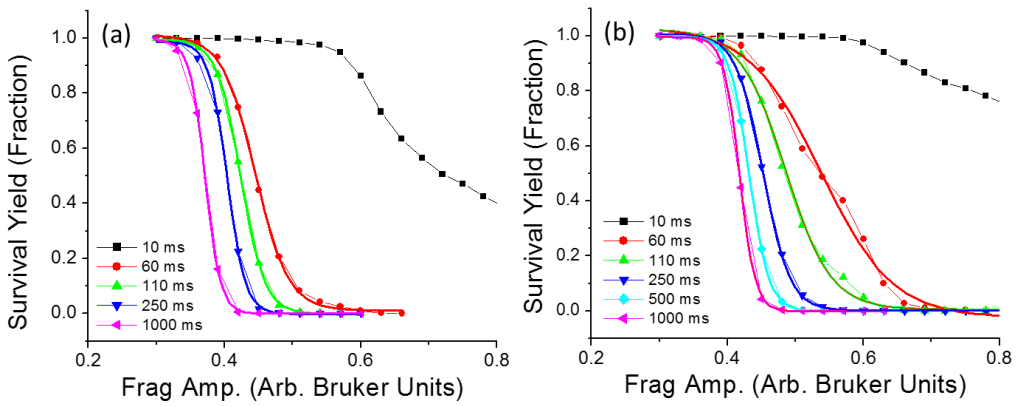

Figure 6.12. Survival yield curves for (a) sucrose and (b) isomaltose. A sigmoidal fit is shown for each curve. Increasing the fragmentation time increases the slope of the sigmoidal fit.

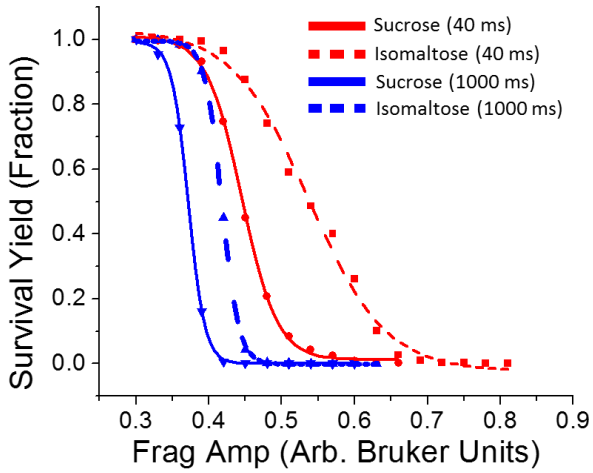

Figure 6.13. A comparison of sucrose and isomaltose survival yield curves. Sucrose shows a much greater degree of dissociation at lower fragmentation amplitudes than isomaltose with either fragmentation time.

6.5 Analysis of Mixtures of Disaccharides

A sample containing cellobiose, laminarbiose, sopherose, and sucrose was analyzed to determine if all four disaccharides could be unambiguously identified. CID of the $[M+Li]^+$ (*m/z* 349) resulted in product ions at m/z 169, 187, 229, 259, 289, and 331. The product ion at *m/z* 289 is unique to cellobiose, and MS^3 of the product ion followed by a water adduction experiment confirmed the identity cellobiose. The cross-ring cleavages at 259 and 229 are unique to laminarbiose and sophorse, respectively, and MS^3 followed by water adduction confirmed their identity. The sucrose in the sample was identified by performing CID at low amplitudes (0.35 V for 250 ms), allowing it to be the only fragmented disaccharide in the sample. The ion at *m/z* 169 was then isolated, and water adduction experiments were used to confirm its identity as sucrose. Analogous experiments were performed with a mixture of cellobiose, nigerose, kojibiose, and sucrose to be sure there was no difference when β and α-glycosidic linkages (of different positions) were mixed in solution, and all 4 disaccharides were identified.

Table 6.3. Comparison of reaction rate and uncreative fractions for a mixture of disaccharides and standards

Mixture of Sophorose, Laminarose, Cellobiose, and Sucrose				
	Reaction Rate		Unreactive Fraction	
	Standard	*Mixture*	*Standard*	*Mixture*
Sophorose	43.4 (0.9)	42.1 (2.3)	0.318 (0.008)	0.327 (0.021)
Laminarose	43.7 (3.8)	42.6 (6.5)	0.290 (0.033)	0.307 (0.015)
Cellobiose	35.2 (2.5)	34.2 (3.7)	0.306 (0.028)	0.317 (0.021)
Sucrose	31.1 (3.3)	33.1 (2.1)	0.688 (0.020)	0.683 (0.023)

Table 6.4. Comparison of reaction rate and uncreative fractions for a mixture of disaccharides and standards

Mixture of Kojibiose, Nigerose, Cellobiose, and Sucrose				
	Reaction Rate		Unreactive Fraction	
	Standard	*Mixture*	*Standard*	*Mixture*
Kojibiose	61.0 (2.2)	61.5 (3.5)	0.419 (0.005)	0.413 (0.039)
Nigerose	68.0 (1.0)	66.8 (4.9)	0.381 (0.027)	0.422 (0.045)
Cellobiose	35.2 (2.5)	33.0 (2.4)	0.306 (0.028)	0.320 (0.029)
Sucrose	31.1 (3.3)	28.8 (3.3)	0.688 (0.020)	0.658 (0.018)

This method was applied to distinguish multiple disaccharide isomers in e-liquids, the medium that is vaped in electronic cigarettes. These e-liquids are typically composed of 50:50 mixture of propelyne glycol and glycerin, but various other compounds are added to give the liquids specific flavorings when vaped. Several ingredients have been identified in e-liquids that are not safe for inhalation, and many others thermally degrade upon heating to produce potentially unsafe byproducts[4]. The e-liquids were diluted in 50:50 methanol:water to a concentration of 40 µg/mL with 100 µM lithium acetate. Some e-liquids were found to contain only one disaccharide, such as Menthol Tobacco that had only sucrose and Black Cherry, which contained only maltose. Three e-liquids were observed to have at least two disaccharides. Black Licorice and a second sample named Menthol Tobacco (from a different batch than the previous sample analyzed in Chapter 4 from the same vendor) showed cross-ring cleavage product ions at m/z 331 and m/z 289, indicative of a disaccharide with 1→4 glycosidic linkage. MS^3 water adduction experiments confirmed the *m/z* 289 and *m/z* 331 were from dissociation of maltose for

both e-liquids. An MS^2 experiment with the fragmentation amplitude set to 0.35 V applied for 250 ms confirmed sucrose was also present in each e-liquid.

Table 6.5. Comparison of reaction rate and uncreative fractions for Menthol Tobacco and standards

Menthol Tobacco				
	Reaction Rate		Unreactive Fraction	
	Sample	*Standard*	*Sample*	*Standard*
Maltose (331)	54.5 (3.2)	53.2 (3.1)	0.537 (0.042)	0.529 (0.015)
Maltose (289)	58.8 (6.5)	58.2 (2.7)	0.401 (0.032)	0.400 (0.039)
Sucrose	32.6 (2.8)	31.1 (3.3)	0.708 (0.013)	0.688 (0.020)

T**able 6.6. Comparison of reaction rate and uncreative fractions for Black Licorice and standards**

Black Licorice				
	Reaction Rate		Unreactive Fraction	
	Sample	*Standard*	*Sample*	*Standard*
Maltose (331)	59.5 (9.2)	53.2 (3.1)	0.521 (0.030)	0.529 (0.015)
Maltose (289)	55.8 (7.2)	58.2 (2.7)	0.385 (0.041)	0.400 (0.039)
Sucrose	37.3 (10.1)	31.1 (3.3)	0.667(0.015)	0.688 (0.020)

One e-liquid titled Mochaccino showed cross ring cleavages at m/z 229, 259, 289, and 331. This indicated the presence of at least one disaccharide with a 1→6 glycosidic linkage or at least three disaccharides containing 1→2, 1→3, and 1→4 glycosidic linkages. There was insufficient signal intensity for MS^3 experiments on the cross-ring cleavages, but an MS^2 experiment with the fragmentation amplitude set to 0.35 V applied for 250 ms confirmed sucrose was also present in Mochaccino.

6.6. Summary

This chapter has shown that measuring that water adduction in a quadrupole ion trap mass spectrometer can be used to determine the relative ratio of two isomeric hexoses. If the two isomers of interest have different unreactive fractions, then the isomer with the larger unreactive fraction will likely form less stable dimers than the isomer with a smaller unreactive fraction. The less stable dimer will fragment more easily in the ion optics, leading to an increased concentration of one isomer in the quadrupole ion trap. These problems with dimers can be corrected by using low concentrations to avoid formation of dimers after ESI and using low voltages in the ion optics to reduce fragmentation of dimers that still form.

This method was also applied to measure the anomeric ratio of glucose in water, based upon a calibration curves of standards with varying percentages of α- and β-methyl glucosides. The methyl glucosides are used as standards because the methyl subsistent at the anomeric carbon prevents the molecule from undergoing mutarotation to the form the other anomer. Plotting the reaction rate or the unreactive fraction versus the percentage of β-methyl glucoside produced linear calibration curves. These calibration curves measured a sample of glucose to be 66.0% β-methyl glucoside (based on unreactive fraction) and 66.3% β-methyl glucoside (based on reaction rate), very close to the accepted value of 64%. A sample of solid α-glucose was dissolved in water, and the unreactive fraction was immediately monitored (after about 5 minutes). The concentration of α-glucose was measured as a function of time until an equilibrium was reached around 150 minutes later.

Disaccharides were distinguished from mixtures containing multiple disaccharides. Reducing disaccharides produce cross-ring cleavages, which result after ring opening of the reducing end of the disaccharide. The cross ring cleavages can be used to distinguish linkage position, but not the anomericity of the disaccharide (see Chapter 4). CID of the cross-ring

cleavages produces the B type ion (*m/z* 169), and water adduction to this B type ion can be used to distinguish the linkage position and anomericity, as long as there are not multiple different disaccharides with the same product ions in the mixture. The reaction rate and unreactive fraction were measured for several different reducing disaccharides. The water adduction reaction rate to the MS^3 B type ion is very similar (less than 10% difference) to the water adduction reaction rate of the MS^2 B type ion, but the unreactive fraction varies greatly when comparing the unreactive fractions of the MS^3 and MS^2 B type ion. Non-reducing disaccharides such as sucrose do not produce cross-ring cleavages. A method was created to distinguish sucrose based on the smaller CID fragmentation amplitudes required for the onset of dissociation compared to reducing disaccharides. It was found that application of the CID voltage for longer periods of time (1000 ms instead of 40 ms) provided better selectivity. Fragmentation times of 250 ms were selected to compromise between increased analysis time and the selectivity achieved with longer fragmentation times.

Two proof-of-principle experiments were used to show that this method would work with a mixture of disaccharide standards. Three vaping liquids were also found to contain mixtures of disaccharides. For two of the vaping liquids, Menthol Tobacco and Black Licorice, maltose and sucrose were identified. Sucrose was identified in a vaping liquid called Mochaccino; however, there was insufficient signal intensity of the cross-ring cleavage product ions for MS^3 experiments to accurately identify the reducing disaccharides also present in the vaping liquid.

REFERENCES

1 P. M. Medeiros and B. R. T. Simoneit, Analysis of sugars in environmental samples by gas chromatography-mass spectrometry, *J. Chromatogr. A*, 2007, **1141**, 271–278.

2 R. U. Lemieux and J. D. Stevens, the Proton Magnetic Resonance Spectra and Tautomeric Equilibria of Aldoses in Deuterium Oxide, *Can. J. Chem.*, 1966, **44**, 249–262.

3 G. Smith, A. Kaffashan and J. A. Leary, Influence of coordination number and ligand size on the dissociation mechanisms of transition metal-monosaccharide complexes, *Int. J. Mass Spectrom.*, 1999, **182/183**, 299–310.

4 A. Khlystov and V. Samburova, Flavoring Compounds Dominate Toxic Aldehyde Production during E-Cigarette Vaping, *Environ. Sci. Technol.*, 2016, **50**, 13080–13085.

CHAPTER 7: SUMMARY AND FUTURE DIRECTIONS

7.1 General Summary

The work presented in this dissertation has been focused on the using water adduction to lithium cationized molecules to distinguish carbohydrate isomers. This includes monosaccharides, which are traditionally difficult to distinguish with mass spectrometry without complicated derivatization, chromatography, or the production of chiral clusters. Disaccharides were also distinguished, including determining the anomercity and linkage position of reducing and non-reducing carbohydrates, something that has not been accomplished previously using only mass spectrometry. The underlying chemistry of water adduction to lithium cationized molecules was also studied using density functional theory in combination with experimental results. The introduction of this dissertation focuses on explaining the challenges of distinguishing the structure of small carbohydrate molecules with various techniques and specifically mass spectrometry. Isomeric compounds are typically distinguished with dissociative methods, but these methods are unable to distinguish monosaccharides without a prior derivatization or separation step. However, when lithium cationized monosaccharides are introduced into a quadrupole ion trap, the ions will adduct water. The reaction rate of the water adduction reaction or the fraction of ions that do not adduct water can be used to distinguish different isomers. The water adduction reaction can also be used to determine the linkage position and the anomericity of the linkage in disaccharides after dissociation. Quantum mechanical calculations were used alongside experimental data to determine the cause of the unreactive fraction. These studies revealed that the number of coordinations between the lithium

cation and the oxygen atoms of the molecule dictates the reactivity of the ion. Finally, the water adduction method is used to determine the ratio of glucose to fructose in a binary mixture and the anomeric ratio of glucose in water. This chapter builds upon the ideas learned from the previous chapters to develop future experiments related to water adduction reaction and distinguishing isomers.

7.2 Distinguishing Larger Saccharides

Chapter 4 demonstrated that the linkage position and anomericity of disaccharides could be distinguished with water adduction. More specifically, the anomericity of the glycosydic linkages could easily be distinguished by measuring the reaction rate and unreactive fraction for the product ions of the non-reducing end (B type ion at *m/z* 169, see Figure 7.1). Linkages in the α-configuration have a higher unreactive fraction and faster reaction rate than the β-linkages. The linkage position can already be easily determined by the cross-ring cleavages, and it has been shown that each linkage position in an oligosaccharide can be determined by sequentially fragmenting the linkages from the reducing end to the non-reducing end and analyzing product ions from cross-ring cleavages with a simple MS^n experiment[1]. Therefore, a need to determine the anomericity of the linkage remains.

CID experiments provide product ion spectra can be used to determine linkage position, and water adduction could be used to determine the anomericity of the linkage. This was tested experimentally with two glucose containing trisaccharides, maltotriose (Glc-α1→4-Glc-α1→4-Glc) and panose (Glc-α1→6-Glc-α1→4-Glc). CID of the $[M+Li]^+$ peak at *m/z* 511 produces several product ions, including B1 type ions (the fragmentation scheme is shown in Figure 7.1). The B1 ions can be isolated, and the water adduction reaction rate and unreactive fractions can be measured. Both the measured reaction rate and unreactive fraction fell into the range expected

for an α-linkage (Figure 7.2). Similarly, the Y2 ion contains the two monosaccharides at the reducing end of the disaccharide. MS^3 of the Y2 ion results in product ions at *m/z* 169, the non-reducing end of the remaining Y2 ion. The water adduction reaction rate and unreactive fraction of the *m/z* 169 product also falls into the range expected for an α-linkage.

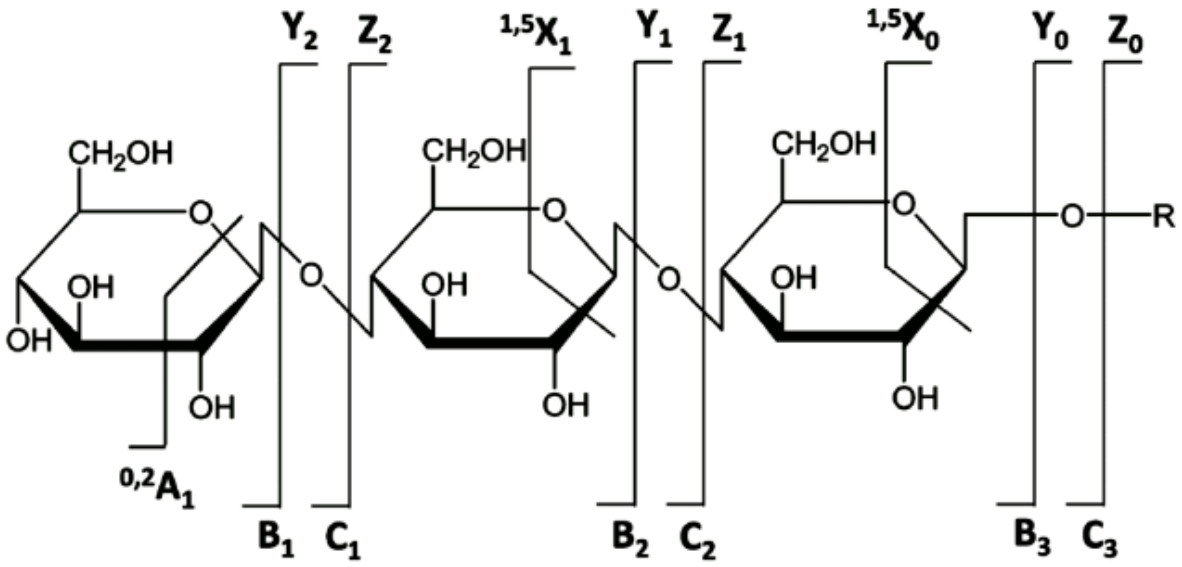

Figure 7.1. Domon-Costello nomenclature for fragmentation of oligosaccharides[2]

These preliminary results suggest that the anomericity of glycosidic linkages could be determined with water adduction, while the linkage position is determined by the product ions after CID. However, more standards are needed to confirm this hypothesis, particularly trisaccharides that have at least one β-linkage. If there is indeed a memory of the anomeric conformation after CID, then this could be a powerful tool for determining the fragmentation pattern and mechanism for larger oligosaccharides.

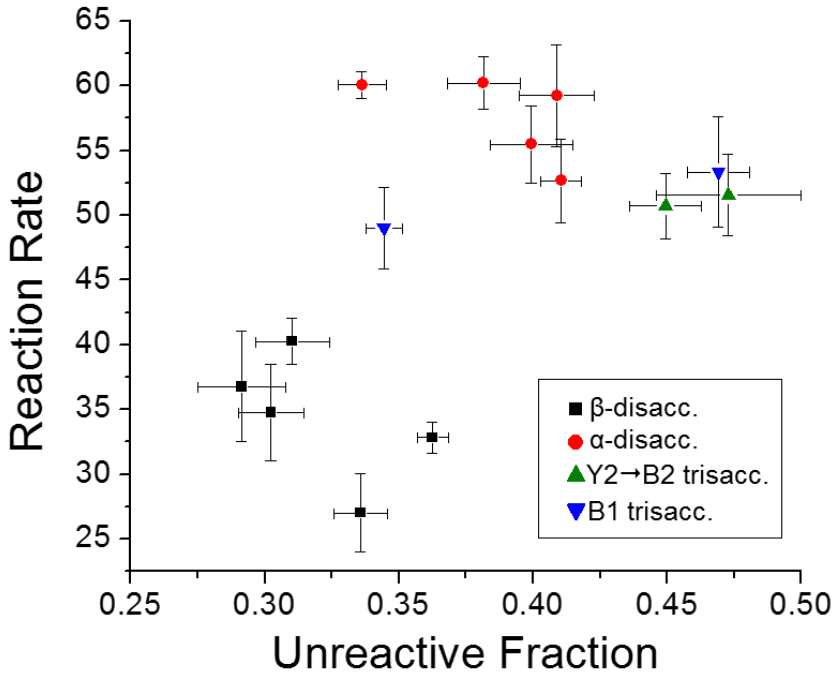

Figure 7.2. Plot of reaction rate versus the unreactive fraction for several different disaccharides and two trisaccharides. Black refers to a disaccharide with a β-linkage, red refers to a disaccharide with an α-linkage, green refers to water adduction to the center monosaccharide (Y2→dissociation of the remaining glycosidic bond) of the trisaccharide, and blue refers to water adduction to the non-reducing monosaccharide (Y2 product ion) of the trisaccharides.

7.3 Using Different ESI solvents to Study Ionization Mechanisms

The results given in chapter 5 of this dissertation explain that the location for the lithium cation binding are dependent on solution phase thermodynamics instead of gas phase thermodynamics. Therefore, modifying the solvent will have an effect on the location of the lithium cation when the molecule is transferred into the gas phase, altering both the reaction rate

and the unreactive fraction. This effect can be observed to a certain degree when comparing the reaction rates and unreactive fractions for glucose, galactose, and mannose from 100% aqueous solutions (Chapter 5) to 50:50 water:methanol (Chapter 3). Aqueous solutions produce the lowest unreactive fractions, and as the concentration of methanol increases, the unreactive fraction increases. In aqueous solution the lithium cation is believed to favor coordinations to water instead of the hexose. Therefore, as the droplet desolvates after ESI, the cation retains as many coordinations to water as possible and as few to the hexose, preferentially forming bidentate structures with the hexose after complete desolvation. The lithium cation has less affinity for methanol than water, so as the droplet is desolvating, coordinations to the hexose hydroxyls may be just as favorable as coordinations to the methanol, so tridentate structures will be more likely to form compared to using water as the solvent. Further experiments should be conducted with other solvents to confirm this idea. As the polarity of the solvent further decreases, the tridentate coordinations are expected to be more favorable.

Measuring the differences in the reaction rate and unreactive fraction after ESI in different solvents helps develop a fundamental understanding of ESI and ESI-like ionization mechanisms, such as extractive electrospray ionization (EESI). EESI is commonly used to extract analytes from aerosol particles. A solvent with no analyte is electrosprayed at passing aerosols that contain the molecules to be ionized. The ionization mechanism is believed to be somewhat similar to ESI, where analyte is extracted from the aerosol into solvent droplets, where ionization occurs. Because the reaction rate and unreactive fraction vary as a function of the solvent used for ionization, water adduction experiments would allow the ionization mechanism to be probed. For example, if the aerosol is a droplet of methanol, but the extraction solvent from

the ESI emitter is water, will the reaction rate and unreactive fraction match those from a solution of methanol or water?

7.4 Further Determination of the Conformation of Unreactive versus Reactive Structures

Isomers can be distinguished by the ratio of unreactive ions (ions that do not adduct water) to total ions. There is believed to be at least two different structures for $[M+Li]^+$, because some ions are able to adduct water and others are unable. This was investigated with quantum mechanical calculations, which demonstrated that for most hexoses there are several locations for the lithium cation to bind. Furthermore, in aqueous solution these different structures are relatively close in free energy, suggesting that several structures are thermodynamically feasible. Finally, calculations showed that a bidentate coordination to the lithium cation allows for water adduction to occur, while a tridentate coordination makes the lithium cation unable to adduct water. The results from these calculations were supported by results obtained experimentally. While these calculations and experiments developed the groundwork for understanding the chemistry causing the unreactive fraction, more experiments could be performed to create a greater understanding of the unreactive fraction. Specifically, methods could be used to separate the unreactive fraction and reactive fraction in the ion trap. Once separated, dissociative methods may provide insight into which oxygen atoms the lithium cation is coordinated. Two methods that could be used to separate the unreactive and reactive ions for given species are discussed below.

Isolation of the precursor mass-to-charge ratio is the first step in a typical tandem MS/MS experiment performed in a quadrupole ion trap. Therefore, after water adduction increases the mass-to-charge ratio of the reacted ion by 18, it would be expected that the reacted ions could be easily isolated. These experiments were performed, but after attempted isolation of the water

adducted ions, only a small peak was observed at the non-hydrated mass-to-charge ratio. This suggests that the adducted water molecule is very labile and dissociates upon excitation and ejection of other ions with other mass-to-charge ratio from the ion trap. An analogous experiment was performed by isolating the unreacted species after a 1000 ms delay. This resulted in isolation of the unreactive species, plus some reactive species where the adducted water dissociated. A second 1000 ms reaction allows the ions to once again react, and the unreacted ions can be isolated once again. This isolates the unreactive species once more, but again, the reactive ions are only partially removed from the ion trap. This experiment was continued with several more isolation and reaction steps. The unreactive fraction was again measured and found to be increasing after each sequential isolation. This suggests that the unreactive ions are slowly being "purified" in the ion trap. However, signal intensity decreases after each successive isolation step, and not enough ions remained to produce meaningful product ion mass spectra. This experiment could be repeated with a sample with greater hexoses concentration to try and retain enough signal so that reproducible CID spectra can be obtained after the several necessary isolation and reaction steps. Recent experiments have also shown that the reacted species can be isolated with a wide isolation window on the HCT, and analogous experiments could be explored to try and isolate the reactive fraction for a given set of ions.

A second method for separating the unreactive and reactive ions is to use ion mobility spectrometry (IMS). IMS is a post-ionization separation technique, often coupled to mass spectrometry for further separation and detection. Ions are separated based on differences in their mobility in an electric field. IMS has been used separate identical molecules with different protonation sites[3] and could possibly be used to distinguish different lithiation sites. Furthermore, the unreactive ions could be separated from the reactive ions by adding a dopant into the IMS

drift gas. Dopants have been shown to cluster (or adduct) to isomeric compounds differently, enhancing the separation between them[4]. Because some lithiated molecules adduct water and others do not, adding a dopant into the IMS device should only change the mobility of the ions that can adduct water, and leave the mobility of the unreactive species unchanged. Once the unreactive or reactive species are filtered out with IMS, CID can be used to determine the location of the lithium cation on the carbohydrate molecule.

7.5 Using Water Adduction to Distinguish Nucleobases

The water adduction reaction can be applied to molecules other than just carbohydrates. ESI of a solution containing a nucleobase and a lithium salt produces some $[M+Li]^+$, though some protonated species may still be observed. Water adduction has been used to distinguish cytosine and isocytocine based on reaction rate or the unreactive fraction. Additionally, three different methylated isomers of adenine (3-methyladenine, 7-methyladenine, and 9-methyladenine) could be distinguished. The different methylations are markers for different disease states. Previously, experiments were conducted to determine the relative concentration of the 7-H tautomer and the 9-H tautomer of adenine in methanol based on mixtures with known concentrations of 7- and 9-methyladenine (numbering scheme shown in Figure 7.3). However, these experiments were unsuccessful, because the reaction rates and unreactive fractions measured for all binary combinations did not match those for adenine. These experiments were collected before the importance of dimer formation on binary mixtures was known, and the experiments should be repeated more carefully.

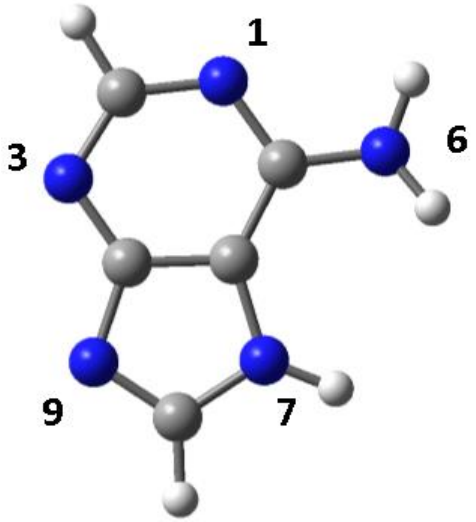

Figure 7.3. The numbering system for the nitrogen atoms in adenine. This example shows the 7-H and 6-H tautomer denoted as Ad (Figure 7.4)

Experimental results monitoring water adduction to adenine also showed only a small percentage of the lithiated molecules were not able to adduct water. Density functional theory calculations were performed similar to those detailed in Chapter 5 to determine unreactive and reactive binding sites for lithium. One caveat to exploring the conformational space of nucleotides is starting calculations from the several different tautomers which can occur in solution. Two different tautomers of adenine are the most favorable in solution, varying the hydrogen between the 7 and 9 positions. Tautomerization is also possible between the 6 and 1 positions, creating two possible structures for each the 7-H and 9-H tautomer: one with an amine (proton at the 6 position) and the other with an imine (proton at the 1 postion) (Figure 7.4). The amine is thermodynamically favored for both tautomers, and the 7-H amine tautomer is favored over the 9-H tautomer with an amine. The following discussion of the four tautomers describes them based on the notation given in Figure 7.4.

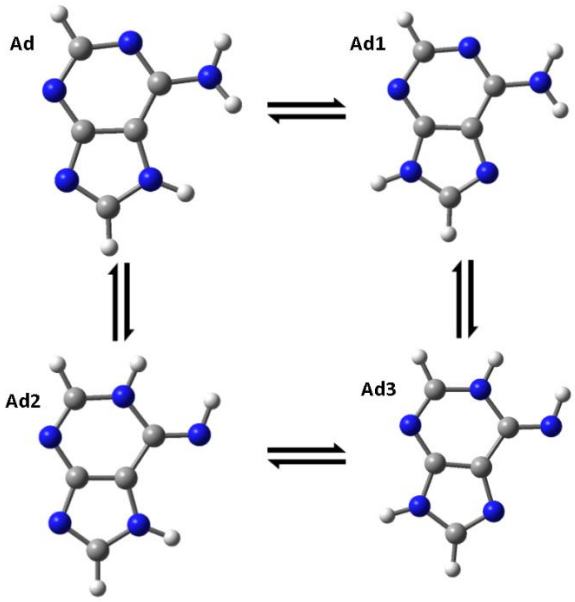

Figure 7.4. The four possible tautomers of adenine. The 7-H, 6-H tautomer is labeled Ad, 9-H,6-H is labeled Ad1, the 7-H, 1-H tautomer is labeled Ad2, 9-H,1-H is labeled Ad3. The relative stabilities are Ad > Ad1 > Ad2 > Ad3

Density functional theory calculations determined the only unreactive structure in all of the four tautomers is a site for the 9-H imine structure. This structure is the least favorable in solution and therefore very unlikely to form. However, this potentially unreactive structure is very favorable in the gas phase (Table 7.1). Therefore, it is possible that the molecule tautomerizes during the final stages of desolvation or in the gas phase. Calculations determined that the transition state for a water catalyzed tautomerization from the amine to the imine of 9-H adenine would has an activation energy of 25 kcal/mol (Figure 7.5).

Table 7.1. All possible lithium cationization sites for each of the four tautomers, and their relative free energies in vacuum and aqueous phases.

Structure	Bound N	Rel. Gibbs Energy (vacuum)	Rel. Gibbs Energy (aqueous)	$\Delta G_{WaterAdduction}$
Ad_1	1	22.98	3.60	-19.91
Ad_2	1,6	19.40	8.77	-16.81
Ad_3	3,9	1.10	0.00	-15.87
Ad1_1	3	13.03	3.27	-19.65
Ad1_2	1,6	10.73	11.78	-17.05
Ad1_3	6,7	8.29	0.27	-15.36
Ad2_1	6	27.07	11.52	-18.63
Ad2_2	3,9	12.74	11.02	-15.83
Ad3_1	6,7	0.00	9.12	-13.38
Ad3_2	3	39.93	14.21	-20.71

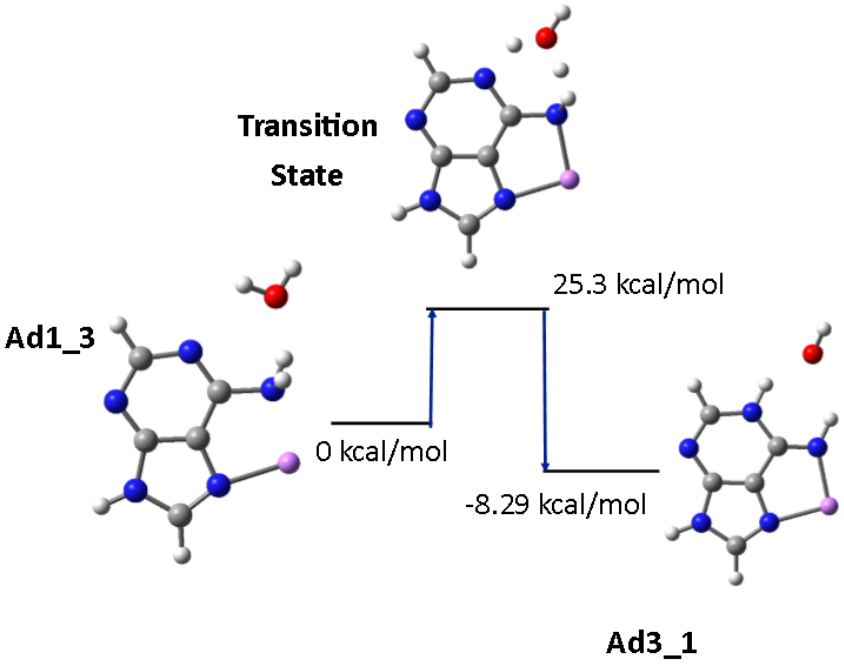

Figure 7.3. Transition state for the water catalyzed tautomerization from Ad1_3, the second lowest energy solution phase structure, to Ad3_1, the most favorable vacuum phase structure and potentially unreactive structure.

This idea was tested experimentally by measuring the unreactive fraction for the 9-methyladenine and the 7-methyladenine (Figure 7.6). Because the lithium cation is bound to the nitrogen in the 7 position in the potentially unreactive structure, only the 9-methyladenine should have an unreactive fraction. The 7-methyladenine was indeed found to be completely reactive, and the 9-methyladenine was found to have unreactive structures. This is in agreement with the results from the DFT calculations, but more experiments are needed to confirm the structure of the unreactive 9-methyladenine. The effect of metal cations on the tautomerization of nucleobases is currently an area of active research, because of the potential effects on DNA during replication and transcription[5–7].

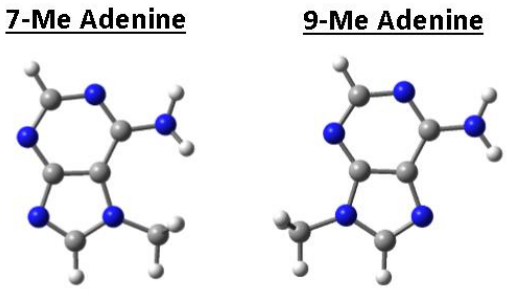

Figure 7.4. 7-methyl and 9-methyl adenine.

Increasing the voltages of the ion transfer optics increases the kinetic energy of the ions, leading to more energetic collisions with neutral molecules and ultimately increasing the internal energy of the ions. This extra internal energy should be able to increase the number of ions that are able to overcome the 25 kcal/mol transition state from the reactive Ad1_3 structure to the unreactive Ad3_1 structure. The voltage difference between the capillary exit and the first skimmer were changed from 10 to 100 V in 10 V increments, and the unreactive fraction was measured at each voltage, similar to experiments from Chapter 5 (Figure 7.7). The 7-methyl adenine did not increase in unreactive fraction as the voltage was increased. The 9-methyl adenine increases in unreactive fraction, and the increase is attributed to increased internal energy allowing for a greater fraction of the ions to tautomerize.

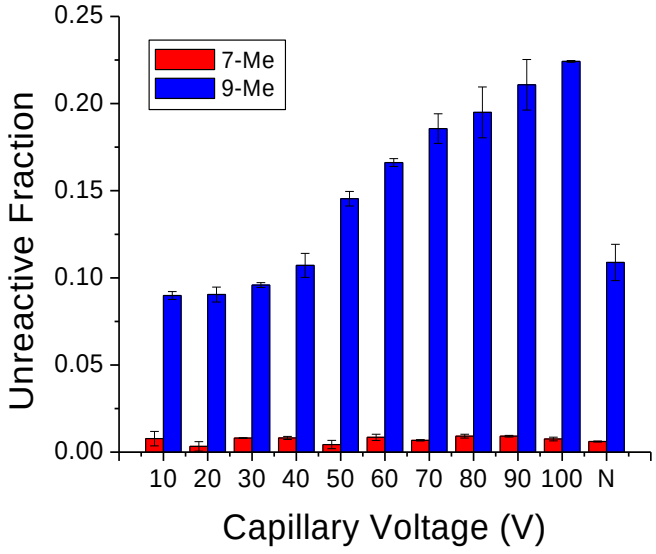

Figure 7.5. The measured unreactive fraction as a function of the capillary offset voltage. The unreactive fraction remains at zero for 7-methyl adenine and increases for 9-methyl adenine as the voltage increases. The label "N" refers to the typical settings of 44.5 V used for maximum transmission of the $[M+Li]^+$ ion.

7.6 Doping Other Alcohols or Other Solvents into the Quadrupole Ion Trap

Control of the water concentration into the ion trap would greatly increase the utility of the water adduction method. Because the unreactive fraction is a thermodynamic property, this property would remain unchanged. However, the reaction rate would increase proportionally to increase in concentration of the water. This would improve the relative standard deviation when measuring the reaction rate of slow reacting species, where the standard deviation of the reaction rate is often near the same magnitude as the standard deviation for species with much faster reaction rates. Increasing the reaction rate would also be useful for experiments with binary mixtures. Doubling the reaction rate will essentially double the slope (and therefore double the sensitivity) of the calibration curve plotting reaction rate versus concentration.

To this point, the only means for adding water into the trap is teeing into the line that provides the heated desolvation gas. The solvent is added at a rate controlled by a syringe pump. This has been used to add several gas modifiers to the ion trap including water, methanol, ethanol, 1-propanol, isopropanol, tertbutanol, and deuterium oxide. Addition, of water into the ion trap with a syringe pump flow rate of 20 µL/min only changed the reaction rate of glucose by less than 5%. When adding deuterium oxide at the same rate, the peak 20 mass-to-charge units greater was only barely noticeable after reaction times of 1000 ms. Doping in organic alcohols had a much more interesting effect. Because the ambient water remains in the ion trap, both an adduction of water and the organic dopant are observed (Figure 7.9). After reaction times of 1000 ms, very little methanol adduction is observed. However, as the size of the alcohol increased, the reaction rate of the alcohol increased as well. Another interesting observation is that the unreactive fraction, measured as the percentage not adducted to water or the alcohol after 3000 ms, decreases when adding an organic alcohol. This suggests the alcohol can bind to structures of $[M+Li]^+$ where water is unable to coordinate. The unreactive fraction continually decreases as the size of the alcohol increases from methanol to tertbutanol.

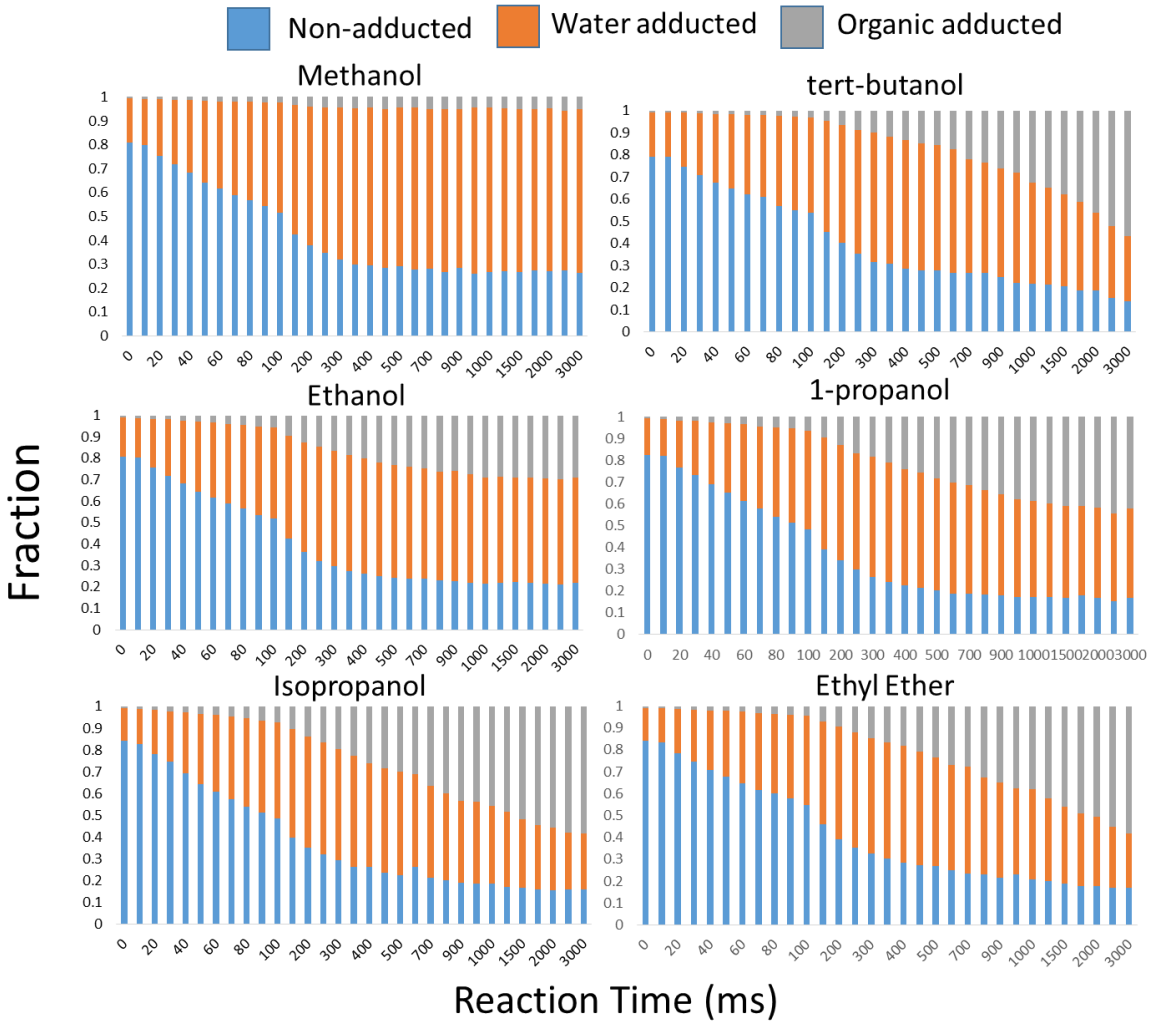

Figure 7.6. The relative signal intensity of non-adducted glucose (blue), water adducted glucose (orange), and organic adducted glucose (grey) at different delay times.

The results found from these experiments could be useful, and the method for adding dopants could be generally improved. Because different unreactive fractions are observed for different alcohols, it's possible that compounds with the same unreactive fraction for water may have different unreactive fractions for some alcohols. A better understanding of why the organic alcohols can react where water cannot is still needed. Doping the solvent in through the dry gas is less than ideal. Even with the syringe pump set to very fast flow rates, the amount of dopant

that reaches the trap is much lower than the amount of ambient water already present. Another problem with using the dry gas is that the adduct is only observed after adding 600 µL of solvent. After 600 µL the dopant adduct peak is observed in the mass spectrum, but total ion signal intensity decreases by about a factor of 2. This is believed to be caused by a gradual coating of the glass inlet capillary as the dopant is first added. A more efficient way to add dopant would be to add it directly into the ion trap through a leak-valve. One ion trap in the lab already has a hole drilled through the top of the ring electrode, and a vacuum fitting on the housing above the hole to mount the leak-valve and solvent reservoir.

REFERENCES

1 M. R. Asam and G. L. Glish, Tandem mass spectrometry of alkali cationized polysaccharides in a quadrupole ion trap, *J. Am. Soc. Mass Spectrom.*, 1997, **8**, 987–995.

2 B. Domon and C. E. Costello, A systematic nomenclature for carbohydrate fragmentations in FAB-MS/MS spectra of glycoconjugates, *Glycoconj. J.*, 1988, **5**, 397–409.

3 J. L. Campbell, J. C. Y. Le Blanc, B. B. Schneider, J. C. Y. Le Blanc and B. B. Schneider, Probing electrospray ionization dynamics using differential mobility spectrometry: The curious case of 4-aminobenzoic acid, *Anal. Chem.*, 2012, **84**, 7857–7864.

4 G. A. Eiceman, E. V Krylov, N. S. Krylova, E. G. Nazarov and R. A. Miller, Separation of Ions from Explosives in Differential Mobility Spectrometry by Vapor-Modified Drift Gas, *Anal. Chem.*, 2004, **76**, 4937–4944.

5 Y. Zhu, L. A. Hamlow, C. C. He, J. K. Lee, J. Gao, G. Berden, J. Oomens and M. T. Rodgers, Gas-Phase Conformations and N-Glycosidic Bond Stabilities of Sodium Cationized 2′-Deoxyguanosine and Guanosine: Sodium Cations Preferentially Bind to the Guanine Residue, *J. Phys. Chem. B*, 2017, **121**, 4048–4060.

6 Y. Zhu, L. A. Hamlow, C. C. He, H. A. Roy, N. A. Cunningham, M. U. Munshi, G. Berden, J. Oomens and M. T. Rodgers, Conformations and N-glycosidic bond stabilities of sodium cationized 2'-deoxycytidine and cytidine: Solution conformation of [Cyd+Na]+is preserved upon ESI, *Int. J. Mass Spectrom.*, , DOI:10.1016/j.ijms.2017.04.005.

7 T. E. Akinyemi, R. R. Wu, Y.-W. Nei, N. A. Cunningham, H. A. Roy, J. D. Steill, G. Berden, J. Oomens and M. T. Rodgers, Influence of Transition Metal Cationization versus Sodium Cationization and Protonation on the Gas-Phase Tautomeric Conformations and Stability of Uracil: Application to [Ura+Cu]+ and [Ura+Ag]+, *J. Am. Soc. Mass Spectrom.*, 2017, **28**, 2438–2453.